1998

Computational investigation of subsonic torsional airfoil flutter

Kakkavas, Constantinos

Monterey, California. Naval Postgraduate School

NAVAL POSTGRADUATE SCHOOL
Monterey, California

THESIS

COMPUTATIONAL INVESTIGATION OF SUBSONIC TORSIONAL AIRFOIL FLUTTER

by

Constantinos Kakkavas

December 1998

Thesis Advisor: Max. F. Platzer
Co-Advisor / Second Reader: Kevin. D. Jones

Approved for public release; distribution is unlimited.

REPORT DOCUMENTATION PAGE

Form Approved OMB No. 0704-0188

1. AGENCY USE ONLY *(Leave blank)*	2. REPORT DATE	3. REPORT TYPE AND DATES COVERED
	December 1998	Master's Thesis

4. TITLE AND SUBTITLE
COMPUTATIONAL INVESTIGATION OF SUBSONIC TORSIONAL AIRFOIL FLUTTER

5. FUNDING NUMBERS

6. AUTHOR(S)
Kakkavas Constantinos

7. PERFORMING ORGANIZATION NAME(S) AND ADDRESS(ES)
Naval Postgraduate School
Monterey, CA 93943-5000

8. PERFORMING ORGANIZATION REPORT NUMBER

9. SPONSORING / MONITORING AGENCY NAME(S) AND ADDRESS(ES)

10. SPONSORING / MONITORING AGENCY REPORT NUMBER

11. SUPPLEMENTARY NOTES
The views expressed in this thesis are those of the author and do not reflect the official policy or position of the Department of Defense or the U.S. Government.

12a. DISTRIBUTION / AVAILABILITY STATEMENT
Approved for public release; distribution is unlimited.

12b. DISTRIBUTION CODE

13. ABSTRACT

In this thesis single-degree-of-freedom torsional airfoil flutter is investigated using an incompressible potential flow code, a compressible inviscid Euler code and a compressible viscous Navier-Stokes code. It is found that the classical linearized incompressible and compressible flow theories yield unconservative flutter estimates. The computations based on the non-linear codes show for NACA 0006, NACA 0009, NACA 0012 and NACA 0015 airfoils that the regions of torsional flutter instability increase as the airfoil thickness and the flight Mach number is increased. On the other hand, the comparison of the flutter boundaries computed with the viscous Navier-Stokes code versus the inviscid Euler code shows that the effect of viscosity is stabilizing. Also, the computed flutter boundaries display the effect of pitch axis location on flutter. Axis locations in the range between half a chord upstream of the leading edge of the airfoil and the leading edge are most prone to induce flutter. Axis locations downstream of the quarter chord are flutter free.

14. SUBJECT TERMS
One degree-of-freedom flutter, reduced frequncy, Mach effect, airfoil thickness effect, viscosity

15. NUMBER OF PAGES
111

16. PRICE CODE

17. SECURITY CLASSIFICATION OF REPORT	18. SECURITY CLASSIFICATION OF THIS PAGE	19. SECURITY CLASSIFI- CATION OF ABSTRACT	20. LIMITATION OF ABSTRACT
Unclassified	Unclassified	Unclassified	UL

NSN 7540-01-280-5500

Standard Form 298 (Rev. 2-89)
Prescribed by ANSI Std. 239-18

Approved for public release; distribution is unlimited

COMPUTATIONAL INVESTIGATION OF SUBSONIC TORSIONAL AIRFOIL FLUTTER

Constantinos Kakkavas
Captain, Hellenic Air Force
B.S., Hellenic Air Force Academy, 1989

Submitted in partial fulfillment of the
requirements for the degree of

MASTER OF SCIENCE IN AERONAUTICAL ENGINEERING

from the

NAVAL POSTGRADUATE SCHOOL
December 1998

Author: [redacted]
Constantinos Kakkavas

Approved by: [redacted]
Max F. Platzer, Thesis Advisor

[redacted]
K.D. Jones, Co-Advisor / Second Reader

[redacted]
G. Lindsey, Chairman
Department of Aeronautics &
Astronautics

ABSTRACT

In this thesis single-degree-of-freedom torsional airfoil flutter is investigated using an incompressible potential flow code, a compressible inviscid Euler code and a compressible viscous Navier-Stokes code. It is found that the classical linearized incompressible and compressible flow theories yield unconservative flutter estimates. The computations based on the non-linear codes show for NACA 0006, NACA 0009, NACA 0012 and NACA 0015 airfoils that the regions of torsional flutter instability increase as the airfoil thickness and the flight Mach number is increased. On the other hand, the comparison of the flutter boundaries computed with the viscous Navier-Stokes code versus the inviscid Euler code shows that the effect of viscosity is stabilizing. Also, the computed flutter boundaries display the effect of pitch axis location on flutter. Axis locations in the range between half a chord upstream of the leading edge of the airfoil and the leading edge are most prone to induce flutter. Axis locations downstream of the quarter chord are flutter free.

TABLE OF CONTENTS

LIST OF FIGURES

LIST OF TABLES

LIST OF SYMBOLS

a_∞	free-stream speed of sound
b	airfoil half chord
c	airfoil chord length
Cl	lift coefficient per unit span
Cm	pitching moment coefficient per unit span
Cp	pressure coefficient
e	total energy per unit volume
E	energy
f	frequency
h	vertical displacement in plunge defined positive downward
I_α	dimensional moment of inertia
i_α	non-dimensional moment of inertia $i_\alpha = \frac{I_\alpha}{\pi \rho_\infty c^4 / 4}$
J	transformation Jacobian flux of momentum
k	reduced frequency, $2\pi fc / U_\infty$
k_α	reduced natural pitching frequency
k_h	reduced natural plunging frequency
K_α	spring constant for pitching
K_h	spring constant for plunging
L	lift per unit span
m	mass
M_∞	free-stream Mach number
M_α	aerodynamic moment per unit span
p	pressure
q	flow field vector
Re	Reynolds number

S_α	static moment ($= x_a m$)
t	time
T	period of oscillation
U_∞	free-stream velocity
u,w	velocity components at x,z direction respectively
V_F	reduced flutter velocity, $U_\infty / c\omega_\alpha = 1/k_\alpha$
W	work
x_a	center of mass to elastic axis location distance
Xp	leading edge to elastic axis location distance
x,z	coordinates in physical plane
α	airfoil angle of attack
Γ	circulation
γ_w	vorticity strength
λ	wavelength of oscillation
μ	viscosity
ξ,ζ	coordinates in transformed plane
ρ	density
τ	non-dimensionalized time
Φ	velocity potential
ω_α	uncoupled natural torsional frequency, $\sqrt{K_\alpha / I_\alpha}$
ω_h	uncoupled natural pitching frequency, $\sqrt{K_h / m}$

Operators

$\dot{(\,)}$	differentiation with respect to time
$(\,)'$	differentiation with respect to non-dimensional time

Δ	incremental change
∇	del operator

ACKNOWLEDGEMENT

I would like to express my sincere appreciation to my thesis advisor, Professor Platzer. His experience and deep knowledge in aeroelasicity proved to be extremely beneficial for me. He has his own way to make the student understand the essence of this science. The study of aeroelasticity phenomena is an extremely difficult job but becomes fun when working with Professor Platzer. I owe most of this work to him.

Many thanks to Dr. K.Jones. None of this work could have been completed without his help on the computer codes and the use of software. He spent a lot of his valuable time in order to show me how I should proceed. He was always there whenever I needed him.

Finally I would like to thank Dr. S. Weber. He was the one who helped me a lot in understanding the way the codes work. He was also the one who advised me what to do when everything seemed to be stuck and the "no way out" seemed to be unavoidable.

I. INTRODUCTION

A. BACKGROUND

The phenomenon of airfoil flutter was first encountered on World War I airplanes. The danger to flight safety posed by this phenomenon stimulated the development of quite sophisticated flutter analysis and testing methods in the ensuing years. References 1,3,4,6 and 7 give good reviews of these developments, where it is also explained that the flutter phenomenon is caused by the interaction of the aerodynamic, inertia and elastic forces. Until very recently, important simplifying assumptions had to be introduced in order to make the problem mathematically tractable. Linearized aerodynamic analysis methods were among the most important simplifications used in the past. For the analysis of low speed flutter phenomena, Theodorsen developed an incompressible flow theory for oscillating flat plates, which was then extended to compressible subsonic flow. This incompressible oscillatory flat plate theory remains the standard aerodynamic analysis tool for flutter calculations. A second important simplification was also introduced by Theodorsen when he proposed to perform the flutter analysis in the frequency domain. In this approach, the aerodynamic forces need to be computed only for the special case where the airfoil is assumed to execute a purely harmonic oscillation at constant small amplitude.

Flutter analyses based on linearized aerodynamic theory in the frequency domain have serious shortcomings. Thin airfoil (flat plate) theory makes it impossible to account for the effect of airfoil geometry on flutter. Frequency-domain methods provide little information about the physics of the flutter problem because the decay of the airfoil motion below the critical flutter speed and the divergence of the motion above this speed cannot be obtained as part of frequency domain flutter analysis.

The recent rapid advances in computational fluid dynamics (CFD), however, made it possible to replace linearized aerodynamic methods by solutions based on the full non-linear Euler or Navier-Stokes equations for inviscid or viscous compressible flow.

As an additional advantage, these modern CFD methods integrate the governing flow equations in time. Therefore, they can easily and naturally be combined with the equations of motion of the airfoil. This leads to the following specific objective for the work attempted in this investigation.

B. OBJECTIVE

A two-dimensional compressible Euler and Navier-Stokes flow solver is coupled with a one degree-of-freedom structural model for the time domain analysis of an airfoil which is free to oscillate about a specific pivot point. The effect of airfoil thickness on torsional flutter is to be determined as a function of pivot location and subsonic Mach number. Also, viscous flow effects on flutter are to be determined by comparing Euler and Navier-Stokes computed flutter boundaries. Furthermore, at low Mach numbers the Euler computed flutter boundaries are to be compared with the flutter boundaries computed with the incompressible unsteady panel code UPOT.

II. GOVERNING EQUATIONS

The equations that describe the compressible viscous fluid flow around a body are the continuity, the momentum and the energy equations. The flow around the body can be computed by the simultaneous solution of these equations. The conservation-law and the vector form of the compressible Reynolds-averaged Navier-Stokes equation is presented in this chapter. A detailed derivation can be found in [Ref 8].

A. CONTINUITY EQUATION

The continuity equation expresses the conservation-of-mass law applied to a fluid passing through a control volume fixed in space

$$\frac{\partial \rho}{\partial t} + \nabla(\rho V) = 0 \tag{2.1}$$

where ρ is the fluid density and V is the fluid velocity. Eq.(2.1) states that the net mass flux through a control volume bounding surface must be equal to the time rate of change of the mass inside the control volume. For two-dimensional Cartesian flow this equation reads

$$\frac{\partial \rho}{\partial t} + \frac{\partial}{\partial x}(\rho u) + \frac{\partial}{\partial z}(\rho w) = 0 \tag{2.2}$$

where u and w are velocity components along the x and z directions, respectively.

B. MOMENTUM EQUATION

The momentum equation expresses Newton's second law as applied to a fluid element flowing relative to a space-fixed coordinate system. The x and z direction momentum equations are:

$$\frac{\partial(\rho V)}{\partial t} + \nabla(\rho VV) = \rho f + \nabla \prod_{ij} \tag{2.3}$$

The first term in Eq.(2.3) represents the time rate of change of momentum per unit volume in the control volume. The second term represents the momentum net flux through the bounding surface of the control volume. Also, f is the body force per unit volume and $\prod_{ij}$ is the stress tensor given by:

$$\prod_{ij} = -p\delta_{ij} + \mu\left[\frac{\partial ui}{\partial xj} - \frac{2}{3}\delta_{ij}\frac{\partial u_k}{\partial x_k}\right] \tag{2.4}$$

where i,j,k = 1,2,3 and δ_{ij} is the Kronecker delta.

By substituting Eq.(2.4) into (2.3) for flow in a two-dimensional Cartesian coordinate system we obtain:

$$\frac{\partial \rho u}{\partial t} + u\frac{\partial \rho u}{\partial x} + w\frac{\partial \rho u}{\partial z} = \rho f_x - \frac{\partial p}{\partial x} + \frac{\partial}{\partial x}\left[2/3\mu(2\frac{\partial u}{\partial x} - \frac{\partial w}{\partial z}\right] + \frac{\partial}{\partial z}\left[\mu\left(\frac{\partial w}{\partial x} + \frac{\partial u}{\partial z}\right)\right]$$

$$\frac{\partial \rho w}{\partial t} + u\frac{\partial \rho w}{\partial x} + w\frac{\partial \rho w}{\partial z} = \rho f_z - \frac{\partial p}{\partial z} + \frac{\partial}{\partial z}\left[2/3\mu\left(2\frac{\partial w}{\partial z} - \frac{\partial u}{\partial x}\right)\right] + \frac{\partial}{\partial x}\left[\mu\frac{\partial w}{\partial x} + \frac{\partial u}{\partial z}\right] \tag{2.5}$$

These equations are known as the Navier-Stokes equations.

C. ENERGY EQUATION

The energy equation is derived by applying the first law of thermodynamics (rate of change of energy = net heat flux into particle + rate of work done on particle).

$$\frac{\partial e}{\partial t} - \frac{\partial Q}{\partial t} - \rho(f_x u + f_z w) + \frac{\partial}{\partial x}(eu + pu - u\tau_{xx} - w\tau_{xz}) + \tag{2.6}$$

$$\frac{\partial}{\partial z}(ew + pw - w\tau_{zz} - u\tau_{xz}) = 0$$

where e is the total energy per unit volume.

D. VECTOR FORM OF FLOW EQUATIONS

The above equations can be rewritten in non-dimensionalized vector form as

$$\frac{\partial Q}{\partial t}+\frac{\partial F}{\partial x}+\frac{\partial G}{\partial z}=\frac{1}{\mathrm{Re}}\left(\frac{\partial F_v}{\partial x}+\frac{\partial G_v}{\partial z}\right) \tag{2.7}$$

where

$$Q=\begin{bmatrix}\rho\\ \rho u\\ \rho w\\ e\end{bmatrix} \qquad F=\begin{bmatrix}\rho u\\ \rho u^2+p\\ \rho uw\\ (e+p)u\end{bmatrix} \qquad G=\begin{bmatrix}\rho w\\ \rho uw\\ \rho w^2+p\\ (e+p)w\end{bmatrix}$$

$$F_v=\begin{bmatrix}0\\ \tau_{xx}\\ \tau_{xz}\\ f_4\end{bmatrix} \qquad G_v=\begin{bmatrix}0\\ \tau_{xz}\\ \tau_{zz}\\ g_4\end{bmatrix}$$

and

$$\tau_{xx}=\frac{4}{3}\mu(u_x-1/2w_z)$$

$$\tau_{zz}=\frac{4}{3}\mu(w_z-1/2u_x)$$

$$\tau_{xz}=\mu(w_x+u_z)$$

$$f_4=u\tau_{xx}+w\tau_{xz}+\frac{\mu}{\mathrm{Pr}(\gamma-1)}a^2$$

$$g_4=u\tau_{xz}+w\tau_{zz}+\frac{\mu}{\mathrm{Pr}(\gamma-1)}a^2$$

$$\mathrm{Re}=\frac{U_\infty L}{\nu}$$

U_∞ is the free stream velocity and L is the reference length. The pressure is related to the other variables by

$$p = (\gamma - 1)\left[e - \frac{1}{2}\rho(u^2 + w^2) \right]$$

In the above equations the ratio of the specific heats, γ is 1.4 and a is the local speed of sound. The density is non-dimensionalized by the free stream density ρ_∞, the velocities by the free stream speed of sound a_∞, and the total energy by $\rho_\infty a_\infty{}^2$.

E. TURBULENCE MODEL

The unsteady Navier-Stokes equations can completely model the fluid flow, but the computational calculations of turbulent flows for realistic geometries at high Reynolds numbers demand very high grid densities and very small time steps. Therefore, in order to compute turbulent flows for configurations of practical interest, turbulence modeling is used. Turbulence models are implemented with the time-averaged forms of the Navier-Stokes equations.

The most commonly used averaging procedures are:

- the standard time averaging procedure for incompressible flow and
- the mass-averaged approach for compressible flows.

The time averaging procedure omits the high frequency information of the turbulence, but the unsteady mean flow information is preserved. For the incompressible case the randomly- changing flow variables are replaced with their averages plus their fluctuations. Thus the u velocity component is represented as $u = \overline{u} + u'$ where $\overline{u}$ is the mean velocity and u' is the fluctuation about the mean. The governing equations are time averaged and the average of the fluctuation terms is set equal to zero.

In the compressible flow case the mass-weighted variable of the Favre averaging approach is used. In this case u is represented as $u = \overline{u} + u''$ where $\overline{u}$ is

$$\overline{u} = \frac{\overline{\rho u}}{\overline{\rho}} \tag{2.8}$$

Here time average of the doubly primed fluctuating quantities is not equal to zero.

After the substitution is carried out for all of the fluctuating flow variables, the entire equation is time averaged. Next, all the time averaged terms that are doubly primed and multiplied by density are defined to be zero. For example

$$\rho u'' \equiv 0 \tag{2.9}$$

The equations of mean motion resulting from the time averaging procedure have more unknowns than equations. This constitutes the closure problem of turbulence. In order to close these equations a turbulence model must be used.

The Baldwin-Lomax (B - L) turbulence model [Ref. 10] is a two-layer eddy viscosity model which simulates the effect of turbulence in terms of the eddy viscosity coefficient μ_t. The term μ in the stress terms is replaced by $\mu+\mu_t$ and the μ/P_r in the heat flux terms is replaced with $\mu/P_r+\mu_t/P_{rt}$. The B-L turbulence model bypasses the need for finding the edge of the boundary layer by using vorticity instead of the boundary layer thickness. This model is adequate for flows which have mild pressure gradients, but it is not very suitable for highly separated flows. The basic equations of the model follow.

In the inner layer, the eddy viscosity is assumed to be proportional to the mixing length squared and vorticity, and in the outer layer it uses an exponentially decaying formula. The inner eddy viscosity is computed up to the point where it is equal to the outer eddy viscosity as shown below.

$$\mu_t = \begin{cases} (\mu_t)_{inner} & for \quad y \le y_{crossover} \\ (\mu_t)_{outer} & for \quad y > y_{crossover} \end{cases}$$

where y is the normal distance from the wall and $y_{crossover}$ taken at its minimum value where it equals y. The inner eddy viscosity is given by:

$$(\mu_t)_{inner} = \rho l^2 |\omega|$$

where

$$l = \kappa y\left[1-\exp(-\frac{y^+}{A^+})\right]$$

$$|\omega| = \sqrt{(\frac{\partial \omega}{\partial x} - \frac{\partial u}{\partial z})^2}$$

$$y^+ = \frac{\rho_w u_\tau y}{\mu_w}$$

A^+ is an experimentally determined damping constant, κ is the Von Karman constant. The outer eddy viscosity is given by

$$\mu_{outer} = dC_{cp}\rho F(y)_{WAKE} F(y)_{KLEB}$$

$F(y)_{KLEB}$ is the Klebanoff intermittency factor given by

$$F(y)_{KLEB} = \left[1 + 5.5\left(\frac{C_{KLEB}\, y}{y_{\max}}\right)^6\right]^{-1}$$

d and C_{cp} are constants. For boundary layers

$$F(y)_{wake} = y_{\max} F_{\max}$$

For wakes and separated boundary layers

$$F(y)_{wake} = C_w k y_{\max} \frac{u^2_{DIF}}{F_{\max}} y_{\max} F_{\max}$$

The quantity y_{max} is the value of y determined for the maximum value of F_{max} and F_{max} is determined by

$$F(y) = y|\omega|\left[1 - \exp(-\frac{y^+}{A^+})\right]$$

III. NUMERICAL FLOW SOLUTIONS

A. INCOMPRESSIBLE INVISCID FLOW

The basic governing equation for two-dimensional, incompressible, irrotational inviscid flow is the Laplace equation $\frac{\partial^2\Phi}{\partial x^2}+\frac{\partial^2\Phi}{\partial z^2}=0$. This comes from the continuity Eq.(2.2) for incompressible flow (ρ=const) and the equation for irrotational flow $\frac{\partial u}{\partial z}-\frac{\partial w}{\partial x}=0$.

A computer code developed by Teng [Ref. 15] was used for the flow calculations. This panel code uses the assumption that the airfoil can be approximated by a number of panels each having a source strength q_j. All the panels are assumed to have the same vorticity strength γ. These sources and vortices induce a velocity at every point around the airfoil. For the flow solution to be found two conditions are applied:

- The flow tangency condition which states that the normal component of the total velocity at the midpoint of each panel due to freestream velocity and the velocities induced by the sources and vortices on all the panels is zero.
- The Kutta condition which states that the pressure on the upper and lower surface of the trailing edge must be equal.

For an oscillating airfoil an additional wake panel is assumed to be attached to the trailing edge. The airfoil motion is divided into small steps. At each step the vorticity of the wake panel is assumed to be concentrated into a single point vortex which detaches from the airfoil with the local velocity such that the Helmholtz theorem can be applied: the change in circulation about the airfoil between time steps k-1 and k is equal and opposite in direction to the vorticity released into the wake or

$$\Delta_k(\gamma_w)_k+\Gamma_k=\Gamma_{k-1}$$

where

Δ is the wake panel length

γ_w is the vorticity strength and

Γ is the circulation about the airfoil

Two more equations are needed in order to determine the length and the orientation of the wake panel. Thus two additional conditions must be specified: The wake panel is oriented in the direction of the local resultant velocity at its mid-point The length of the wake panel is proportional to the magnitude of the local resultant velocity at its mid-point and the time-step. Figure 3-1 shows the unsteady wake and its elements.

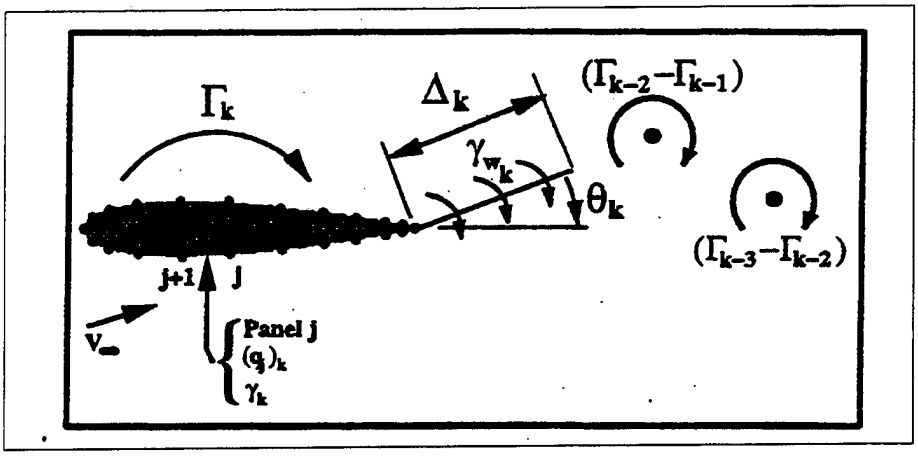

Figure 3-1 Incompressible Flow wake model

B. COMPRESSIBLE FLOW

The governing equations of the compressible flow over airfoils are so complicated that no exact solution can be obtained analytically. Their solution is accomplished with numerical methods which were applied on a mass scale after the advent of high speed computers.

The total process of obtaining flow solutions about problems involving fluid motion can be represented schematically in Figure 3-2.

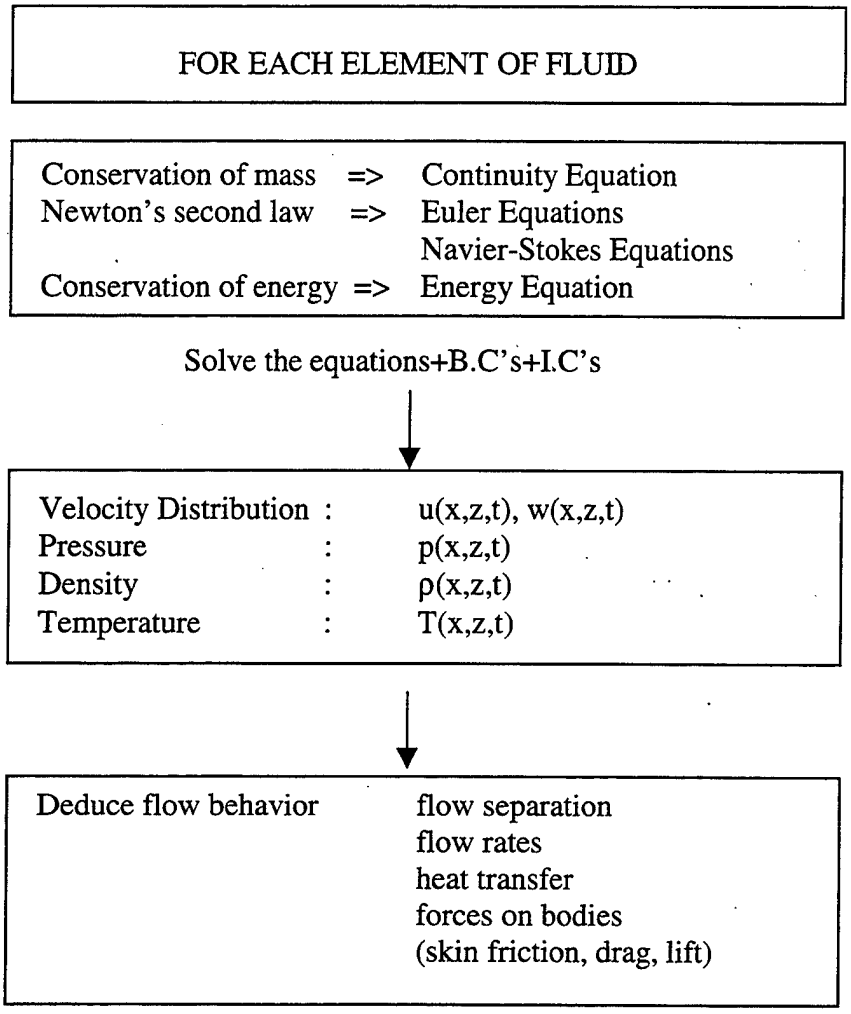

Figure 3-2 Overview of Computational Fluid Dynamics

The governing partial differential equations, are replaced with systems of algebraic equations, so that a computer can be used to obtain the solution. The process of converting the continuous governing equations to a system of algebraic equations is known as discretization.

For finite differencing schemes, a grid of discrete points is distributed throughout the computational domain in time and space. The algebraic equations link together values of the dependent variables at adjacent grid points. The required number of grid points for an accurate solution typically depends on three factors; the dimensionality, the geometric complexity and the severity of the gradients of the dependent variables. At each grid point each dependent variable and certain auxiliary variables must be stored. All of these variables must be stored in main memory for the computation to be efficient.

As the governing equations for flows around an airfoil are nonlinear, the process of the computational solution must be iterative. The iterative process is often equivalent to advancing the solution over a small time step. The number of iterations, or time steps, might vary from a few hundred to several thousand.

The discretization process always introduces an error. As long as the discrete equations are faithful representations of the governing equations, this error can be reduced by refining the grid. If the numerical algorithm that performs the iteration is stable, then the computational solution can be made arbitrarily close to the true solution of the governing equations by refining the grid.

1. Grid Generation by Algebraic Mapping

In order to use an unweighted differencing scheme the flow equations must be transformed to a generalized coordinate system using the following transformations for the case of unsteady two-dimensional flow:

$$\begin{aligned} \xi &= \xi(x,z,t) \\ \zeta &= \zeta(x,z,t) \\ \tau &= \tau(x,z,t) \end{aligned} \tag{3.1}$$

The above equations can be used to transform the governing equations from the physical (x, z,t) to the computational domain (ξ,ζ,τ) with the Jacobian transformation. For more details refer to [Ref.2].

Grid generation has to do with the establishment of the correspondence between points (x, z) in the physical domain and points (ξ,ζ) in the computational domain.

Algebraic mapping techniques interpolate the boundary data in one or more dimensions in order to generate the interior grid. The generated grid should be well-conditioned, i.e., smoothly varying, close to orthogonal and with local grid aspect ratios close to unity. For fluid flow problems, the solution is often changing rapidly close to a particular surface. It is important to construct a grid that is orthogonal, or near-orthogonal, adjacent to such a surface.

Stretching functions on the boundaries are used in order to define the grid points in the interior. Consequently, the two-boundary and multisurface techniques are still able to get smoothly varying near-orthogonal grids with only one-dimensional explicit interpolation.

The distribution of points along the boundary of the domain is handled effectively by defining normalized, one-dimensional, stretching functions along boundary segments, typically corresponding to each side of the computational rectangle in the (ξ,η) plane. Boundary stretching functions are applicable whether the interior grid is generated by solving a partial differential equation or by an algebraic mapping.

2. Numerical Implementation of Algebraic Mapping

Computer programs have been developed capable of generating grids between two bounding curves based on algebraic mapping techniques.

For the domain shown in (Figure 3-3), the bounding surfaces consist of a symmetric slender body extended downstream, ABC, and a farfield boundary, FED. Between these two boundaries half of a C-grid is to be generated. By symmetry the complete C-grid can be obtained by reflection about the x-axis.

As mentioned before, grid generation is split into two parts:

First, grid point locations on all boundaries are determined and a 1-D stretching function is used to control the distribution on the boundaries.

Subsequently, the interior grid is generated by the multisurface technique. Two intermediate surfaces, Z_2, and Z_3, are introduced, one each adjacent to the bounding

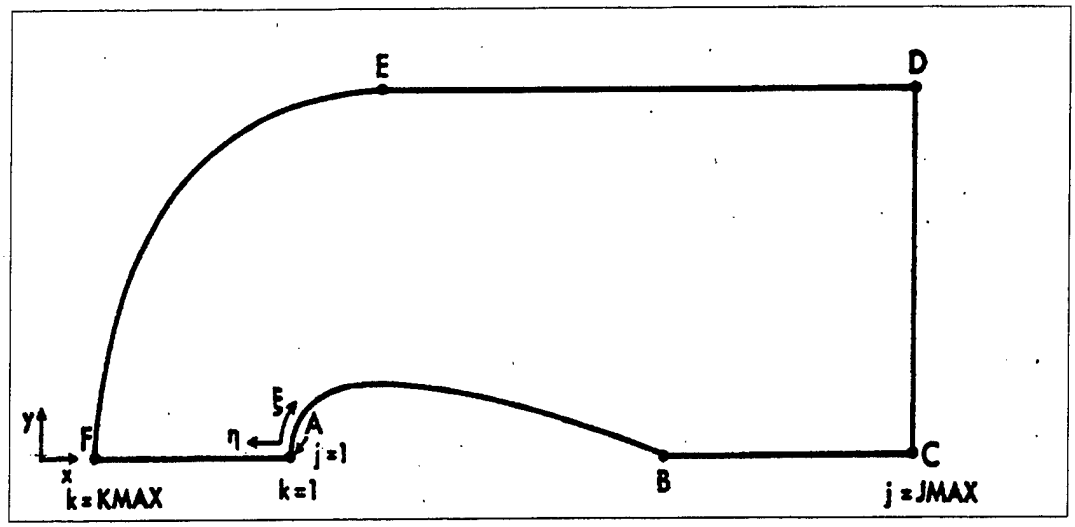

Figure 3-3 Numerical Implementation of Algebraic Mapping

surfaces ABC and FED. The parametric (r) correspondence of surfaces Z_2, and Z_3 to their neighbouring bounding surface is adjusted so that grid lines intersect the bounding surfaces orthogonally. The mechanism of choosing x(r), y(r) on surfaces Z_2, and Z_3 requires an orthogonal projection, conceptually similar to the near-orthogonal grid construction.

3. CFD Techniques

Computational techniques are used to obtain an approximate solution of the governing equations and boundary conditions. For example, for two-dimensional unsteady incompressible flow, velocity and pressure solutions, u(x, z, t), w(x, z, t) and p(x, z, t), would be computed. The computational solution is obtained in two steps that are shown in Figure 3-4.

In the first step, the partial differential equations and boundary and initial conditions are converted into a discrete system of algebraic equations. This step, as

mentioned before, is called discretization. The second step comprises the solution of the system of algebraic equations.

The fact that the differentiated terms in the governing partial differential equations are replaced by algebraic expressions connecting nodal values on a finite grid introduces an error. In order to minimize this error, the most appropriate algebraic expressions should be chosen. Equally important as the error in representing the differentiated terms in the governing equation is the error in the solution.

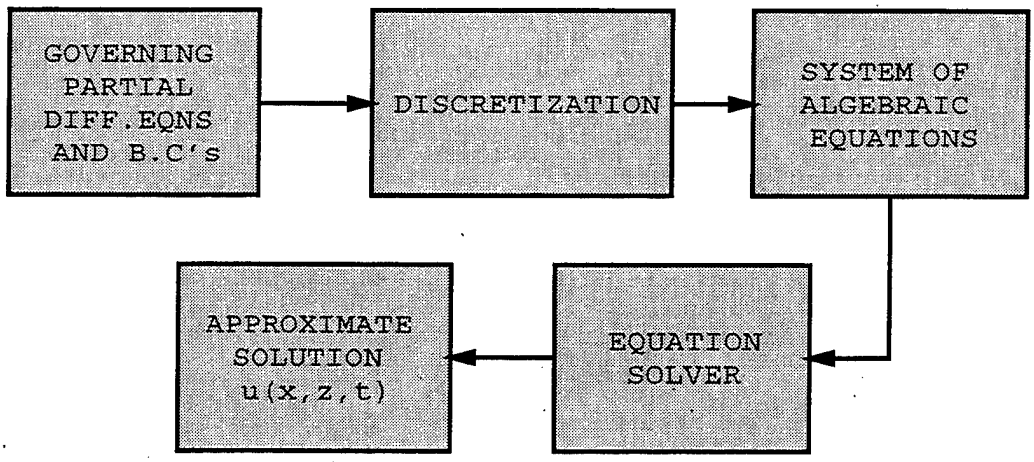

Figure 3-4 Overview of the computational solution procedure

a. Discretisation process example

To convert the governing partial differential equation(s) into a system of algebraic equations (or ordinary differential equations), a number of choices are available. The most common are the finite difference, finite element, finite volume and spectral methods.

The way the discretisation is performed also depends on whether time derivatives (in time dependent problems) or equations containing only spatial derivatives are being considered. In practice, time derivatives are discretized almost exclusively

using the finite difference method. Spatial derivatives are discretized by either the finite difference, finite element, finite volume or spectral method.

The discretization process can be illustrated by considering the scalar equation

$$\frac{\partial u}{\partial t} + \alpha \frac{\partial u}{\partial x} = 0 \tag{3.2}$$

The most direct means of discretization is provided by replacing the derivatives by equivalent finite difference expressions. It is based on forward difference in time and a central difference in space and gives, after multiplying with Δt:

$$u_i^{n+1} - u_{i+1}^n + \frac{\alpha \Delta t}{2\Delta x}\left(u_{i+1}^n - u_{i-1}^n\right) = 0 \tag{3.3}$$

This equation is referred to as explicit in time. That is if we know u_i^n at all grid points in space at time level n, then we have a series of explicit calculations to determine u^{n+1} at all grid points. Further, all values of u_i^{n+1} are obtained independently of each other; they depend only on u_i^n, not on the other u_i^{n+1} terms.

The process of discretizing Eq.(3.2) to give Eq.(3.3) implies that the problem of finding the exact (continuous) solution u(x, t) has been replaced with the problem of finding discrete values u_i^n, i.e. the approximate solution at the (i, n)th node. In turn, two related errors arise, the truncation error and the solution error.

The precise value of the approximate solution between the nodal (grid) points is not obvious. Intuitively, the solution would be expected to vary smoothly between the nodal points. In principle, the solution at some point (x_r, u_r) that does not coincide with a node can be obtained by interpolating the surrounding nodal point solution.

To provide the complete numerical solution at time level (n + 1), Eq. (3.3) must be applied for all the nodes i=2,...I-1, assuming that Dirichlet boundary conditions provide the values u_1^{n+1} and u_I^{n+1}.

The discretization process invariably introduces an error unless the underlying exact solution has a very elementary analytic form. In general, the error for a finite difference representation of a derivative can be obtained by making a Taylor series

expansion about the node at which the derivative is being evaluated. The evaluation of the leading term in the remainder provides a close approximation to the error if the grid size is small. However, the complete evaluation of the terms in the Taylor series relies on the exact solution being known.

b. Convergence

A solution of the algebraic equations that approximate a given partial differential equation is said to be convergent if the approximate solution approaches the exact solution of the partial differential equation for each value of the independent variable as the grid spacing tends to zero. Thus we require

$$u_i^n \to \bar{u}(x_i, t_n) \quad \text{as} \quad \Delta x, \Delta t \to 0$$

where $\bar{u}$ is the exact solution

The difference between the exact solution of the partial differential equation and the exact solution of the system of algebraic equations is the solution error, denoted by e; that is

$$e_i^n = \bar{u}(x_i, t_n) - u_i^n$$

The exact solution of the system of algebraic equations is the approximate solution of the governing partial differential equation. The exact solution of the system of algebraic equations is obtained when no numerical errors of any sort, such as those due to round-off, are introduced during the computation. The magnitude of the error, at the $(i,n)^{th}$ node typically depends on the size of the grid spacings, Δx and Δt, and on the values of the higher-order derivatives at that node, omitted from the finite difference approximations to the derivatives in the given differential equation.

4. Navier – Stokes Solution

If we apply the generalized transformation to the compressible Navier-Stokes equations written in vector form Eq.(2.7), the following transformed equation

is obtained

$$\frac{\partial \hat{Q}}{\partial t}+\frac{\partial \hat{F}}{\partial \xi}+\frac{\partial \hat{G}}{\partial \zeta}=\frac{1}{\mathrm{Re}}\left(\frac{\partial \hat{S}}{\partial \zeta}\right) \tag{3.4}$$

where $\hat{Q}$ is the conservative variables vector:

$$\hat{Q}=\frac{1}{J}\begin{bmatrix}\rho\\ \rho u\\ \rho w\\ e\end{bmatrix}$$

J is defined in Eq.(3.9)

$\hat{F}$, $\hat{G}$ are the inviscid flux vectors:

$$\hat{F}=\frac{1}{J}\begin{bmatrix}\rho U\\ \rho uU+\xi_x p\\ \rho wU+\xi_\zeta p\\ (e+p)u-\xi_t p\end{bmatrix} \qquad \hat{G}=\frac{1}{J}\begin{bmatrix}\rho W\\ \rho uW+\zeta_x p\\ \rho wU+\zeta_z p\\ (e+p)W-\zeta_t p\end{bmatrix}$$

and $\hat{S}$ is the thin layer approximation of the viscous fluxes in the ζ direction:

$$\hat{S}=\frac{1}{J}\begin{Bmatrix}0\\ \mu m_1 u_\zeta+(\mu/3)m_2\zeta_x\\ \mu m_1 w_\zeta+(\mu/3)m_2\zeta_z\\ \mu m_1 m_3+(\mu/3)m_2 m_4\end{Bmatrix}$$

where

$$m_1=\zeta_x^2+\zeta_z^2$$

$$m_2=\zeta_x u_\zeta+\zeta_z w_\zeta$$

$$m_3=(u^2+w^2)/2+\frac{\partial_\zeta(\alpha^2)}{\mathrm{Pr}(\gamma-1)}$$

$$m_4=\zeta_x u+\zeta_z w$$

The U and W are the contravariant velocity components, tangential to the constant ξ and ζ surfaces, respectively, and they are given by:

$$U = u\xi_x + w\xi_z + \xi_t$$

$$W = u\zeta_x + w\zeta_z + \zeta_t$$

Non-dimensionalization of the governing Eq.(3.4) is performed using the following reference quantities: density ρ_∞, length c, time c/a_∞, and energy $\rho_\infty a^2_\infty$

After non-dimensionalization of the governing equations, Euler solutions are obtained setting the viscous terms of Eq.(3.4) zero and applying the flow tangency condition at the airfoil surface. For Navier-Stokes solutions the no-slip condition is applied at the surface.

The numerical integration of the Eq (3.4) is performed using an implicit scheme [Ref. 11] given by

$$\left[I + h_\xi \left(\nabla^b_\xi \hat{A}^+_{i,k} + \Delta_\xi \hat{A}^-_{i,k}\right)\right]^p \times$$

$$\left[I + h_\zeta \left(\nabla^b_\zeta \hat{B}^+_{i,k} + \Delta_\xi \hat{B}^-_{i,k} - \mathrm{Re}^{-1}\,\delta_\zeta \hat{M}_{i,k}\right)\right]^p \times \left(\hat{Q}^{p+1}_{i,k} - \hat{Q}^p_{i,k}\right) = \tag{3.5}$$

$$= -\left[\left(\hat{Q}^p_{i,k} - \hat{Q}^n_{i,k}\right) + h_\xi \left(\hat{F}^p_{i+1/2,k} - \hat{F}^p_{i-1/2,k}\right) + h_\zeta \left(\hat{G}^p_{i,++1/2} - \hat{G}^p_{i,k-1/2}\right) - \mathrm{Re}^{-1} h_\zeta \left(\hat{S}^p_{i,++1/2} - \hat{S}^p_{i,k-1/2}\right)\right]$$

In Eq.(3.5) ∇, Δ and δ are the forward, backward and central difference operators respectively, whereas the $h_\xi = \Delta\tau / \Delta\xi$, $h_\zeta = \Delta\tau / \Delta\zeta$, $A^\pm = \partial\tilde{F} / \partial\tilde{Q}$ and $B^\pm = \partial\tilde{G} / \partial\tilde{Q}$ are the flux Jacobian matrices. The superscript $(.)^n$ refers to the time step and the superscript $(.)^p$ refers to Newton subiterations within each time step.

Time accuracy of the implicit numerical solution is obtained by performing Newton iteration to convergence for each time step. Linearization and factorization errors are minimized because the left hand side of Eq.(3.5) can be driven to zero at each time step. Typically two to three subiterations are sufficient to drop the residuals two orders of magnitude during the Newton iteration process.

IV. AEROELASTIC ANALYSIS

A. FLUTTER – GENERAL

Flutter can be defined as the dynamic instability of an elastic body in an airstream. The aircraft aerodynamic surfaces, such as wings, tails, and control surfaces (i.e. bodies subjected to large lateral aerodynamic loads of the lift type) are the bodies that are most likely to experience flutter. The only air forces necessary to produce it are those due to deflections of the elastic structure from the undeformed state.

The flutter speed U_F and frequency ω_F are defined, respectively, as the lowest airspeed and the corresponding circular frequency at which a given structure flying at given atmospheric density and temperature will exhibit sustained, simple harmonic oscillations. All small motions are stable at speeds below U_F, whereas divergent oscillations can occur in a range of speeds (or even at all speeds) above U_F. In other words, flight at U_F represents a borderline condition or neutral stability boundary above which flutter will happen.

The free vibration of a linear structure in vacuum is a real, or single, eigenvalue problem. In contrast, the theoretical flutter analysis leads to a complex, or double, eigenvalue problem, where two characteristic numbers determine the critical flutter speed and frequency. This is because the simple harmonic motion assumption is made; all dependent variables are proportional to $e^{i\omega t}$, and the problem is to find all the combinations of U and ω for which flutter actually occurs.

There are three main ways in order to study and predict flutter:

- theoretical flutter computation
- wind-tunnel experiments on scaled dynamic models,
- flight testing of full-scale aircraft.

The decision as to which of these is most economical in a given case is very difficult and depends on a multitude of factors such as:

- the purpose and the phase of the study
- anticipated margin of safety from flutter,
- the Mach number range,
- the number of different mass and structural configurations to be analyzed.

Current regulations require that flight flutter testing must be preceded by flutter analysis and wind tunnel testing.

B. THE PHENOMENON OF FLUTTER

The phenomenon of flutter can be described with a simple experiment: consider a cantilever wing, mounted in a wind tunnel at a small angle of attack and with the root rigidly built in. Then when there is no flow in the tunnel we deliberately deflect and then release the wing. We observe that the oscillation decays gradually. Then we increase the speed of flow in the wind tunnel and repeat the experiment; the oscillation of the disturbed airfoil dies out. With further increase of the flow speed, however, a point is reached at which the oscillation maintains itself with steady amplitude. This is the critical flutter speed. If the wind tunnel speed is increased, flutter will occur with increasing amplitude. It is obvious that during the aircraft flight at speeds above the critical, an initial disturbance (coming from a gust for example) will cause an oscillation of great violence. In such circumstances the airfoil suffers from oscillatory instability and is said to flutter.

The above experiment on wing flutter shows that the oscillation is self-excited; i.e., no further external disturbance is required. The motion can maintain itself or grow for a range of wind speeds, which depends on the design of the wing and the conditions of the test.

An aerodynamic surface, as an elastic body, has infinitely many degrees of freedom (d.o.f). But often it is sufficient to consider only three variables, namely the flexure (plunge), the torsion (pitch), and the control-surface rotation. A flutter mode consisting of all three elements is called a ternary flutter. In special cases, however, two of the variables predominate, and the corresponding flutter modes are called binary flutter modes. In fact, many airplanes can be replaced by a system of simple beams, so that the elastic deformation can be described by the deflection and torsion of the beams, in addition to the rotation of control surfaces about their hinge lines.

For the oscillatory motion of a wing only the first two components of flutter are often considered: the flexural (plunge) and the torsional (pitch). In general, the coupling of those two degrees of freedom is an essential feature for wing flutter. The oscillation that occurs at the critical speed is harmonic. Experiments on cantilever wings show that the flexural movements at all points across the span are approximately in phase with one another, and likewise the torsional movements are all approximately in phase, but the flexure is considerably out of phase from the torsional movement. As will be seen later, it is this phase difference that is responsible for the occurrence of flutter.

A rigid airfoil in a low-speed attached flow which is constrained in torsion and can only plunge (flexural d.o.f) does not flutter. In contrast, a rigid airfoil with only the torsional d.o.f can flutter for some special mass distributions and elastic-axis locations. In this text we will restrict the term "flutter" to the oscillatory instability in a flow which does not experience flow separation or strong shocks.

For a control surface, such as a flap or an aileron, its flexural and torsional elastic deformation are not so important as its freedom to turn about the hinge line. Consequently, the deflection of a control surface can simply be described by the angle of rotation about its hinge line.

The degrees of freedom of flutter mentioned before, together with the freedom of the airplane to move as a rigid body, offer a large number of possible combinations of binary, ternary, and higher modes of flutter. Since it is not clear which of these modes

correspond to the actual critical speeds, it is necessary either to resort to experiments or, in a theoretical approach, to analyze all cases. This is why a successful flutter analysis depends so much on the analyst's experience. He must be able to choose, among all possible modes, those that are likely to be critical for a given structure.

As one can easily understand, flutter analysis is an extensive subject; for this reason it is preferable to divide its presentation in sections. Some basic definitions are given in Section C. The role of the elastic stiffness in flutter prevention are explained on an empirical basis in Section D. The origin of flutter from the aerodynamic point of view is then considered in Section E. It will be shown that flutter occurs because the speed of flow affects the amplitude ratios and phase shifts between motion in various degrees of freedom in such a way that energy can be absorbed by the airfoil from the airstream passing by. The physical explanation and the equations of motion for the one d.o.f flutter will be discussed in Section F, whereas the two d.o.f flutter will be explained in Section G. A practical way to find the flutter condition with the Panel Code (UPOT) will be shown in Section H.

C. NONDIMENSIONAL PARAMETERS

In flutter analysis any non-dimensional quantity relating to the motion can be expressed as a function of two parameters:

$$\rho/\sigma \quad \text{and} \quad K/\sigma l^3 U^2$$

where

l	Typical linear dimension
U	Air speed
ρ	Air density
σ	Typical density of structural material
K	Typical torsional stiffness constant (ft-lb per rad)

If we consider the energy dissipation of the structure, the viscosity and the compressibility of the fluid in flutter analysis then three more non-dimensional variables must be added:

g	Material damping coefficient
Re	Reynolds number
M	Mach number

For two systems to be dynamically similar they should have equal variables g, Re, and M in addition to the above parameters. In general, g is important in control-surface flutter, Re is important in stall flutter, and M is important in high-speed flight; otherwise their effects are small.

The non-dimensional form of the frequency of oscillation ω (radians per second, with dimension T^{-1}) is:

$$k = \frac{\omega l}{U} \tag{4.1}$$

which is called the reduced frequency.

Two similar systems having the same values of ρ/σ and $K/\sigma l^3 U^2$ flutter at the same reduced frequency. Since all derived concepts relating to the motion can be expressed in functional relations as above, it is clear that the equality of the values of the parameters ρ/σ and $K/\sigma l^3 U^2$ is sufficient to guarantee dynamic similarity of the two systems.

The reduced frequency characterizes the variation of the flow with time. Its inverse, $U / \omega l$ is called the reduced speed. The physical meaning of the reduced frequency is given as follows: Consider that a disturbance occurs at a point on a body and oscillates together with the body. The fluid element influenced by the disturbance moves

downstream with a mean velocity U. Let the frequency of oscillation of the body and the disturbance be ω. Then the spacing, or "wave length" of the disturbance, is $\lambda = T \cdot U$ or $\lambda = 2\pi U/\omega$. So the reduced frequency for the airfoil of chord c is:

$$k = \frac{\omega c}{U} = 2\pi \frac{c}{\lambda} \tag{4.2}$$

Therefore, the reduced frequency represents a ratio of the characteristic length of the body (chord) to the wave length of the disturbance. In other words, the reduced frequency characterizes the way a disturbance is felt at other points of the body. Since every point of an oscillating body disturbs the flow, one may say that the reduced frequency characterizes the mutual influence between the motion at various points of the body.

The reduced natural pitching frequency is defined as

$$k_\alpha = \frac{\omega_\alpha c}{U} \tag{4.3}$$

where

$$\omega_\alpha = \sqrt{\frac{K_\alpha}{I_\alpha}} \tag{4.4}$$

is the uncoupled natural torsional frequency of the system, K_α is the spring constant for pitching and I_α is the moment of inertia about the pivot point per unit span. From Eq.(4.3) and (4.4) we have:

$$k_\alpha = \frac{c}{\sqrt{I_\alpha} U} \sqrt{K_\alpha} \tag{4.5}$$

The reduced flutter velocity is defined:

$$V_F = \frac{U}{\omega_\alpha c} = \frac{1}{k_\alpha} \tag{4.6}$$

D. STIFFNESS CRITERIA

As mentioned before, wing-flutter occurs when the reduced frequency is lower than the following critical value:

$$k_{cr} = \frac{\omega_\alpha c}{U}$$

where U is the mean speed of flow, ω_α is the undamped natural pitching frequency of the wing, and c is the chord length of the vibrating portion of the wing.

For safety against flutter, the reduced frequency should be higher than k_{cr}, or the design speed of the airplane should be lower than

$$U_{cr} = \frac{\omega_\alpha c}{k_{cr}} \tag{4.7}$$

The frequency ω_α, which may be determined by ground vibration experiments or computed by a theoretical analysis, increases with increasing stiffness of the structure. Therefore, the critical speed can be raised by increasing the wing stiffness. It is obvious that when the lower limit of U_{cr} is defined (e.g., the maximum speed of flight) we can determine the minimum value of ω, and hence the minimum value of the torsional rigidity.

E. VERTICAL TRANSLATORY OSCILLATION

The fundamental role played by the aerodynamic forces in inducing flutter is that they are the means through which kinetic energy is transferred from the airstream to the airfoil as elastic and kinetic energy. Hence, the possibility of flutter can be discussed by considering the energy relation. From the analysis we can find the amount of energy exchanged between the airstream and the airfoil; if the oscillating body gains energy from

the airstream in completing a cycle then the oscillation is aerodynamically unstable; if it gives energy to the airstream the oscillation is going to be aerodynamically stable.

In order to determine the energy transfer consider an airfoil performing a vertical translatory oscillation with a constant amplitude h_0. Then the vertical displacement can be described by

$$h = h_0 e^{i\omega t} \tag{4.8}$$

where h is defined to be as positive downward. The speed of downward motion is therefore

$$\dot{h} = i\omega h_0 e^{i\omega t} \tag{4.9}$$

where the prime indicates a differentiation with respect to time. If $\dot{h}$ is a constant, the downward motion will induce a lift force L_0 on the airfoil:

$$L_0 = \frac{1}{2}\rho U^2 S \frac{dC_L}{d\alpha}\frac{\dot{h}}{U} \tag{4.10}$$

where $\frac{\rho U^2}{}$ is the dynamic pressure and S is the wing area. This value L_0 is the quasi-steady lift and is defined as positive upward in the usual sense. As the airfoil performs a translatory oscillation, the true instantaneous lift acting on the airfoil differs from L_0 both in magnitude and in phase and its value can be stated in the form

$$L = L_0 r e^{i\psi} \tag{4.11}$$

In this expression r represents the ratio of the absolute value of the instantaneous lift to that of the quasi-steady lift, and ψ the phase angle by which the actual lift leads the quasi-steady value. The quantities r and ψ depend on the reduced frequency k, the Mach number M, and the Reynolds number Re. For a nonviscous incompressible fluid, r and ψ are functions of k alone. The ratio $L/L_0 = re^{i\psi}$ can be plotted as vector with length r and angle ψ. Using incompressible oscillatory thin airfoil theory von Karman and Sears derived the vector diagram of Figure 4-1.

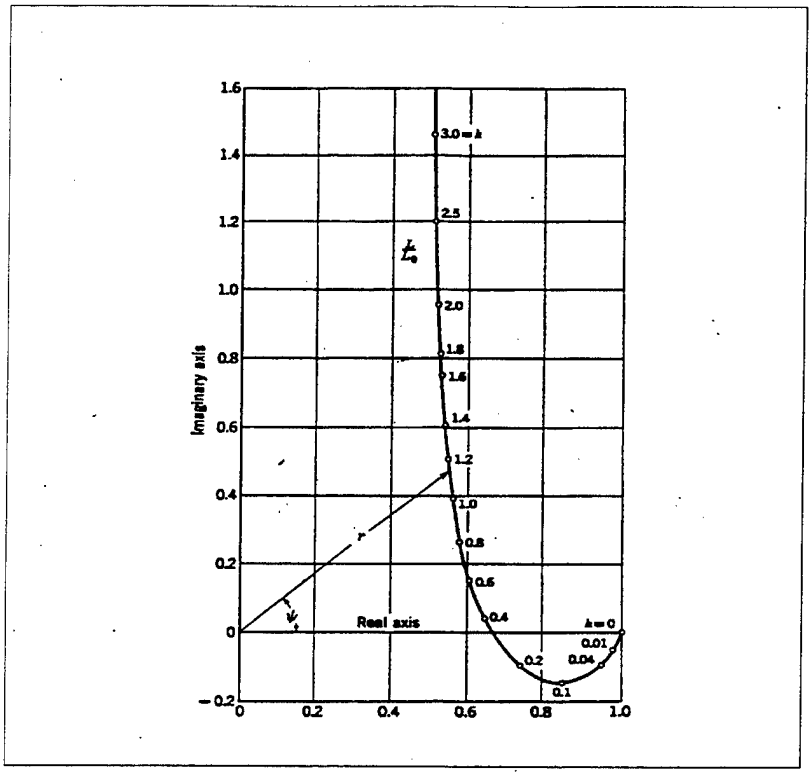

Figure 4-1 Vector diagram of lift in vertical translation oscillation. (From Y.C.Fung Ref. 1)

When the airfoil moves through a distance *dh*, the differential work done by the lift is

$$dW = -Ldh = -L\dot{h}dt \tag{4.12}$$

and therefore the total work done by the air on the airfoil during one cycle of oscillation, as given by Y.C Fung, [Ref.1] is:

$$W = -\int_0^{2\pi/\omega} \mathrm{Re}[L]\cdot \mathrm{Re}[\dot{h}]\cdot dt = -\frac{1}{2}\rho US\frac{dC_L}{d\alpha}(\omega h_0)^2 r\int_0^{2\pi/\omega} \sin(\omega t+\psi)\cdot\sin(\omega t)dt =$$

$$= -\frac{\pi}{2}\rho US\frac{dC_L}{d\alpha}\omega h_0{}^2 r\cos\psi \tag{4.13}$$

Hence, the gain of energy *W* by the airfoil from the airstream is proportional to -cosψ, where ψ is the phase angle by which the actual lift leads the quasi-steady value. If $-\pi/2 < \psi < \pi/2$, then *W* is negative; i.e., the oscillating airfoil will give energy to the

airstream and the oscillation is therefore stable. If we refer back to Figure 4-1, it is seen that the condition $-\pi/2 < \psi < \pi/2$ is satisfied. Hence, in a nonviscous incompressible fluid, the vertical translation oscillation is aerodynamically stable.

This example shows the importance of the phase angle between the aerodynamic force and the oscillatory motion. Based on this phase angle we can conclude that purely translational flutter in one degree of freedom is impossible.

However as shown in the next Section, this conclusion does not hold for single-degree-of–freedom torsional motion.

F. ONE DEGREE OF FREEDOM FLUTTER (TORSIONAL)

In this section one degree of freedom torsional flutter will be examined. In Subsection 1 the negative damping at low reduced frequency k will be explained qualitatively. In Subsection 2 the time and frequency domain analysis will be presented.

1. Physical Explanation

Consider an airfoil in an incompressible airflow of speed U, subjected to a slow (low k), nearly sinusoidal torsional motion. Assume that the rotational axis is at the leading edge (L.E.), but similar results are obtained if it is anywhere in front of the quarter chord point.

Examine now step by step how flutter may occur for this one degree of freedom oscillating airfoil with the help of Figure [illegible] given by Bisplinghoff et al [Ref.4]. At stage (a) when the airfoil is at the highest angle of attack all the vortices shed during the preceding last half cycle have counter-clockwise vorticity. Between (a) and (c) the airfoil pitches down resulting in vortices of clockwise vorticity. As k is low, the counter-clockwise vortices are far away from the trailing edge (T.E.) and do not contribute significantly in inducing the upwash. Therefore, as the airfoil pitches through the zero AOA position, stage (b), a lift L_2 is induced which is in the same direction as the motion and therefore net positive work is done on the airfoil.

When the airfoil increases the angle of attack from steps (c) to (a) the counter-clockwise vortices dominate inducing a wake upwash and therefore a lift L_2 and moment which is in the same sense as the angular velocity and again does positive work on the wing.

This transfer of energy from the airstream to the airfoil is the origin of the negative damping. At higher values of k the wave length of the vertical wake becomes shorter so that vortices from previous half-cycles can contribute. The net effect is an eventual change of the aerodynamic damping from negative to positive.

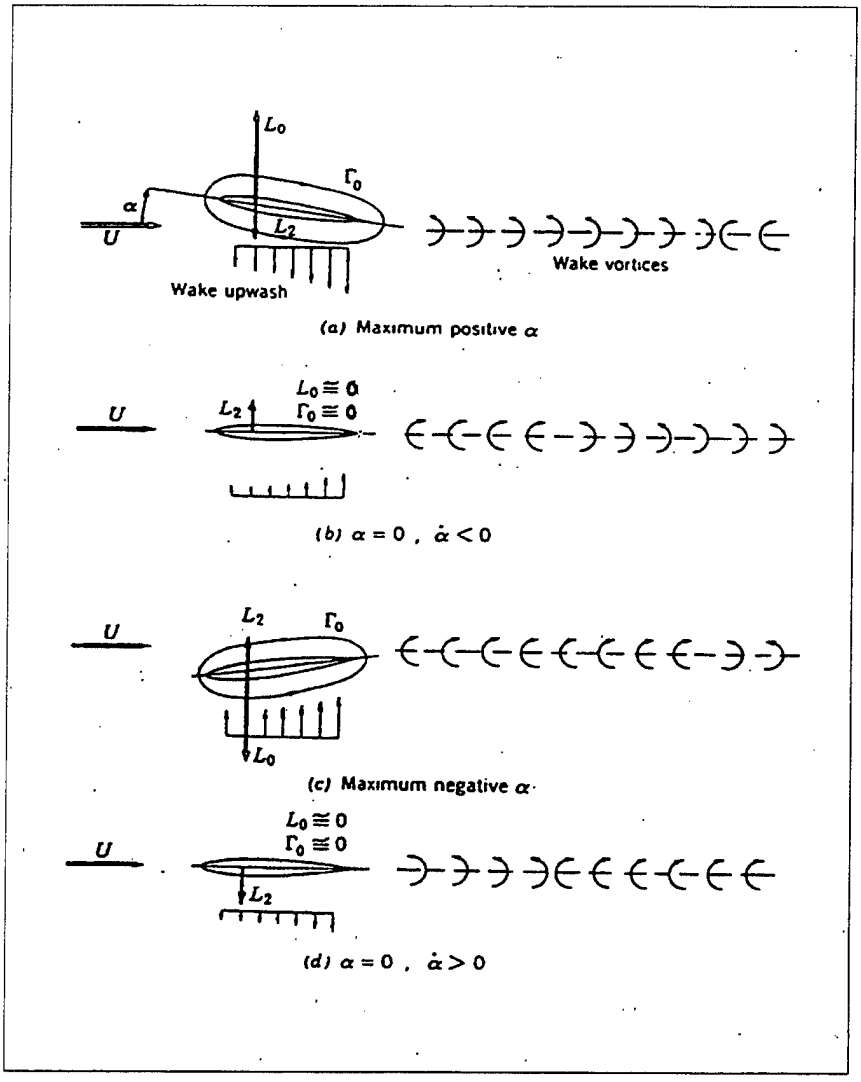

Figure 4-2 Oscillating airfoil about a pivot point in front of ¼ chord

The phenomenon of upwash and lift induced by the wake vortices can be visualized by the incompressible panel code UPOT. The airfoil wake vortices are shown in Figure 4-3 as squares. The solid ones are the clockwise vortices whereas the dotted ones are the counterclockwise vortices. The airfoil is shown in the same four positions as in Figure 4-2. It is clearly seen that the rotation of the vortices sketched by Bisplinghoff et al is reproduced by the panel code.

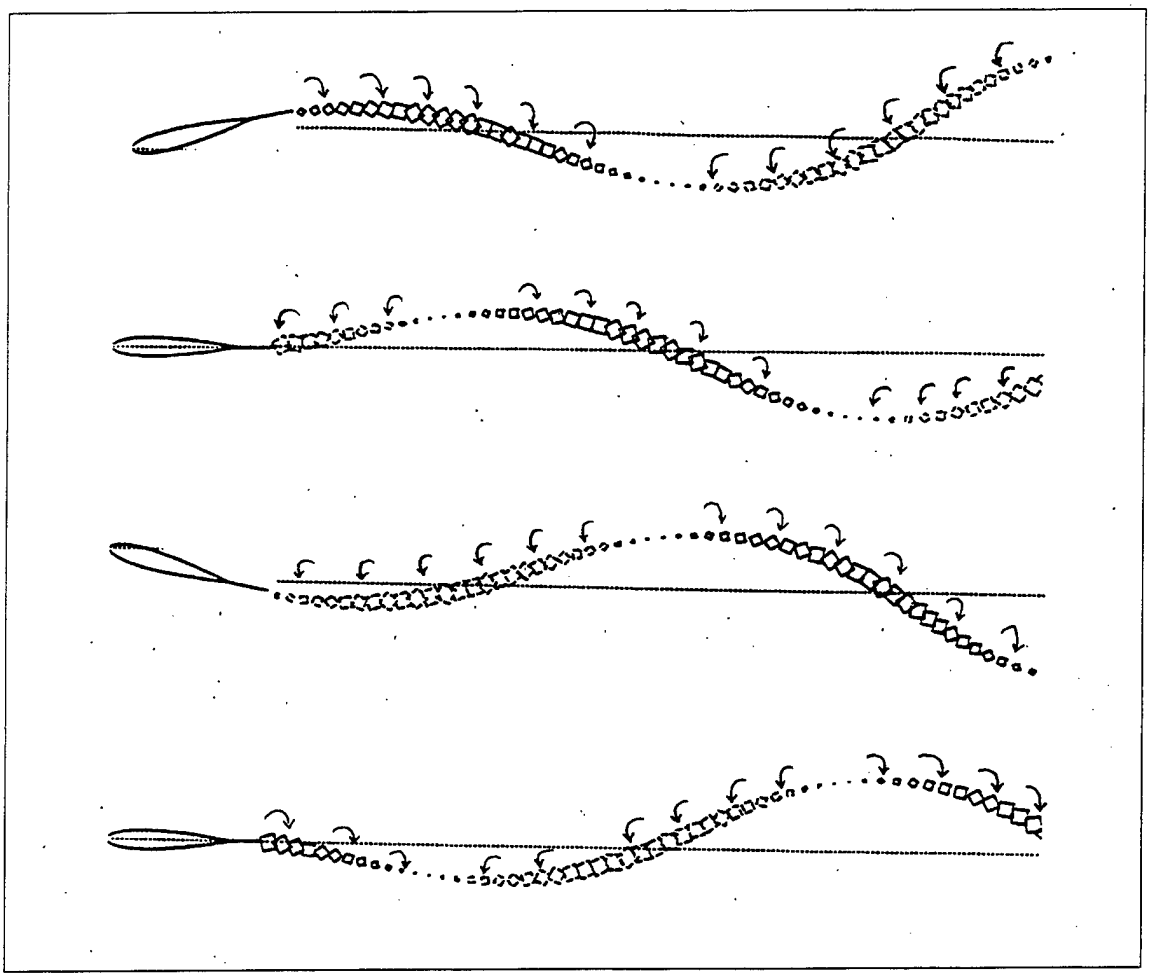

Figure 4-3 Incompressible flow wake visualization (from UPOT)

The essence of the foregoing discussion is the inclusion of unsteady effects. If only quasi-steady aerodynamics had been used (without vortex shedding), the possibility of torsional flutter would have been overlooked. For a more detailed analysis refer to Bisplinghoff et al [Ref. 4 pages 262-263].

2. Flutter Analysis

Flutter analysis can be done with two methods. The first is the time-domain analysis in which the airfoil motion is found as a function of time. It is based on discretisation of the ordinary differential equation of motion. The second method is the classical theoretical approach based on frequency-domain analysis with which the critical flutter speed and frequency are calculated. For both methods we consider a simple system of a two-dimensional, rigid airfoil of unit span, which is hinged at a specific point (pivot) but elastically restrained from rotating about this axis by a torsion spring with constant K_α. The airfoil, which has a moment of inertia about the pivot point I_α, is placed in an airstream so that the unstrained position of the spring corresponds to zero angle of attack α (Figure 4-4). Then we let the airfoil perform a torsional oscillation.

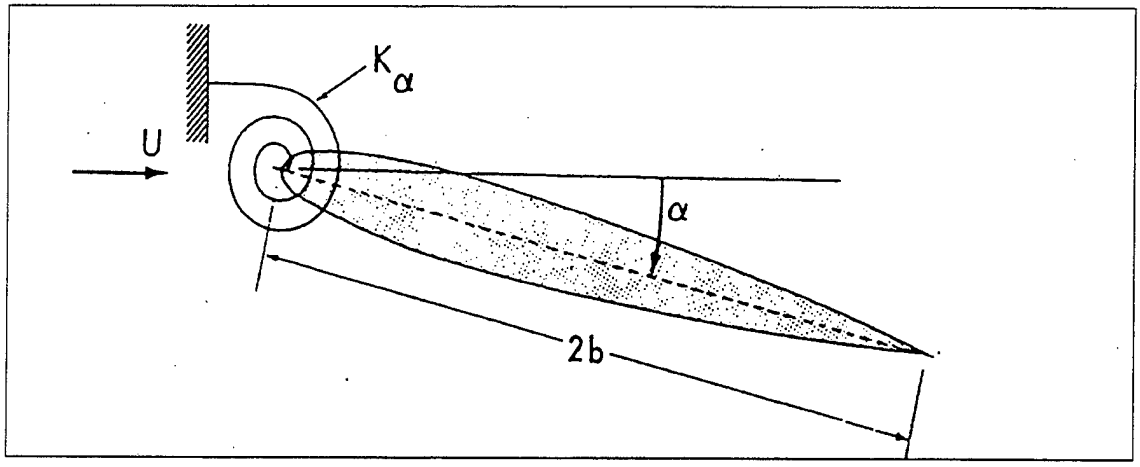

Figure 4-4 Rigid, symmetrical airfoil restrained to rotate about L.E

The equation of motion for this single-degree-of-freedom system is

$$I_\alpha \ddot{\alpha} + \alpha K_a = M_\alpha \tag{4.14}$$

where M_α is the aerodynamic moment due to $\alpha(t)$.

a. Time domain analysis

The equation of motion (4.14) can be non-dimensionalized using the following definitions:

Dimensionless aerodynamic moment coefficient

$$c_m = \frac{M_\alpha}{1/2\rho_\infty U_\infty^2 c^2} \tag{4.15}$$

Dimensionless moment of inertia

$$i_\alpha = \frac{I_\alpha}{\pi\rho_\infty c^4/4} \tag{4.16}$$

Dimensionless time

$$\tau = \frac{tU_\infty}{c} \tag{4.17}$$

Then (4.14) becomes:

$$i_\alpha \alpha'' + i_\alpha k_a^2 \alpha = \frac{2}{\pi} c_m$$

or

$$\alpha'' = -k_\alpha^2 \alpha + \frac{2}{i_\alpha \pi} c_m$$

where the primes refer to differentiation with respect to nondimensional time, τ, and k_α is given by Eq.(4.3). This second-order ordinary differential equation can be rewritten as a system of two first-order differential equations using $\alpha' = s$:

$$\alpha' = s \tag{4.18}$$

$$s' = -k_\alpha^2 \alpha. + \frac{2}{i_\alpha \pi} c_m \tag{4.19}$$

This is the system of equations used for the incompressible flutter analysis where c_m is computed at each time step using the panel code UPOT.

For the compressible flutter analysis the time can be non-dimensionalized using the free stream speed of sound, a_∞, instead of the freestream velocity U_∞. Thus the dimensionless time can be defined as

$$\tau = \frac{t a_\infty}{c} \tag{4.20}$$

Using this non-dimensional c_m, i_α and τ, the equation of motion (4.19) becomes:

$$s' = -k_\alpha^2 \alpha. + \frac{2}{i_\alpha \pi} M_\infty^2 c_m$$

The reduced natural frequency k_α for this case is based on the freestream speed of sound, whereas in the incompressible case it is based on the freestream velocity. In order to have compatibility between the values of k_α found for incompressible and compressible flow we have to convert the latter into the former values. The procedure will be shown in Section H.

Integration of Eq.(4.18) and (4.19) can be done with a first-order Euler scheme, a second order modified Euler scheme or a fourth order Runge-Kutta scheme.

The second-order modified Euler scheme is derived by applying the trapezoidal rule to integrate an equation $\dot{y} = f(x,t)$ as follows:

$$y_{n+1} = y_n + h/2[f(y_{n+1}, t_{n+1}) + f(y_n, t_n)]$$

and using an initial value for y(0).

The fourth-order Runge-Kutta scheme is derived by applying the following equation:

$$y_{n+1} = y_n + (1/6)[k_1 + 2k_2 + 2k_3 + k_4]$$

with

$$k_1 = hf(y_n, t_n) \qquad k_2 = hf(y_n + k_1/2, t_n + h/2)$$

$$k_3 = hf(y_n + k_2/2, t_n + h/2) \quad k_4 = hf(y_n + k_3, t_n + h)$$

Panel codes, like UPOT, typically use large time steps and therefore use of the fourth-order Runge-Kutta scheme is advisable. In contrast, the stability limits of Euler/N-S codes typically require small time steps and therefore the first-order Euler scheme gives satisfactory accuracy.

b. Frequency domain analysis

In order to perform the classical flutter analysis in the frequency domain we assume that the airfoil executes a torsional oscillation with a constant amplitude α_0.

The angle of attack α at any time can be described by

$$\alpha = \alpha_0 e^{i\omega t} \tag{4.21}$$

and after substituting (4.16) into (4.14), and dividing through by $\pi\rho b^4 \omega^2 \alpha_0 e^{i\omega t}$ we get

$$\frac{I_\alpha}{\pi\rho b^4}\left[1 - \left(\frac{\omega_\alpha}{\omega}\right)^2\right] + c_m = 0 \tag{4.22}$$

where ω_α is the undamped natural frequency of torsional vibration and c_m is the dimensionless aerodynamic coefficient which is a complex number.

Hence (4.18) can be split into real and imaginary parts

$$\mathrm{Re}\{c_m\} = \frac{I_\alpha}{\pi\rho b^4}\left[\left(\frac{\omega_\alpha}{\omega}\right)^2 - 1\right] \tag{4.23}$$

$$\mathrm{Im}\{c_m\} = 0 \tag{4.24}$$

Flutter occurs only at those values of the reduced frequency that make the out-of-phase component of the aerodynamic moment Eq.(4.24) vanish, provided that the corresponding in-phase part is of such magnitude that Eq.(4.23) yields a non-imaginary flutter frequency ω. The latter condition is met when the rotational axis is ahead of the

one quarter chord line. Hence by this method we can find the flutter airspeed and frequency.

The variation of the real and imaginary parts of the aerodynamic moment, based on Theodorsen's thin airfoil theory, for k defined as $\omega c/2U_\infty$, is shown in Figure 4-5. For the definition ok k according to Eq.(4.2), the imaginary moment becomes zero at a reduced frequency of k=0.076. This is consistent with the previous discussion which showed that torsional flutter occurs only at low reduced frequencies. For further details refer to [Ref. 6] pages 528-532.

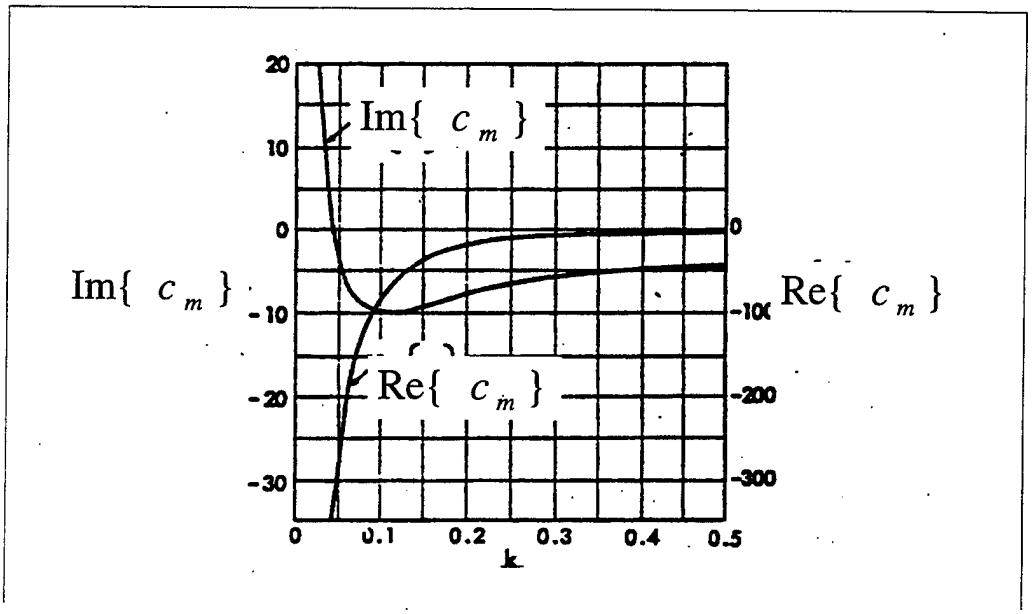

Figure 4-5 Variation with reduced frequency k of the real and imaginary parts of the dimensionless aerodynamic moment m_α due to pitching of an airfoil about its leading edge in incompressible flow (for k defined as $\omega c/2U_\infty$).

G. TWO DEGREE OF FREEDOM FLUTTER

1. Physical Explanation

For the two-degrees-of-freedom flutter we will consider two cases: a) the torsional deflection leads the bending deflection by 90 degrees as shown in Figure 4-6 whereas b) the torsional deflection and bending are in phase with each other as shown in Figure 4-8.

In both figures the solid arrows indicate the airfoil motion whereas the dotted arrows indicate the airfoil lift.

For simplicity we will assume purely steady state values for the lift corresponding to the instantaneous position of the airfoil.

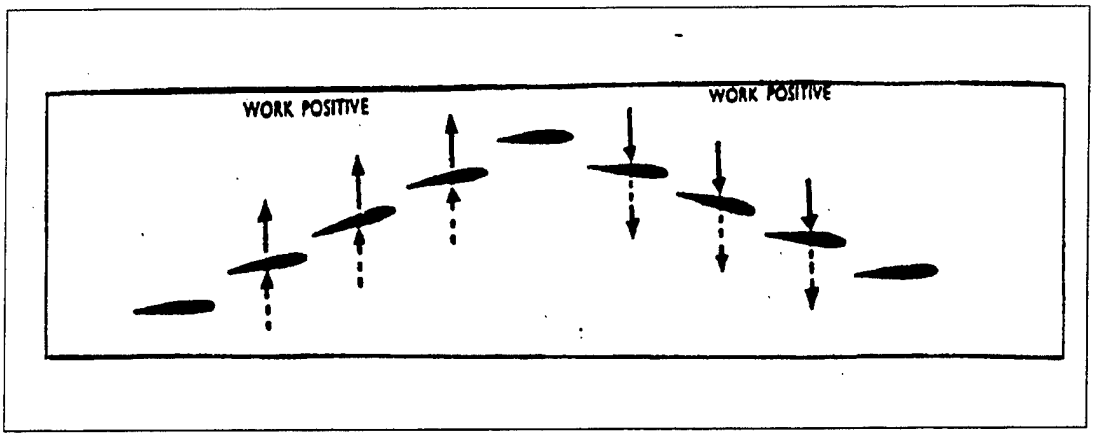

Figure 4-6 Two degrees of freedom airfoil motion – phase difference 90°

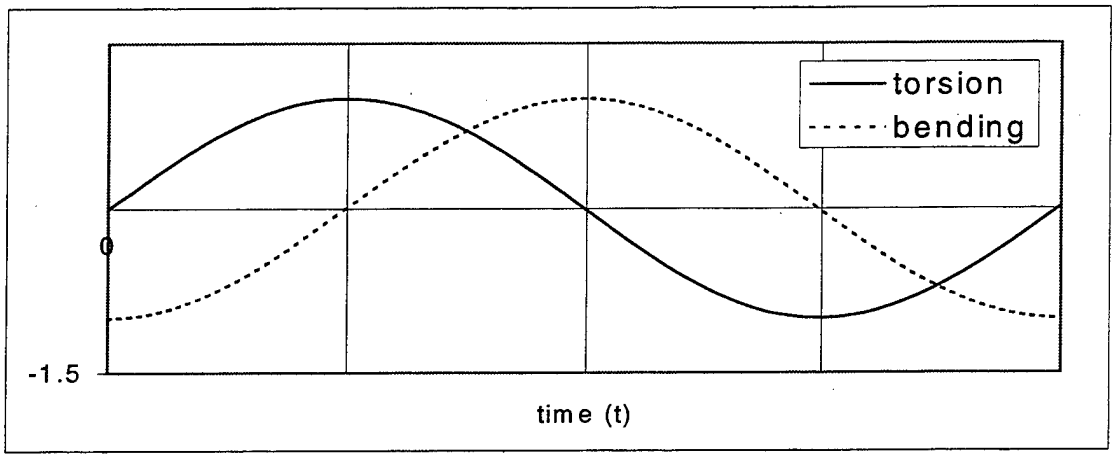

Figure 4-7 Torsion - Bending diagrams– phase difference 90°

From Figure 4-7 we can see that for the two first quarters of the cycle, both lift L and displacement dh are positive whereas for the two last quarters of the cycle, both lift L and displacement dh are negative. As a result over the whole cycle work is done on the airfoil.

When the torsional deflection is in phase with the bending deflection then from

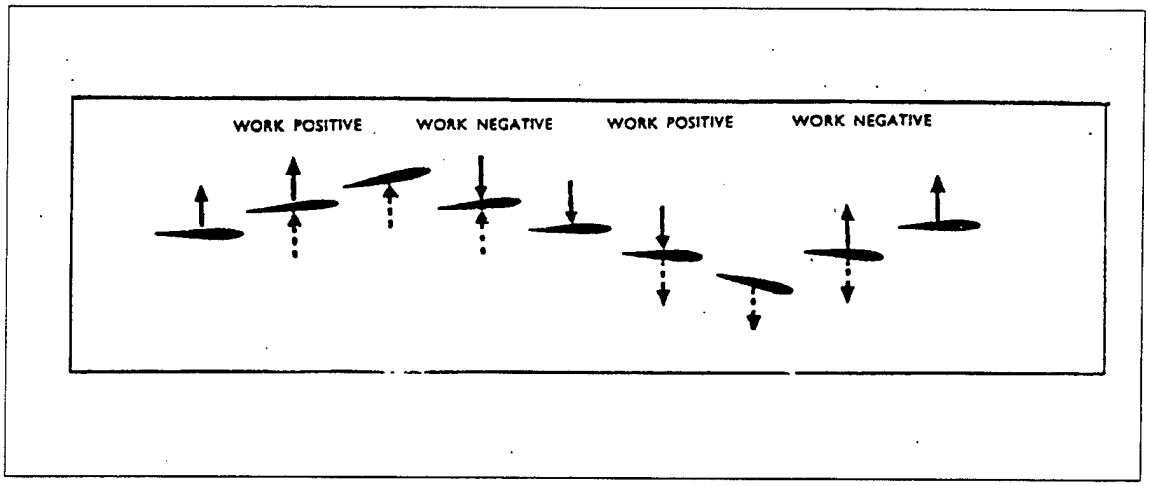

Figure 4-8 Two degrees of freedom airfoil motion – phase difference 0°

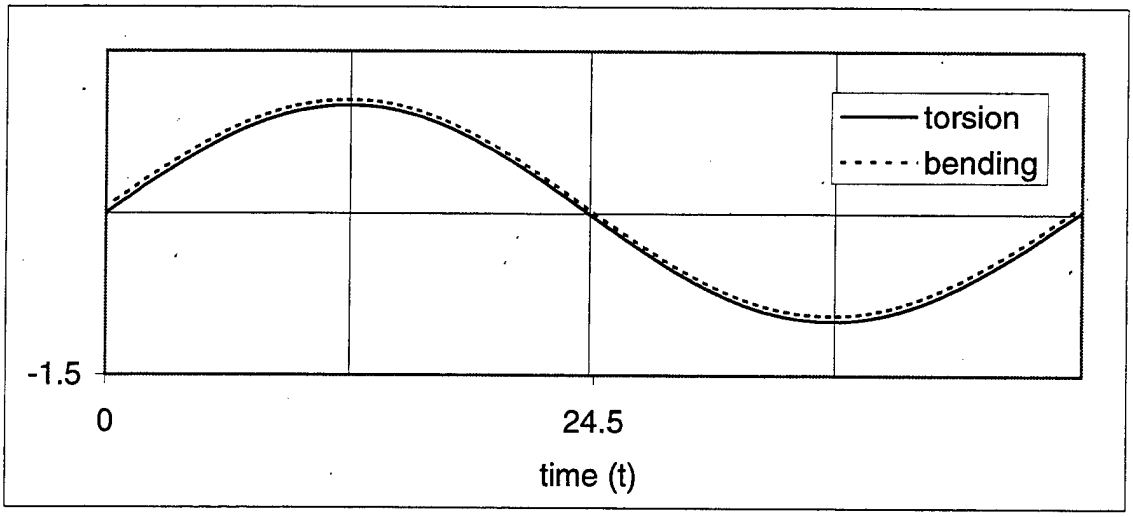

Figure 4-9 Torsion - Bending diagrams– phase difference 180°

Figure 4-9, we can see that for the first quarter of the cycle, the lift L and the displacement dh are positive so positive work is done on the airfoil. For the second quarter of the cycle, the lift L is positive whereas the displacement dh is negative so negative work is done on the airfoil. Similarly positive and negative work are done on the airfoil during the third and fourth quarter of the cycle. As a result zero work is done on the airfoil.

2. Equations of motion

The equations of motion for the two-degree-of-freedom system with no mechanical damping shown, for example, by Fung [Ref.1] pages 210-211, can be written as:

$$m\ddot{h} + S_\alpha \ddot{\alpha} + hK_h = -L \tag{4.25}$$

and

$$S_\alpha \ddot{h} + I_\alpha \ddot{\alpha} + \alpha K_a = M_\alpha \tag{4.26}$$

where S_α is the static moment about the elastic axis.

I_α is the airfoil moment of inertia

L is the airfoil aerodynamic lift

and M_α is the aerodynamic moment about the elastic axis

a. Time domain analysis

For the incompressible flow case the equations of motion (4.25) and (4.26) can be non-dimensionalized using the same non-dimensional coefficients that were used for the one degree of freedom case Eq.(4.15)-(4.17).

Then the system of equations (4.25) and (4.26) becomes:

$$mh'' + S_\alpha \alpha'' + mk_h^2 h = -2c_l / \pi$$

and $$S_\alpha h'' + i_\alpha \alpha'' + i_\alpha k_\alpha^2 = 2c_m / \pi$$

where the primes refer to differentiation with respect to nondimensional time τ.

In a matrix form the above system of equations becomes:

$$[M]\{X\}'' + [k]\{X\} = \{F\} \tag{4.27}$$

with $$[M] = \begin{bmatrix} m & S_\alpha \\ S_\alpha & i_a \end{bmatrix} \qquad [k] = \begin{bmatrix} mk_h^2 & 0 \\ 0 & i_a k_a^2 \end{bmatrix}$$

$$\{X\} = \begin{Bmatrix} h \\ \alpha \end{Bmatrix} \qquad \{F\} = \frac{2}{\pi} \begin{Bmatrix} -c_l \\ c_m \end{Bmatrix}$$

For the compressible flow case (N-S Code) the equations of motion (4.25) and (4.26) can be non-dimensionalized using the free-stream speed of sound, a_∞, instead of the free-stream velocity U_∞ such that the dimensionless time can be defined from Eq.(4.20).

Then the system of equations have the same form as Eq.(4.27) with the difference that the vector $\{F\}$ now is defined as

$$\{F\} = \frac{2}{\pi} M_\infty^2 \begin{Bmatrix} -c_l \\ c_m \end{Bmatrix}$$

Eq.(4.34) can be rewritten as:

$$\{X\}'' = [M]^{-1}\{F\} - [M]^{-1}[k]\{X\} \tag{4.28}$$

Defining $\{X\}' = \{Y\}$, we can solve Eq.(4.28) as a system of two first-order differential equations

$$\{X\}' = \{Y\}$$

$$\{Y\}' = [M]^{-1}\{F\} - [M]^{-1}[k]\{X\}$$

As we mentioned for the one degree of freedom case, the integration of this system of equations is done with the fourth-order Runge-Kutta scheme in the panel code, and with a first-order Euler scheme in the Euler/N-S codes.

b. Frequency domain analysis

Assuming constant amplitude time harmonic oscillation including plunge and torsion

$$h = h_0 e^{i\omega t}$$
$$\alpha = \alpha_0 e^{i\omega t}$$

the equations of motion become:

$$e^{i\omega t}\left[-\omega^2 M h_0 - \omega^2 \alpha_0 S_\alpha + h_0 K_h\right] = L \qquad (4.29)$$

$$e^{i\omega t}\left[-\omega^2 I_\alpha{}^2 \alpha_0 - \omega^2 h_0 S_\alpha + \alpha_0 K_\alpha\right] = M_\alpha \qquad (4.30)$$

The aerodynamic lift L and moment M_α are assumed to be linear functions of h_0 and α_0 so Eqs. (4.30) and (4.31) constitute a system of homogeneous equations. Therefore the determinant of these equations must be set to zero in order to obtain a solution. As discussed in [Ref. 1 and 6] the solution of the flutter determinant normally requires an iterative procedure. For further details refer to these text books.

H. NS – UPOT REDUCED FREQUENCY COMPATIBILITY

As mentioned before, the reduced frequencies calculated with the Euler and N.S codes need to be redefined in order to be compatible with the conventional definition of k. This is done as follows:

The non-dimensional time used in UPOT is defined as

$$\tau_{UPOT} = \frac{tU_\infty}{c} \tag{4.31}$$

whereas in the N.S code it is defined as

$$\tau_{NS} = \frac{ta_\infty}{c} \tag{4.32}$$

In order to have comparable results from the compressible and incompressible flow solutions we have to adjust the reduced frequency values of the NS code to those of the UPOT code. From the definition of the reduced frequency:

$$k = \frac{\omega c}{U_\infty} \tag{4.33}$$

we get

$$k = \frac{2\pi}{T}\frac{c}{U_\infty} \tag{4.34}$$

where T is the period of airfoil oscillation.

For the results computed with the UPOT code and because of (4.1) we have

$$k = \frac{2\pi}{\frac{T_{UPOT}c}{U_\infty}}\frac{c}{U_\infty} = \frac{2\pi}{T_{UPOT}} \tag{4.35}$$

Similarly for the NS results from (4.4) and because of (4.2) we get

$$k = \frac{2\pi}{\frac{T_{NS}c}{a_\infty}}\frac{c}{U_\infty} = \frac{2\pi}{\frac{T_{NS}c}{a_\infty}}\frac{c}{M_\infty a_\infty} = \frac{2\pi}{T_{NS}}\frac{1}{M_\infty} \tag{4.36}$$

The last equation shows that we have to divide the reduced frequencies that come from the NS code ($2\pi / T_{NS}$) with the Mach number (M_∞) in each case in order to find the reduced frequency which is compatible with the UPOT results.

I. FLUTTER PREDICTION WITH UPOT CODE

One practical way to find the flutter condition for a given airfoil with the UPOT code is to see the resulting diagram of the moment coefficient with respect to AOA. The work is proportional to the integrated area in the loop. Positive area means that work goes into the flow. Negative area means that work goes into the airfoil. Zero area means that the airfoil flutters. Running the code for low values of reduced frequency it is seen that the aerodynamic moment coefficient forms a clockwise elliptic path as the AOA changes during the airfoil oscillation (Figure 4-10), so net positive work is done on the airfoil.

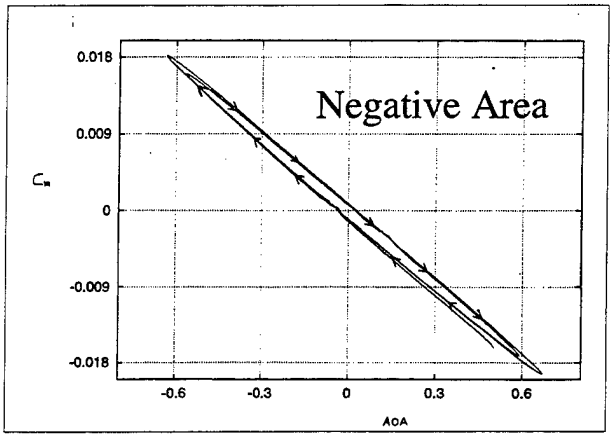

Figure 4-10 Aerodynamic moment coefficient graph for low k values

For high values of reduced frequency the path has a counterclockwise direction as shown in Figure 4-11 and the work is negative.

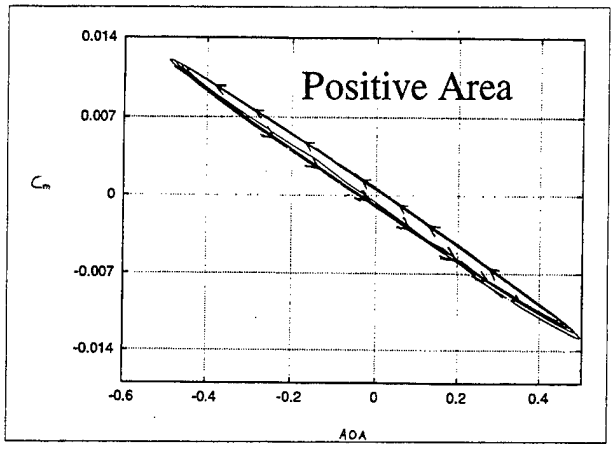

Figure 4-11 Aerodynamic moment coefficient graph for high k values

At last, when the critical value of reduced frequency is used the path becomes a straight line as shown in Figure 4-12, so no work is done on the airfoil.

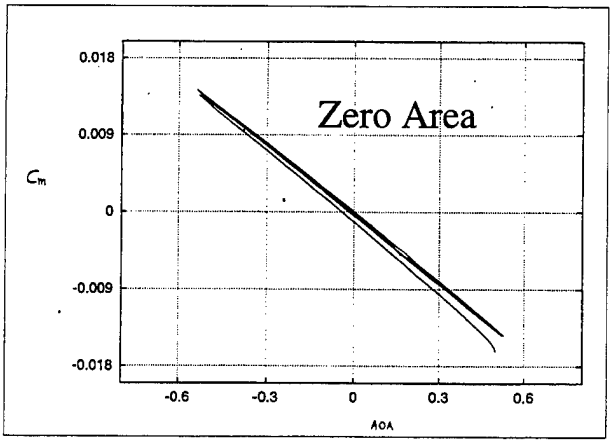

Figure 4-12 Aerodynamic moment coefficient graph for the critical flutter k value

V. RESULTS

A. GENERAL

All the results presented in this thesis were obtained with the time domain method described in Chapter IV, and the flow field solutions at each time step were computed based on the Navier-Stokes, Euler or unsteady potential flow (UPOT) solution, described in Chapter III.

The reduced frequency values used in the Navier-Stokes and Euler codes were redefined in order to be compatible with the UPOT definition. The grid generation for the airfoils and the input data for the Navier - Stokes code are presented in Sections B and C. The procedure for extracting the results is described briefly in Section D. Then the calculation for the non-viscous (Euler) case is presented in Section E. The calculation for a wide range of pivot points is shown in Section F. The effect of Mach number and airfoil thickness on torsional flutter is presented in Sections G and H. The influence of the viscous effects and a comparison between viscous and non-viscous flow are shown in Sections I and J. In Section K a comparison between UPOT and NS results for low subsonic Mach numbers (M=0.1-0.3) is presented.

B. GRID GENERATION

Airfoil grids for NACA 0006, 0009, 0012 and 0015 were computed with ALGEM. In Figure 5-1 the NACA 0015 grid for the Euler calculations is presented whereas in Figure 5-2 the grid details close to the airfoil are shown. This NACA 0015 coarse grid size is 201X41 points.

For viscous flow different grids were used because of the necessity to resolve the flow close to the airfoil. The grid size is 201X61 points.

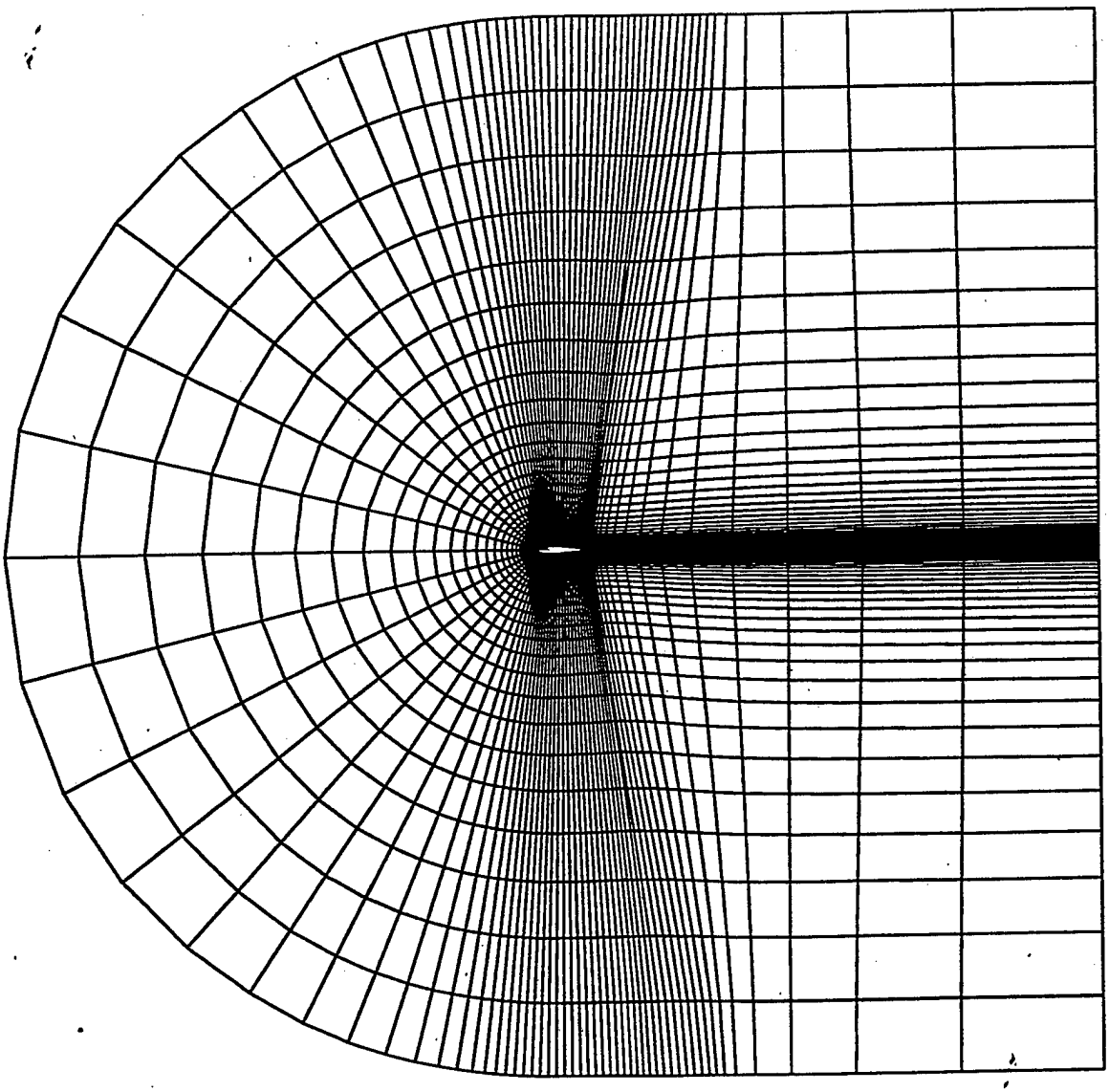

Figure 5-1 C-grid for NACA 0015 (non-viscous flow – every other grid line shown)

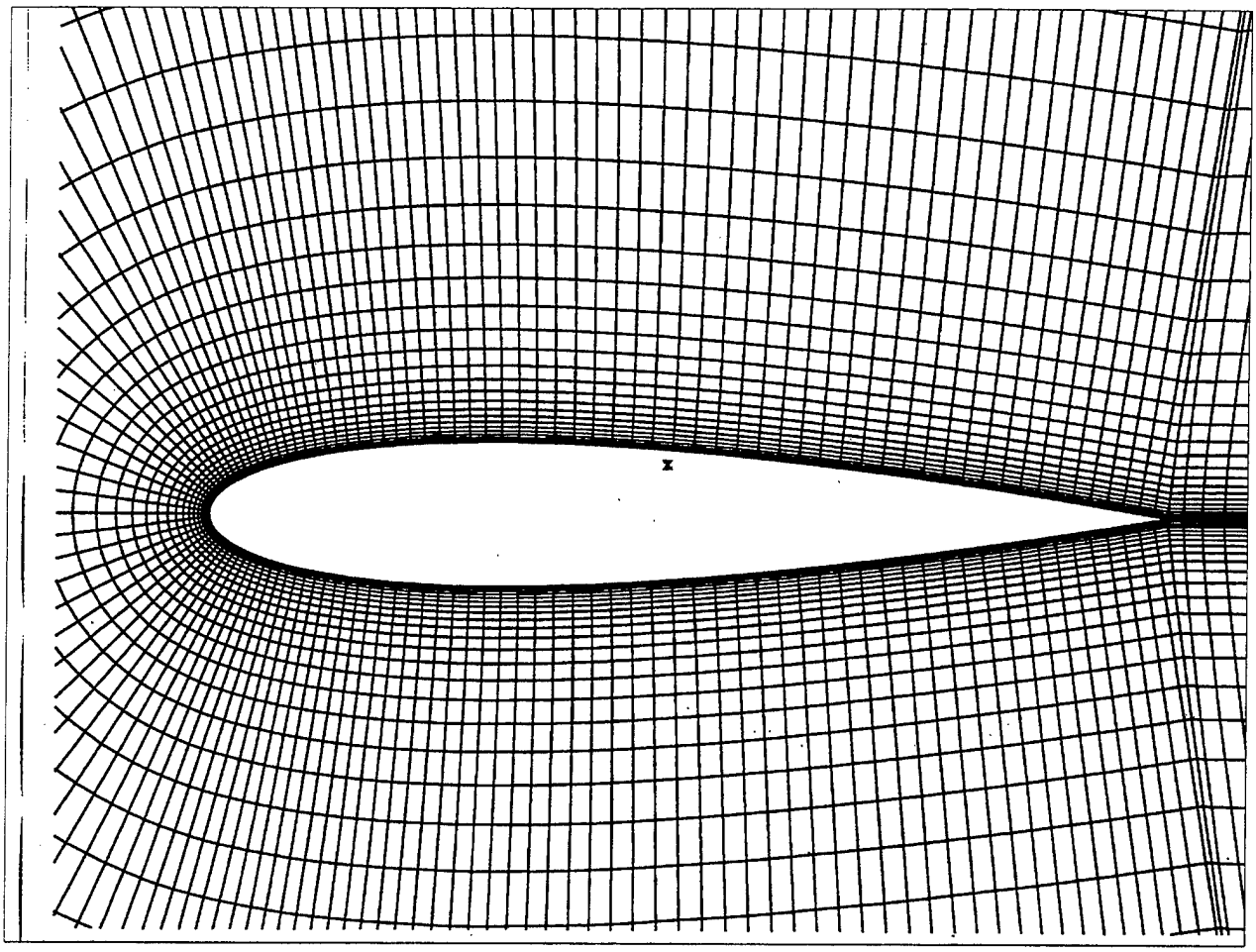

Figure 5-2 NACA 0015 C-grid details (non-viscous flow)

C. INPUT DATA DESCRIPTION

The input data file includes many variables, some of which have to be changed during the calculation procedure. A typical input file for the initial calculation of the steady solution for the non-viscous flow is presented next. The use of the input file variables is also explained in this section.

INPUT FILE :

```
# IREAD   ITER    NPRINT  NLOAD   ODVAR
     0    10000      1       1       1.00
# ALPHA   OSCIL   RAMP    REDFRE  ALFAMND ALFAMXD
    0.5     false   false    0.100    -.500     0.500
# PLUNGE  PLMX    PLMY    PLPHSXD PLFREQ
   false      0.      0.10    0.        0.1
# MACH    RE      VISC    TURBL
  0.700     0.     false   false
# TIMEAC  COUR    NEWTIT
   false    30.00     1
# free   mass   ialpha  ka    kh    xp    xa
  false  0.0    100.0  0.200 0.0   0.0   0.0
# aneut  hneut  h0
  0.0    0.0    0.0
```

INPUT VARIABLES EXPLANATION:

IREAD	0	No initial solution, free stream conditions initialize the flowfield in the startup steady-state computations
	1	Initial solution is read from a binary file saved from the previous run (default, at the end of each run, solution file is saved as binary)
	2	Initial solution is read as formatted (plot3d form)
	-1	Initial solution is read as binary, unsteady motion starts
	-2	Initial solution is read as formatted (plot3d form), unsteady motion starts
ITER		# of timesteps
NPRINT		Residuals are printed out at every nprint timesteps
NLOAD		Aerodynamic loads are printed out in ns.out and written into lo.d file at every nload timesteps
ODVAR		Solution variables, q array, are written into "qp.d" file at every delta odvar change in unsteady motions (degrees in oscillatory motion, amplitude change in plunge)
ALPHA		Steady state AOA (do not set it to zero, instead set it to 0.0001)

OSCIL	false N/A true sinusoidal oscillations in pitch
RAMP	false N/A true straight ramp motion in pitch
REDFRE	Reduced frequency of the unsteady pitching motion, based on the half chord, chord length is assumed to be 1.
ALFAMND	Min AOA of the pitching motion
ALFAMXD	Max AOA of the pitching motion
PLUNGE	false N/A true plunging motion
PLMX	Plunge amplitude in x
PLMY	Plunge amplitude in y
PLPHSXD	The phase angle between x and y amplitudes, in degrees
PLFREQ	The reduced frequency of the plunging motion, based on the half chord, chord length is assumed to be 1.
REYNOLD	Reynolds number of the freestream flowfield
MACH	Mach number of the freestream flowfield
VISC	false Euler solution true Viscous Navier-Stokes solution
TURBL	false Laminar flow is assumed true Baldwin-Lomax turbulence model is applied
TIMEACC	false Variable local time stepping in the computational grid, used in the computations of steady state and/or attached flowfields. true Constant time stepping everywhere in the computational grid, used in the computations of unsteady and separated flowfields
COUR	Courant number of the timestepping (50-1500), determines the time step of the computations based on the minimum grid size and the freestream conditions. Its value depends on the computational grid. For diverging computations, its value needs to be reduced.

If the residuals in the output file increases in time, it is the sign that Courant number is to be reduced.

NEWTIT Number of Newton subiterations in each timestep, applied in unsteady flows (2-3), for steady flowfields it is set to 1.

D. CALCULATION PROCEDURE

For every flutter calculation initially the steady solution had to be found. For the non-viscous cases the code was run for 6000 iterations (1000 with COUR Number of 1, 1000 with COUR Number of 2, 2000 with COUR Number of 4 and 1000 with COUR Number of 8). For the viscous case and due to the increased number of nodes of the grid the calculation needed over 12000 iterations in order to converge to a steady solution. The steady solution was assumed to be satisfactory when the step variation of Cl coefficient was found to be less than 10^{-5} or when the five first digits of Cl remained constant.

After the steady solution was found the oscillating airfoil calculation started. From Chapter III Section G we saw that for pivot points behind the quarter chord point (0.25c) a statically stable solution is always obtained. Therefore the calculations were performed for pivot points ahead of the quarter chord point. The pivot points that were chosen for the flutter calculations were: 0.15·c, 0, -0.25·c, -0.50·c, -0.75·c and -0.85·c. For every case an initial value of the uncoupled reduced natural pitching frequency k_α (Eq. 4.3) was assumed (which corresponds in Eq.(4.4) to an airfoil spring constant K_α) and the time variation of the airfoil angle of attack (AOA) was computed. If the AOA was found to decrease, the assumed value of k_α was adjusted until the motion started to diverge. For every computation the slope of the AOA amplitude was determined and an interpolation procedure was implemented in order to find the value of k_α which gives the critical flutter condition. After the critical condition was found the reduced frequency of oscillation was calculated.

E. NON – VISCOUS (EULER) CALCULATION

The whole procedure described above will be shown for the non-viscous flow over an oscillating airfoil NACA 0015 at M=0.7. The elastic axis of oscillation is the L.E of the airfoil (pivot point Xp=0). An initial AOA disturbance of 0.5° will be imposed on the airfoil in order to start the motion.

The input file for the steady solution is as follows (4th run for COUR Number :8):

```
# IREAD   ITER   NPRINT  NLOAD   ODVAR
   1    2000    1       1       1.00
# ALPHA   OSCIL   RAMP    REDFRE  ALFAMND ALFAMXD
   0.5    false   false   0.100   -.500   0.500
# PLUNGE  PLMX    PLMY    PLPHSXD PLFREQ
  false   0.      0.10    0.      0.1     0.0     0.0
# MACH    RE      VISC    TURBL
  0.700   0.      false   false
# TIMEAC  COUR    NEWTIT
  false   8.00    1
# free    mass    ialpha  ka      kh      xp      xa
  false   0.0     100.0   0.00000 0.0     0.0     0.0
# aneut   hneut   h0
  0.0     0.0     0.0
```

The steady solution is presented in Figure 5-3. It is seen that Cl reaches a steady value of 0.1017 after τ =5 sec.

The final result for the steady solution is presented in Table 5-1.

τ	AOA	Cl	Cd	Cm
32.3321342	0.5	0.1017382	0.0040226	-0.0257816

Table 5-1 Steady state solution for NACA 0015 M=0.7 (Euler case)

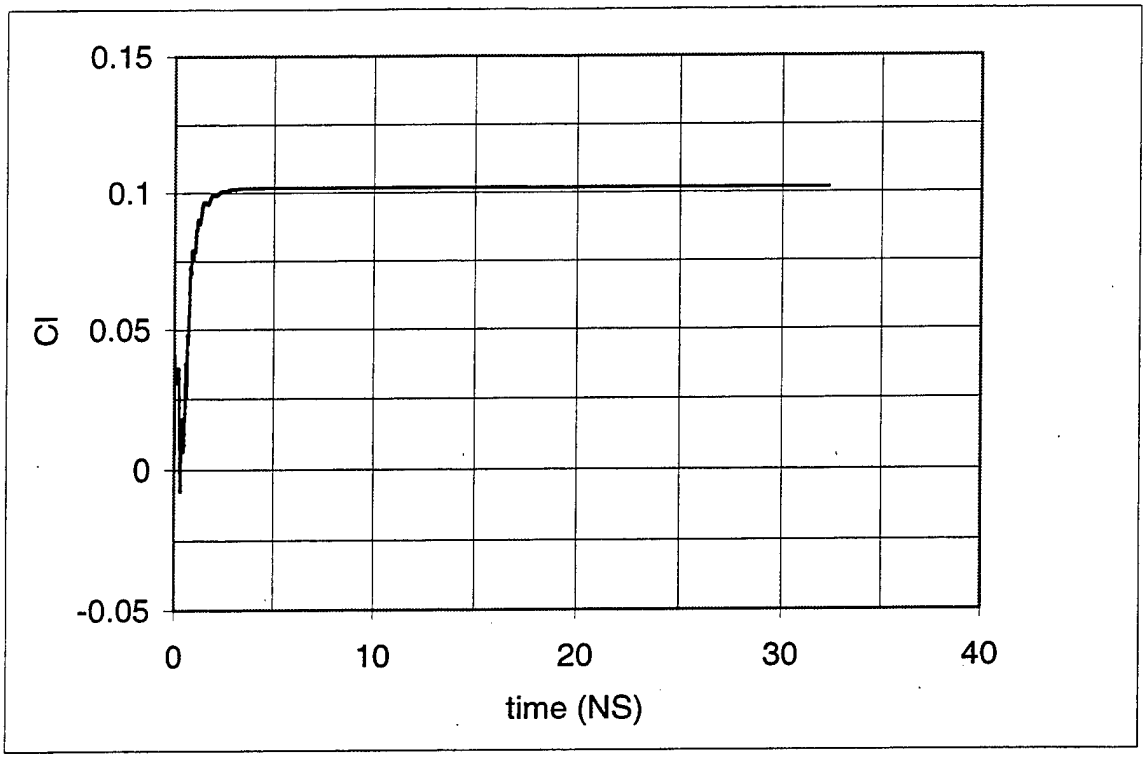

Figure 5-3 Steady state solution for NACA 0015 M=0.7 (Euler case)

After the steady solution is calculated, the critical value of the reduced natural pitching frequency k_α for flutter is found, by first assuming an initial value of 0.36, as shown in the input file

```
#   IREAD    ITER     NPRINT   NLOAD    ODVAR
      -1     10000      1        1       1.00
#   ALPHA    OSCIL    RAMP     REDFRE   ALFAMND  ALFAMXD
     0.5     false    false    0.100    -.500    0.500
#   PLUNGE   PLMX     PLMY     PLPHSXD  PLFREQ
    false    0.       0.10     0.       0.1       0.0      0.0
#   MACH     RE       VISC     TURBL
    0.700    0.       false    false
#   TIMEAC   COUR     NEWTIT
    true    15.00      3
```

```
#   free     mass     ialpha   ka         kh       xp       xa
    true     0.0      100.0    0.360000   0.0      0.0      0.0
#   aneut    hneut    h0
    0.0      0.0      0.0
```

As one can see, seven variables changed values comparing with the steady case input file: the *IREAD* was turned to –1, the number of iterations to 10000, the *TIMEAC* to true, the *COUR* number to 15.0 , the *NEWTIT* to 3 and the *free* to true. Also *ialpha* (non–dimensional moment of inertia) was chosen to be 100 and the *ka* to be 0.36.
The plot of the resulting airfoil motion is presented in Figure 5-4 .

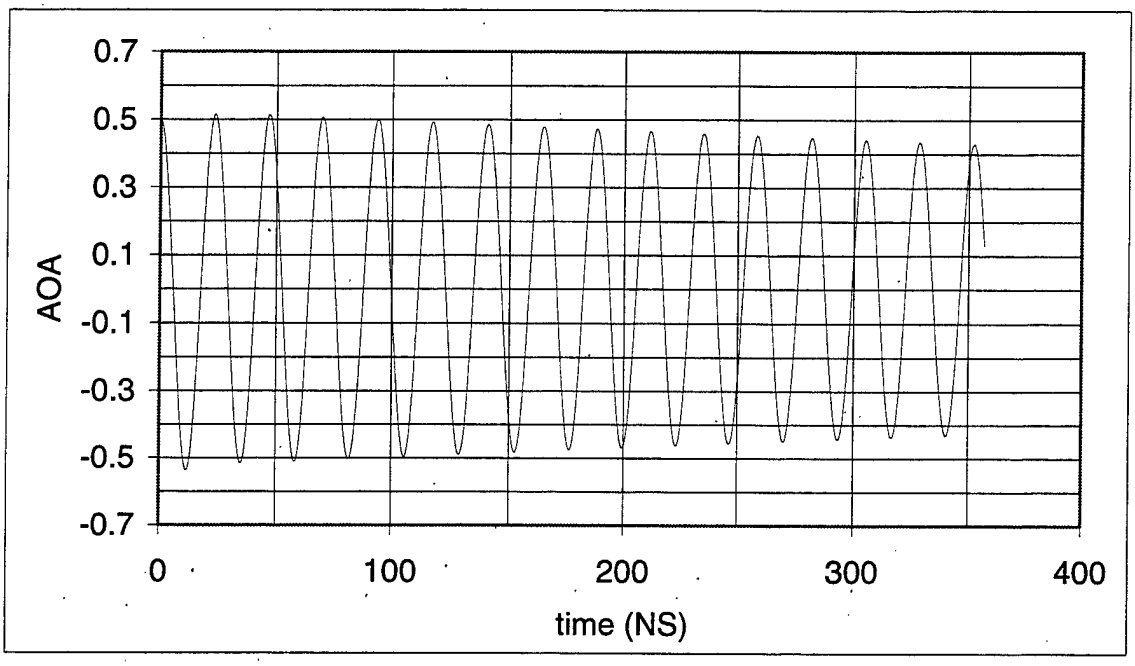

Figure 5-4 Unsteady case solution - K_α=0.36 (Euler case)

From the plot we can see that the airfoil motion decays with time so the assumed value of k_α was too high. In order to determine the critical k_α value the maximum AOA values of the graph are input into a regression equation to find the slope of the maximum AOA values, namely -2.860E-04 (Figure 5-5):

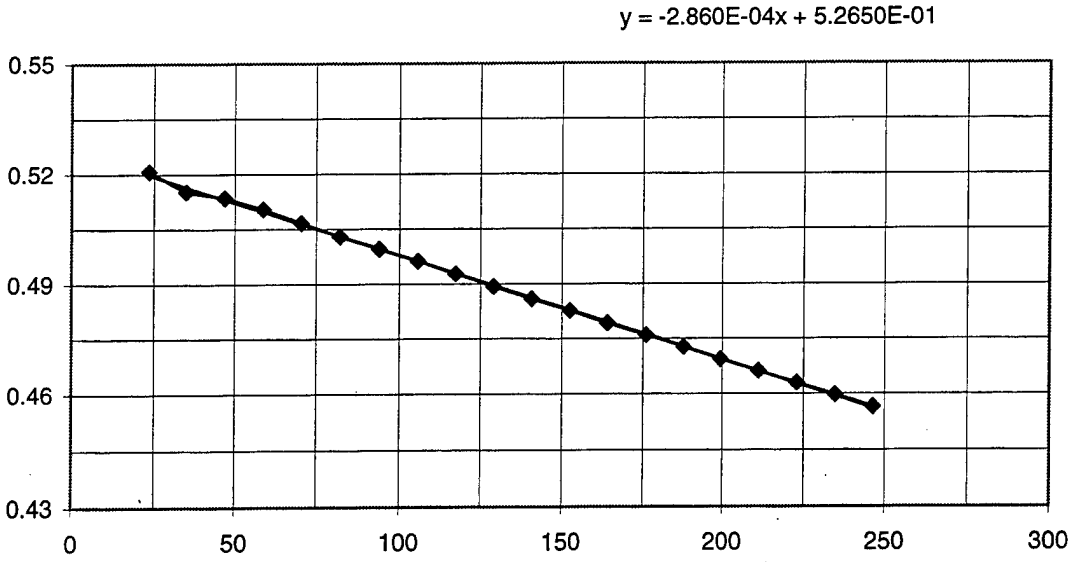

Figure 5-5 Time rate of change of AOA amplitude of airfoil motion K_α=0.36 (Euler case)

Repeating this process for k_α of 0.25 we get the AOA history presented in Figure 5-6:

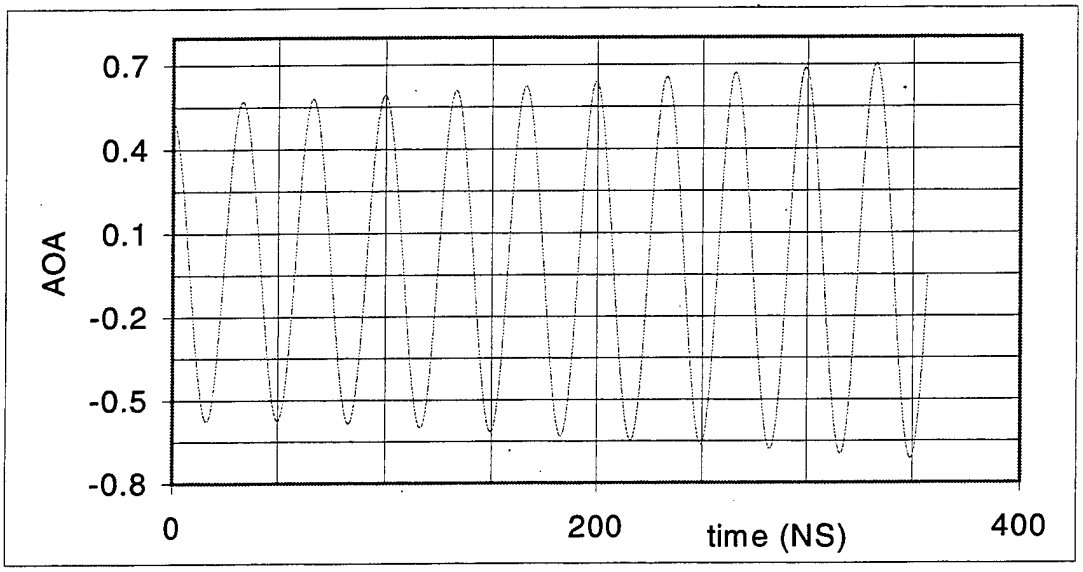

Figure 5-6 Unsteady case solution - K_α=0.25 (Euler case)

From this plot we observe that the airfoil motion diverges. Therefore the assumed value of k_α is too low. Then applying again a regression equation for the maximum AOA values of the graph yields a slope of 4.566E-04 (Figure 5-7):

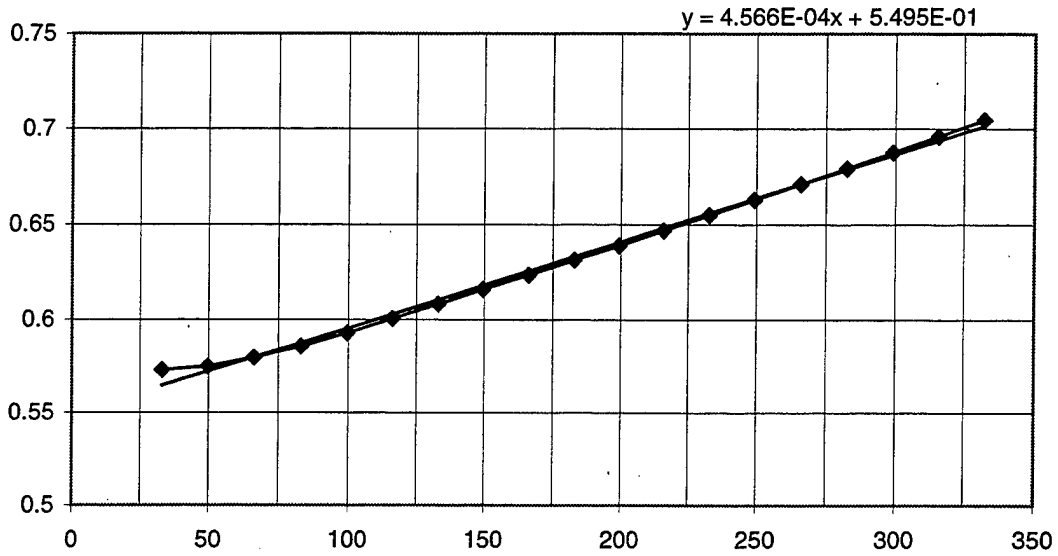

Figure 5-7 Time rate of change of AOA amplitude of airfoil motion K_α=0.25 (Euler case)

Now we can interpolate the values of the slope found for the two assumed values of the reduced natural pitching frequency k_α. In order to have more accurate results we can follow the same procedure for another value of k_α (here assumed 0.30). Finally we get the results shown in Table 5-2.

Ka	Slope
0.36	-2.860E-04
0.30	1.669E-04
0.25	4.5664E-04

Table 5-2 Regression equation slope values for various k_α values

Making a curvefit in EXCEL for the above results (Figure 5-8) we can find that the value of the k_α for which the slope of the extreme points is zero, is k_α=0.324.

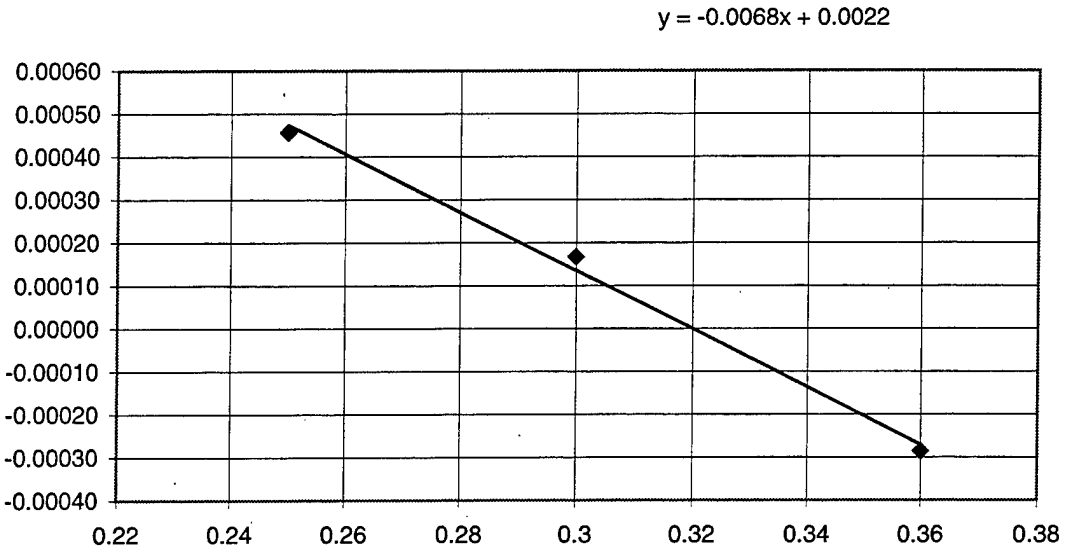

Figure 5-8 Curvefit of K_α vs time rate of change of AOA amplitude (Euler case)

To verify whether this k_α value is indeed the critical reduced natural pitching frequency, the code was run for k_α =0.324 which yielded the airfoil motion presented in Figure 5-9:

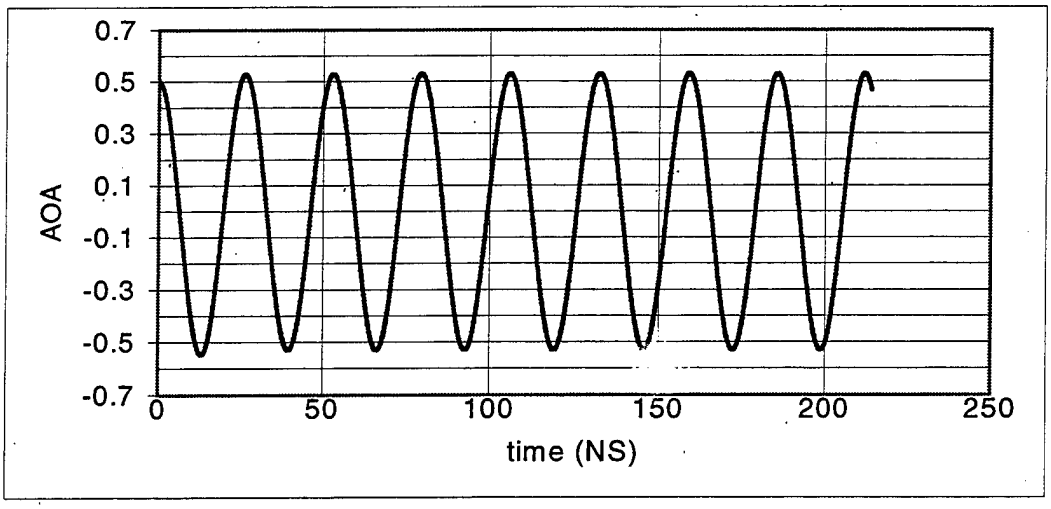

Figure 5-9 Unsteady case solution - Ka=0.324 Critical flutter case (Euler)

Omitting the first peaks, which are caused by the starting transient, and applying again a regression equation for the maximum points, we find that the slope is $6.638591 \cdot 10^{-7}$, which is very close to zero (Figure 5-10). Therefore the reduced natural pitching frequency k_α of 0.324 is accepted as the critical value. If this value didn't give the flutter condition (slope not close to zero), the new slope value would be interpolated again until finding the k_α for zero slope.

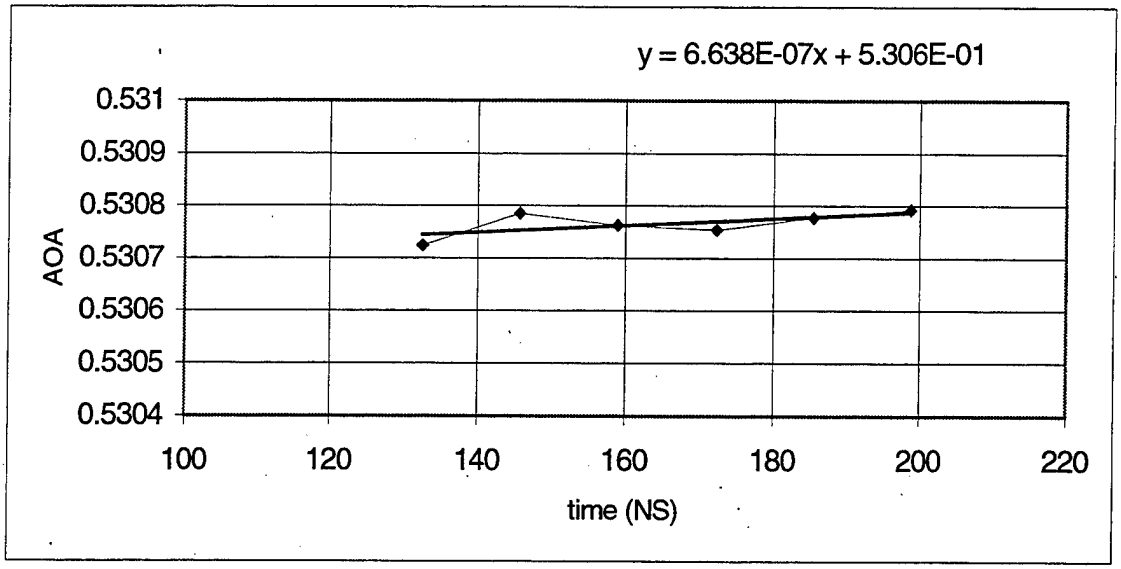

Figure 5-10 Time rate of change of AOA amplitude of airfoil motion K_α=0.324 Critical flutter (Euler case)

The reduced frequency of oscillation is found using (4.36)

$$k = \frac{2\pi}{T_{NS}} \frac{1}{M_\infty}$$

In order to find the period of oscillation the initial transient exhibiting variable peaks are ignored, and the average period between the minimum and maximun peaks is computed as shown in Table 5-3.

Min peaks	T (NS)	Max peaks	T (NS)
92.6997		105.954	
119.209	26.5092	132.465	26.51039
145.721	26.51206	158.977	26.51233
	Average T (NS) =	26.511	

Table 5-3 Average period T calculation for NACA 0015 flutter - Ka=0.324

The average period of oscillation (non-dimensionalized) is 26.511. Then applying Eq.(4.36) for Mach number of 0.7 we find that the reduced frequency of oscillation is 0.339.

The pressure distribution around the airfoil for a whole cycle of oscillation at 30° increments is shown in Figure 5-11.

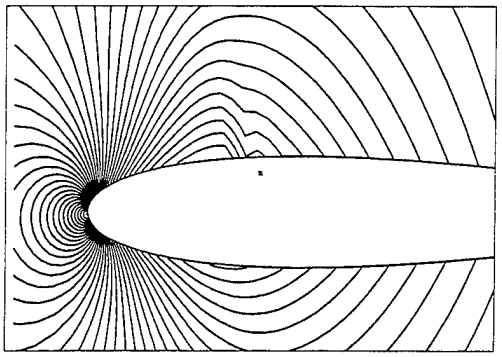

AOA=30°

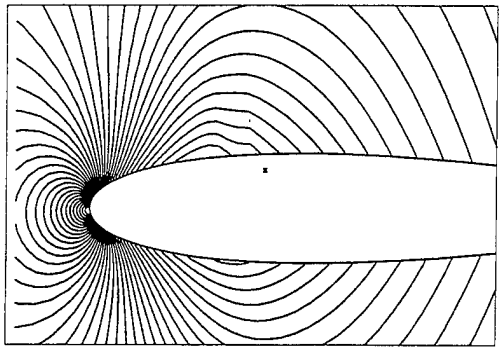

AOA=60°

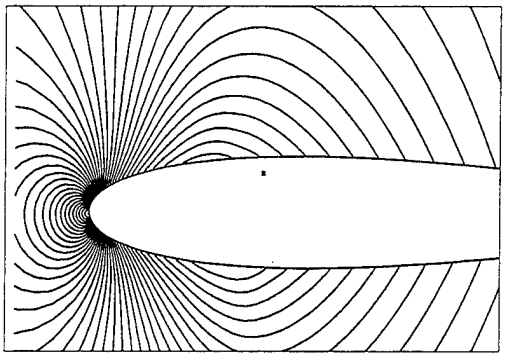

AOA=90°

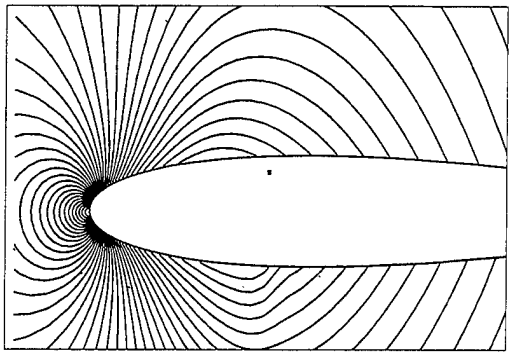

AOA=120°

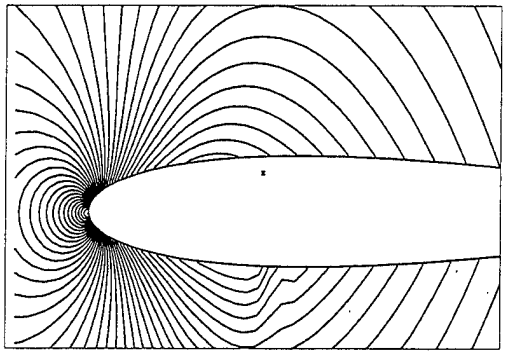

AOA=150°

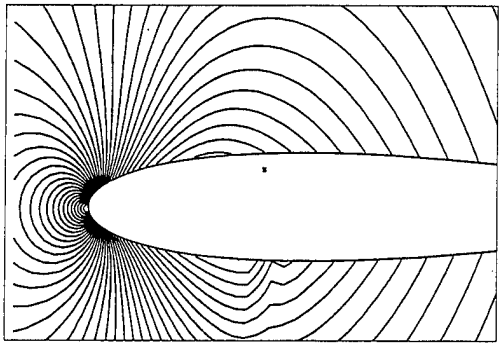

AOA=180°

Figure 5-11 Pressure Contours around NACA 0015 for a whole cycle of oscillation M=0.7 Xp=0.0

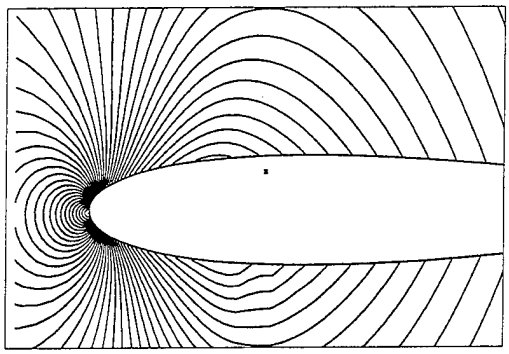

AOA=210°

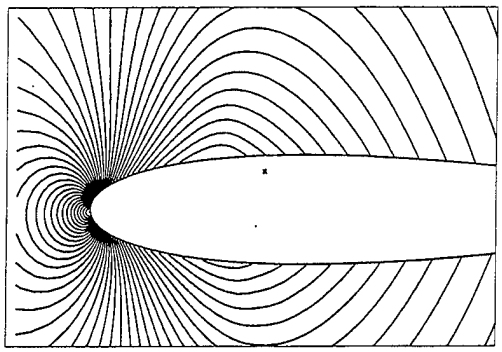

AOA=240°

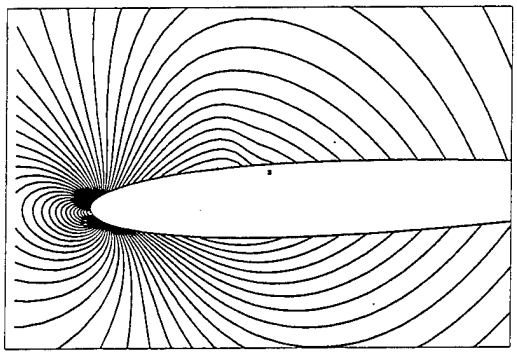

AOA=270°

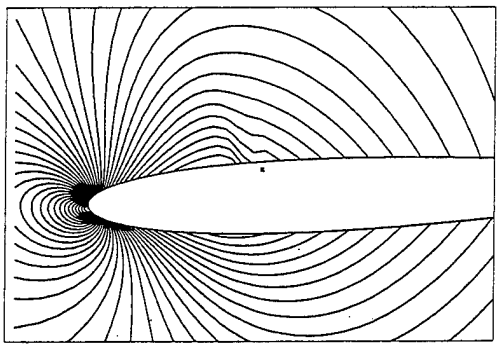

AOA=300°

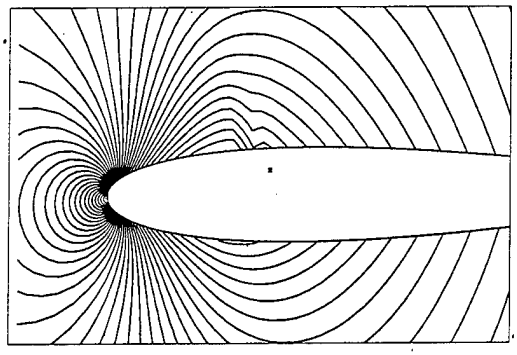

AOA=330°

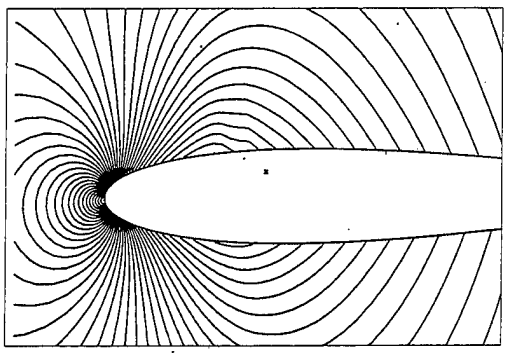

AOA=360°

Fig.5-11 Pressure Contours around NACA 0015 for a whole cycle of oscillation M=0.7 Xp=0.0 (cont.)

F. EFFECT OF PIVOT POINT ON TORSIONAL FLUTTER

The previously described procedure was applied to obtain the effect of pivot location, Mach number and airfoil thickness on single degree of freedom torsional flutter. Figure 5-12 shows the variation of the flutter reduced frequency with pivot point for the NACA 0015 airfoil at M=0.7.

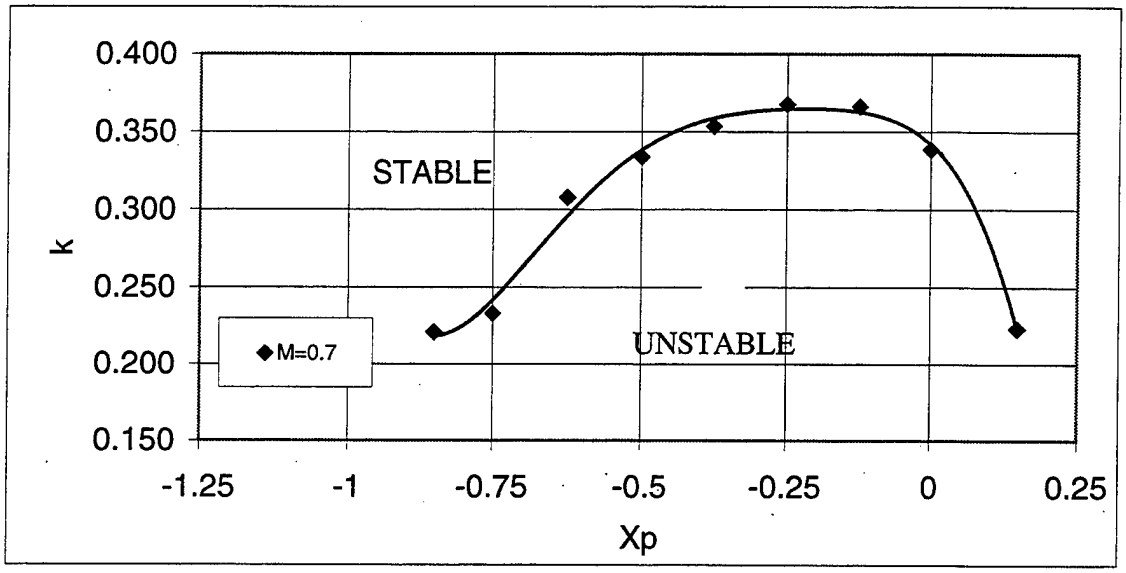

Figure 5-12 Effect of Pivot Point on reduced frequency for NACA 0015 and M=0.7 (Euler case)

The area below the curve is an unstable region for the airfoil; that is if the frequency of oscillation is lower than the value corresponding to the curve for a certain pivot point, then flutter is triggered by an initial disturbance of 0.5 degrees. In contrast the area above the curve is the stable region and every oscillation will die out.

It is readily seen that the most flutter prone range of pivot points is between 0 and -0.50·c. The pivot point most likely to induce flutter is Xp=-0.25·c, i.e when the pivot point of oscillation is one quarter chord ahead of the L.E.

The above information can be shown in terms of the reduced natural pitching frequency k_α required to avoid flutter. It should be noted that for elastic axis locations of -0.85<Xp<0.15 the used value of moment of inertia i_α was 100. For Xp=0.15 and –0.85

the solutions were always decaying with this value of i_α so an increased value of 300 was used.The resulting graph is shown in Figure 5-13:

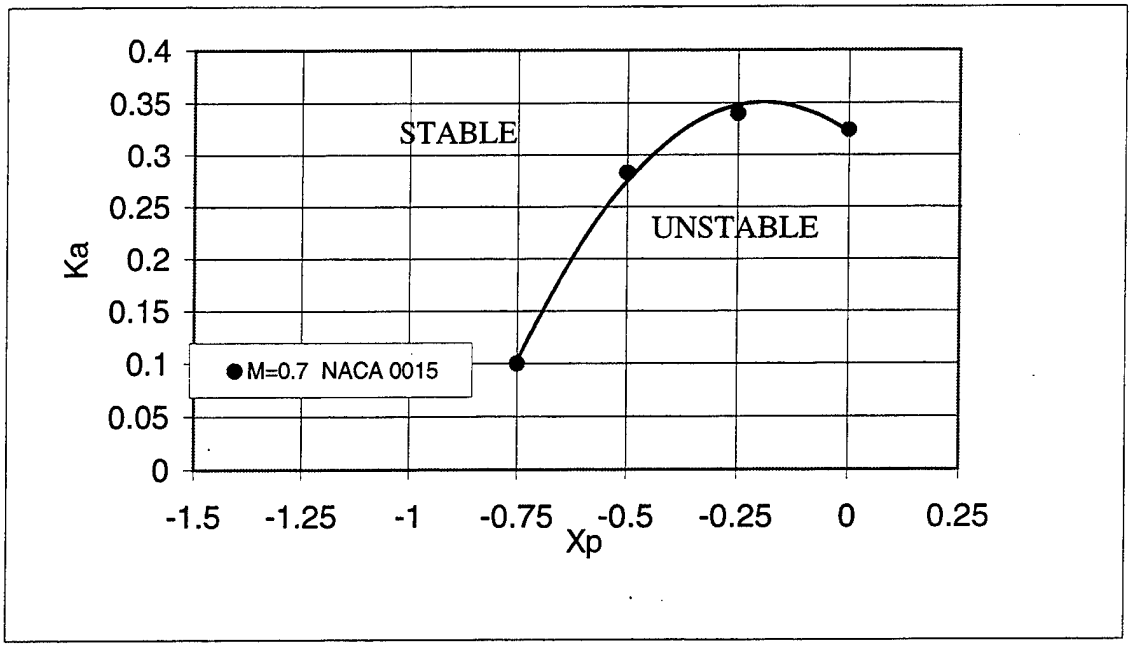

Figure 5-13 Effect of Pivot Point on critical k_α for NACA 0015, M=0.7 and i_α=100 (Euler case)

Again, the area below the curve is an unstable region for the airfoil; if the airfoil spring constant K_α is lower than the value that corresponds to the curve for a certain pivot point (low torsional stiffness), then flutter is induced by an initial disturbance of 0.5 rees.

G. EFFECT OF MACH NUMBER ON TORSIONAL FLUTTER

Figure 5-14 expands the information presented in Figure 5-12 by displaying the effect of Mach number on torsional flutter.

An increase in Mach number significantly increases the region of instability for the whole range of pivot points.

Another important result that comes from this graph is that the values of reduced frequency tend to become constant when reducing the Mach number to very low subsonic speeds of M=0.1-0.2.

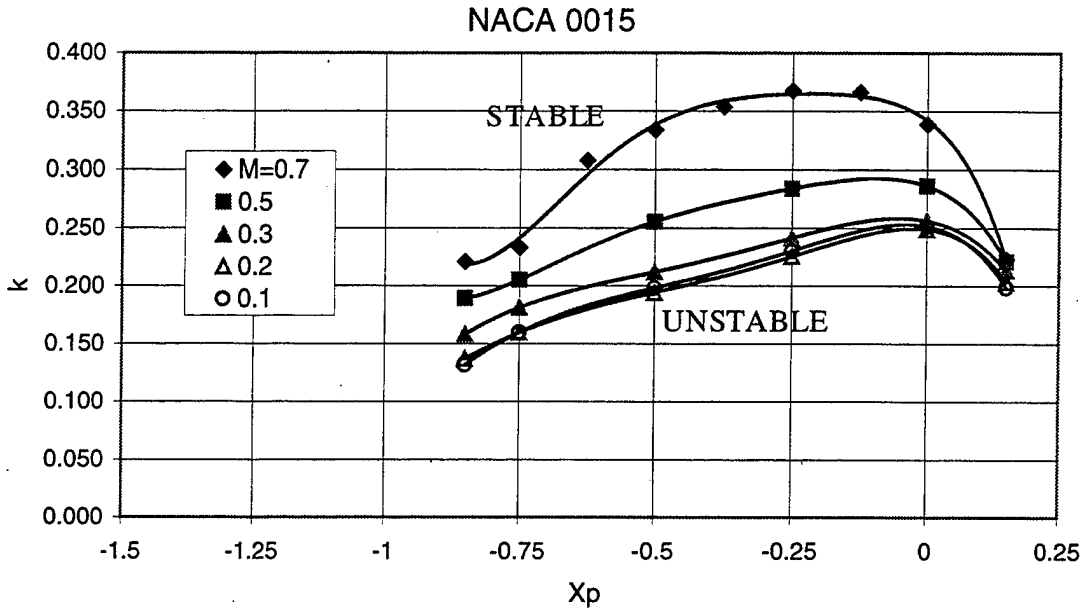

Figure 5-14 Effect of Mach Number and Pivot Point for NACA 0015 (Euler case)

This information is shown in bar chart form in Figure 5-15:

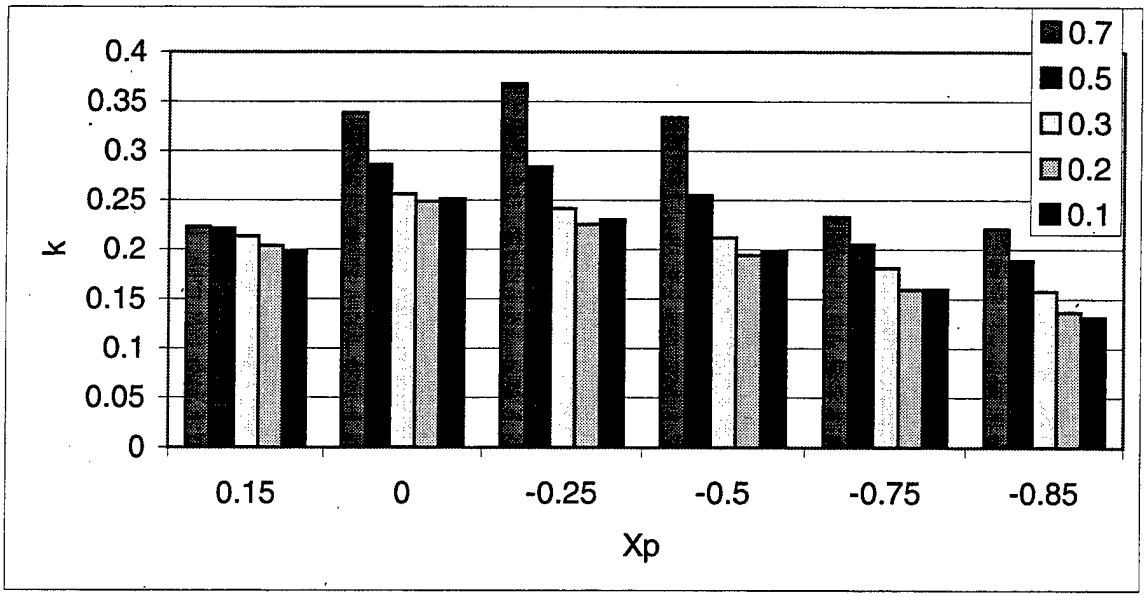

Figure 5-15 Reduced frequency variation with Mach number for Pivot Points -0.85<Xp<0.15 (NACA 0015)

The percentage increase of the reduced flutter frequency with Mach number and pivot points is tabulated in Table 5-4.

M \ Xp	0.15	0	-0.25	-0.5	-0.75	-0.85
0.7	12.4%	34.6%	59.8%	68.6%	45.8%	67.6%
0.5	11.4%	13.8%	23.4%	28.9%	28.3%	43.5%
0.3	7.4%	1.9%	4.9%	6.9%	13.3%	20.0%
0.2	2.4%	-1.1%	-2.1%	-2.0%	-0.1%	4.0%
0.1	0	0	0	0	0	0

Table 5-4 Percentage Increase of k with Mach number and Pivot Points

Another way to display the effect of pivot location and Mach number is to plot the reduced natural torsional frequency k_α needed to suppress flutter. Again it is seen from Figure 5-16 that an increase in Mach number is destabilizing.

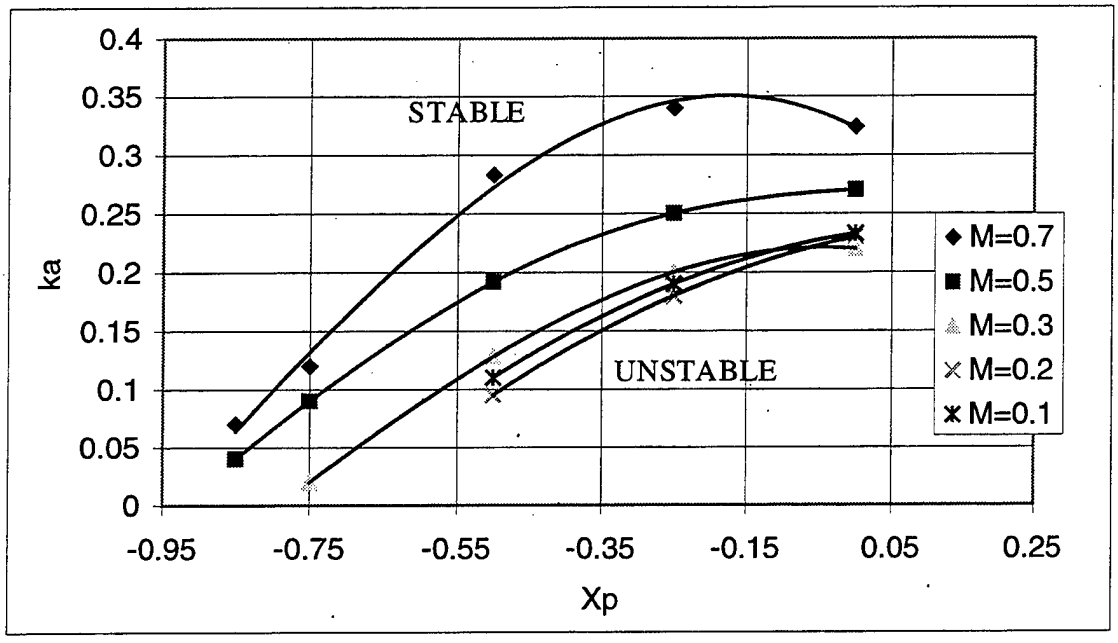

Figure 5-16 Effect of Mach number and pitch axis location on torsional flutter of NACA 0015 airfoil, i_α=100

Another useful way of representing the results is to show the variation of the reduced flutter velocity with Mach number for every pivot point. As discussed in Chapter III the reduced flutter velocity is defined as $V_F = \frac{U}{\omega_\alpha c} = \frac{1}{k_\alpha}$ and can be used in order to find the speed U for which flutter occurs for given values of K_α. Figure 5-17 shows the decrease of the flutter speed as the Mach number is increased. The results shown are only for pivot points $-0.85<Xp<0$ for which $i_\alpha=100$.

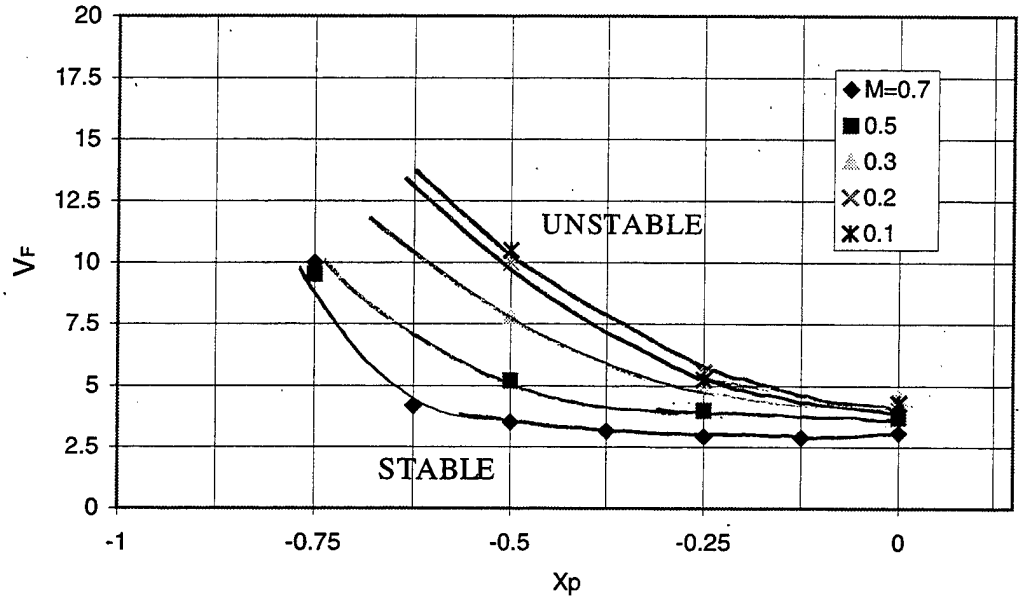

Figure 5-17 Variation of flutter speed with Mach Number for NACA 0015, $i_\alpha=100$

H. EFFECT OF AIRFOIL THICKNESS

The same procedure was applied to study the effect of airfoil thickness. Calculations were done for the airfoils: NACA 0006, NACA 0009, NACA 0012 and NACA 0015 for a Mach number of 0.7. The variation of critical reduced frequency with the airfoil thickness is presented in Figure 5-18 and Figure 5-19 showing that over the whole pivot point range any increase in airfoil thickness has a destabilizing effect.

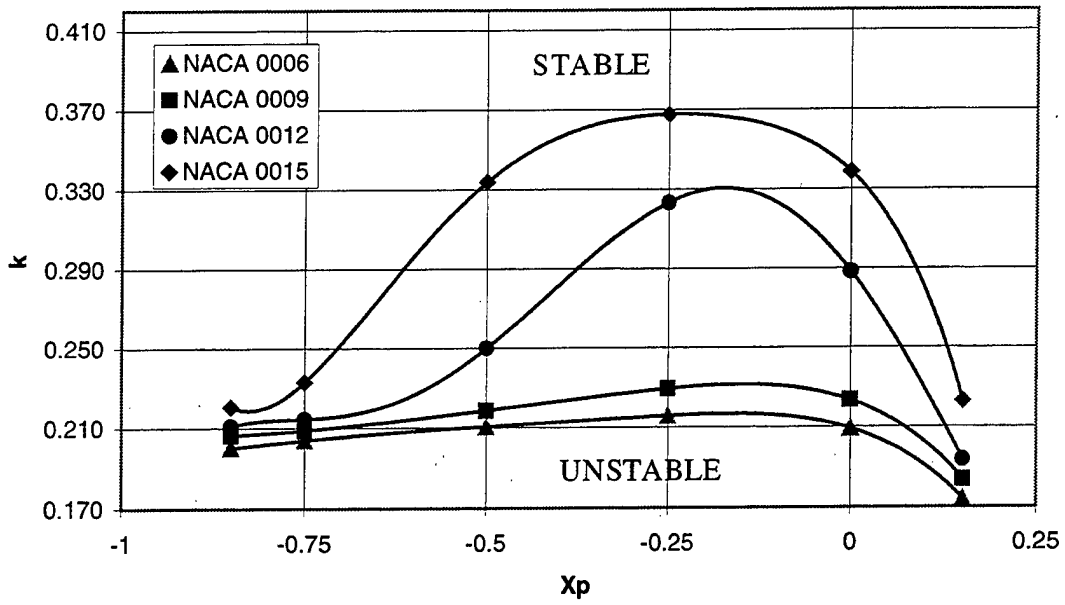

Figure 5-18 Effect of airfoil thickness on critical reduced frequency at M=0.7

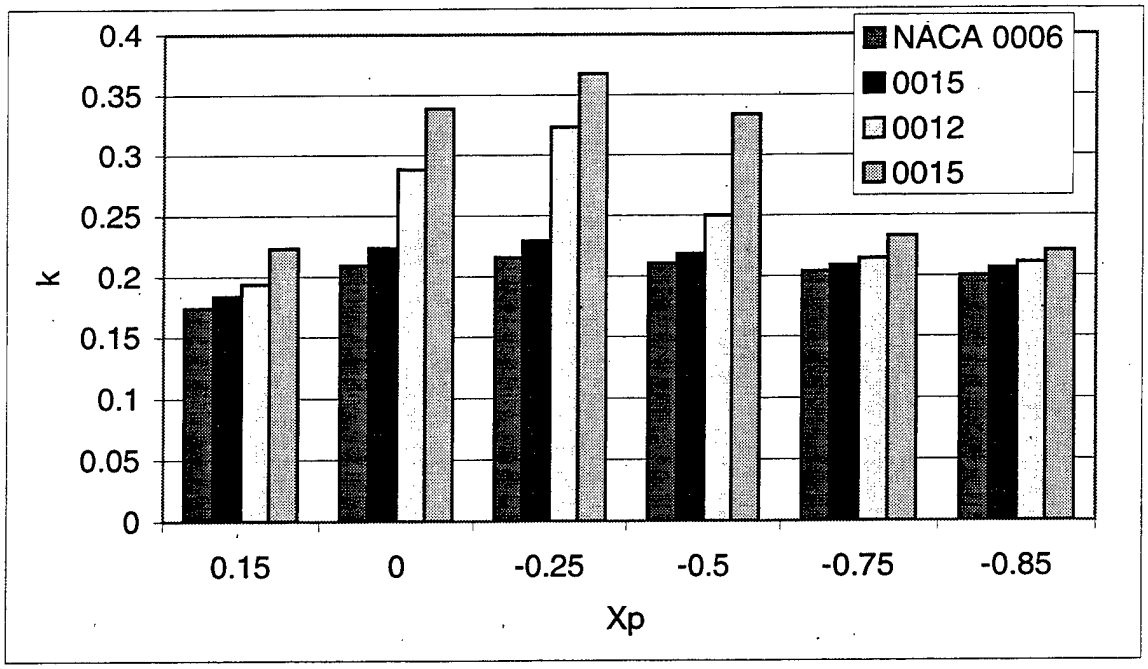

Figure 5-19 Effect of airfoil thickness at M=0.7

This destabilizing influence of airfoil thickness is quantified in Table 5-5 where the percentage increase of the reduced flutter frequency k is tabulated.

Airfoil thickness	0.15	0	-0.25	-0.5	-0.75	-0.85
6	0	0	0	0	0	0
9	5.6%	6.8%	6.3%	3.8%	2.4%	3.2%
12	11.2%	37.8%	49.8%	18.8%	5.2%	5.4%
15	28.1%	61.8%	70.4%	58.6%	14.3%	10.3%

Table 5-5 Percentage increase of k with airfoil thickness and pivot point location

Similarly, Figure 5-20 displays the reduced natural pitching frequency k_α needed to suppress flutter. Again it is seen that the NACA 0015 airfoil requires a much higher torsional frequency than the NACA 0006 airfoil. Again the results shown are for elastic

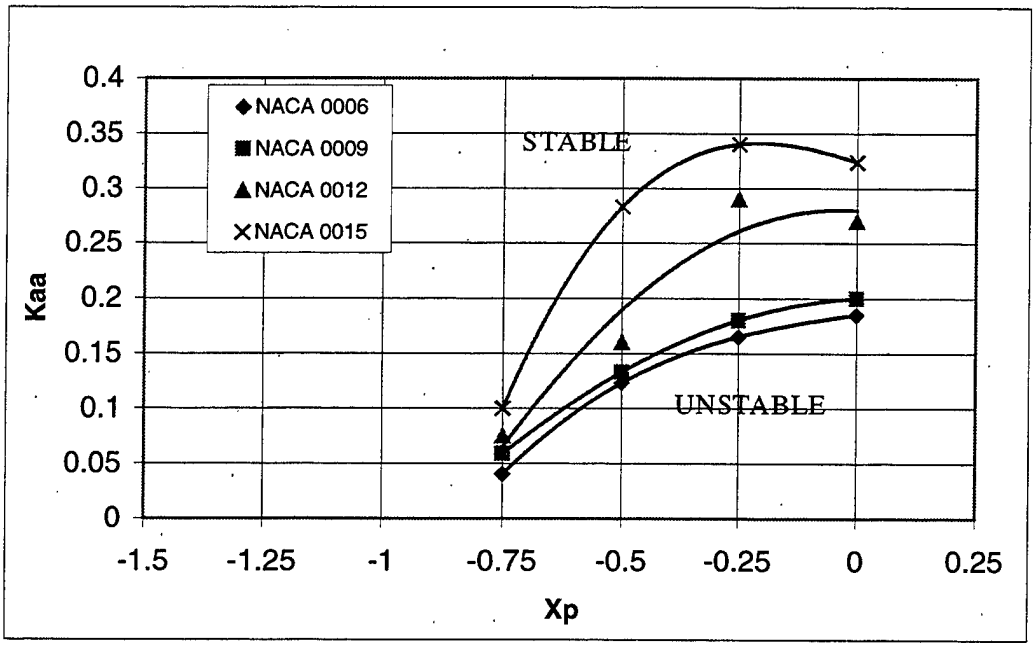

Figure 5-20 Effect of airfoil thickness on torsional flutter at M=0.7, i_α=100

axis locations of -0.85<Xp<0.15 for which the used value of moment of inertia was 100.

Finally the destabilizing effect is also shown in Figure 5-21. Increasing the airfoil thickness results in a significant decrease in the flutter speed.

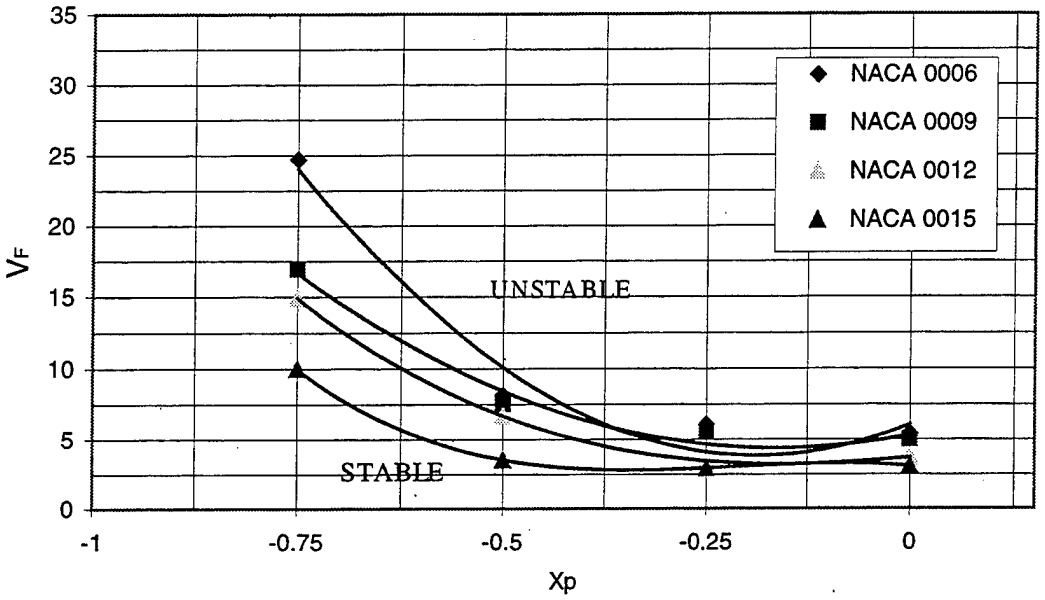

Figure 5-21 Variation of flutter speed with airfoil thickness at M=0.7, i_α=100

I. VISCOUS (NAVIER-STOKES) CASE CALCULATION

The same procedure previously described for Euler case will be shown for the viscous flow over the same oscillating airfoil (NACA 0015), the same Mach number (M=0.7) and the same elastic axis of oscillation (L.E of the airfoil - pivot point Xp=0).

The input file for the steady solution is as follows:

```
#    IREAD     ITER      NPRINT    NLOAD     ODVAR
       0       20000       1         1        1.00
#    ALPHA     OSCIL     RAMP      REDFRE    ALFAMND   ALFAMXD
       0.5     false     false     0.100     -.500     0.500
#    PLUNGE    PLMX      PLMY      PLPHSXD   PLFREQ
     false     0.        0.10      0.        0.1        0.0       0.0
#    MACH      RE        VISC      TURBL
     0.700     1.0e6     true      true
```

```
#    TIMEAC    COUR      NEWTIT
     true      1000.0      1
#    free      mass      ialpha    ka         kh         xp         xa
     false      0.0      100.0     0.00000    0.0        0.0        0.0
#    aneut     hneut     h0
     0.0       0.0       0.0
```

The steady solution is presented in Figure 5-22.We can see that Cl reaches a steady value of 0.08977 after t =40 sec.

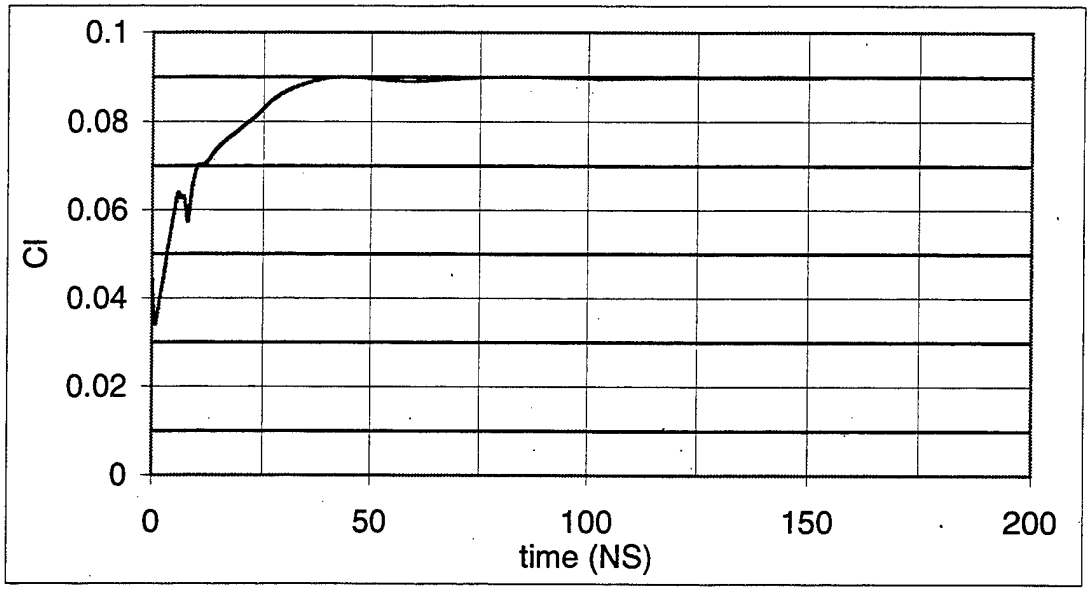

Figure 5-22 Steady state soln for NACA 0015 M=0.7 (N-S case)

The final result for the steady solution is shown at

Table 5-6:

T	Aoa	Cl	Cd	Cm
153.6969	0.5	0.089777	0.006215	0.000665

Table 5-6 Steady state solution for NACA 0015 M=0.7 (N-S case)

After the steady solution is obtained, the flutter condition can be found using the same procedure described for the Euler calculations. We start with a pivot point of Xp=0.0 and an assumed value of 0.36 for k_α. The following is the input file for the N.S. code:

```
#    IREAD     ITER      NPRINT    NLOAD     ODVAR
       -1      30000       1         1        1.00
#    ALPHA     OSCIL     RAMP      REDFRE    ALFAMND   ALFAMXD
      0.5      false     false     0.100     -.500     0.500
#    PLUNGE    PLMX      PLMY      PLPHSXD   PLFREQ
     false     0.        0.10      0.        0.1        0.0       0.0
#    MACH      RE        VISC      TURBL
     0.700     1.0e6     true      true
#    TIMEAC    COUR      NEWTIT
     true     700.00       3
#    free      mass      ialpha    ka        kh        xp         xa
     true      0.0      100.0     0.340000  0.0       0.0       0.0
#    aneut     hneut     h0
     0.0       0.0       0.0
```

The plot of the resulting airfoil motion is presented in Figure 5-23.

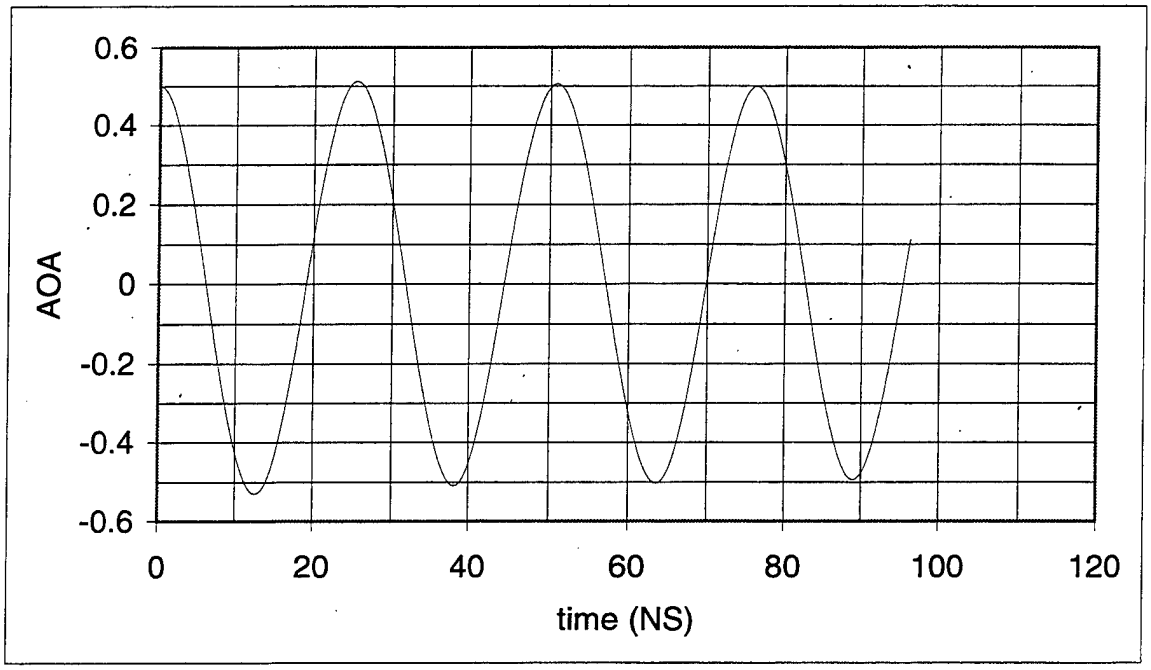

Figure 5-23 Unsteady case solution - Ka=0.34 (N-S case)

Since the airfoil motion is seen to decay the assumed value of k_α is too high. After finding the maximum points of the graph and applying a regression equation we find that the slope of the maximum points is -3.188E-04 (**Figure 5-24**).

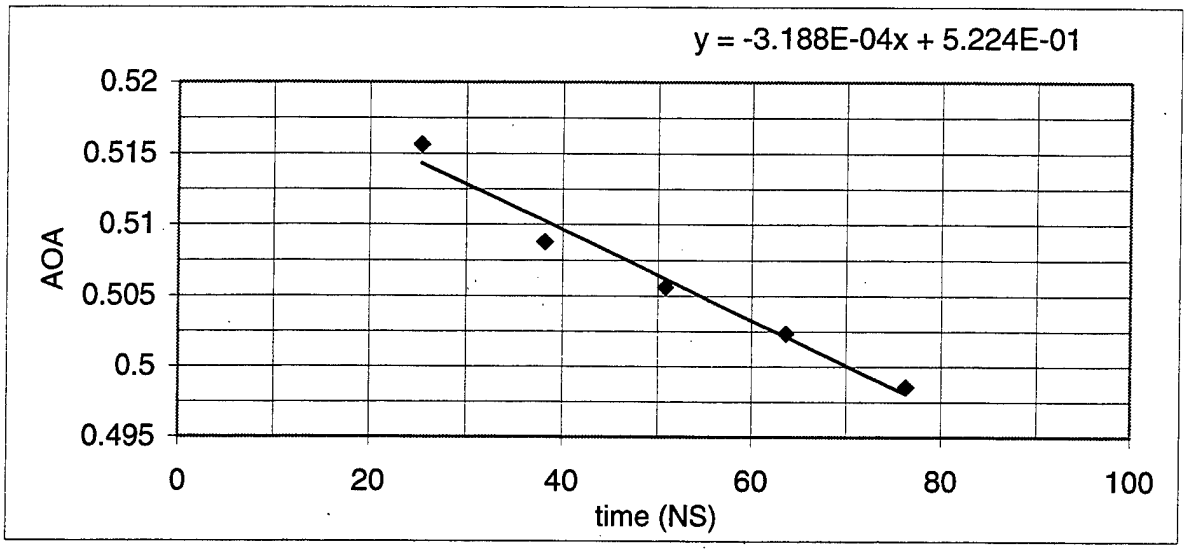

Figure 5-24 Time rate of change of AOA amplitude for K_α=0.34 (N-S case)

Similarly for k_α=0.20 the diverging motion presented in **Figure 5-25** is obtained.

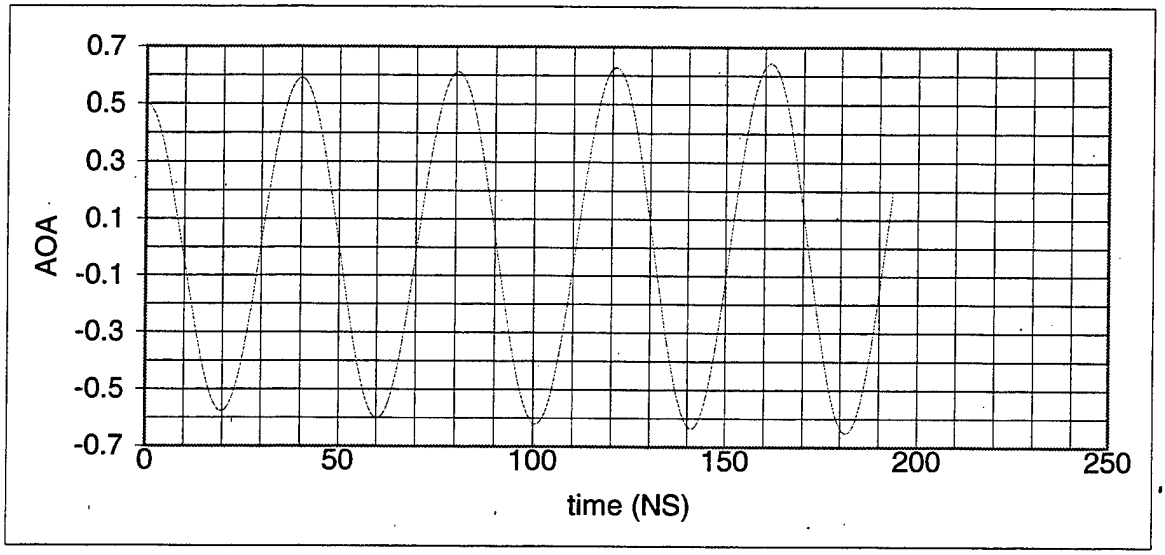

Figure 5-25 Unsteady case solution - Ka=0.20 (N-S case)

Then applying a regression equation for the maximum points of the graph, the slope is found to be 4.566E-04 (Figure 5-26):

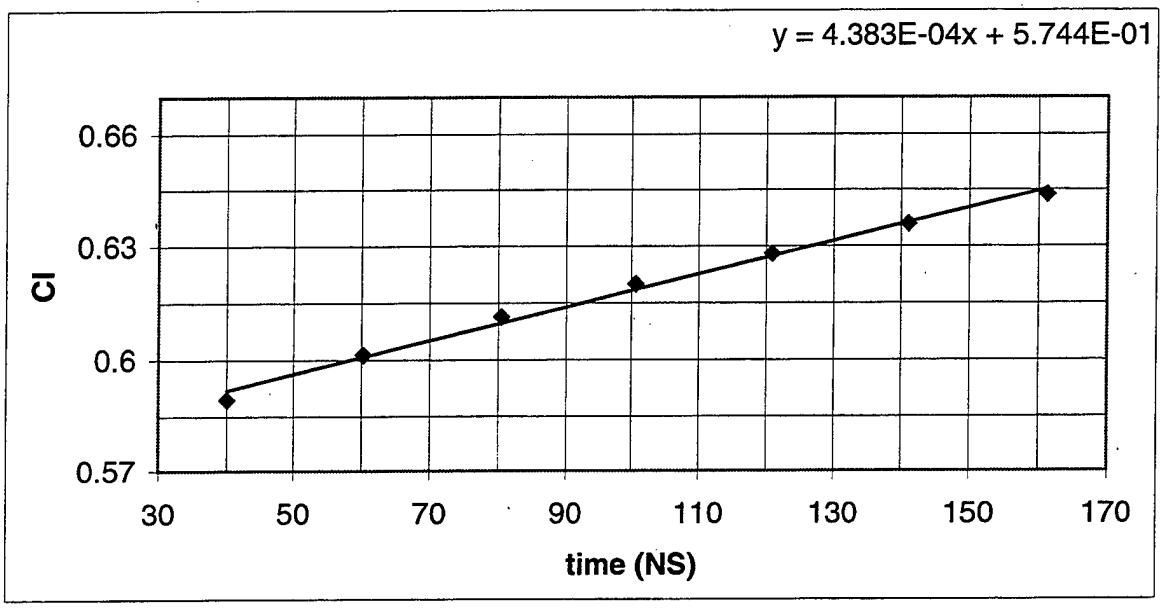

Figure 5-26 Time rate of change of AOA amplitude for Ka=0.20 (N-S case)

The results for the two trials are shown in Table 5-7 which make it possible to interpolate the value of k_α which produces a constant amplitude of oscillation. As shown in Figure 5-27 this value is k_α=0.252.

Ka	Slope
0.34	-2.860E-04
0.20	4.383E-04

Table 5-7 Regression equation slope values for various k_α values

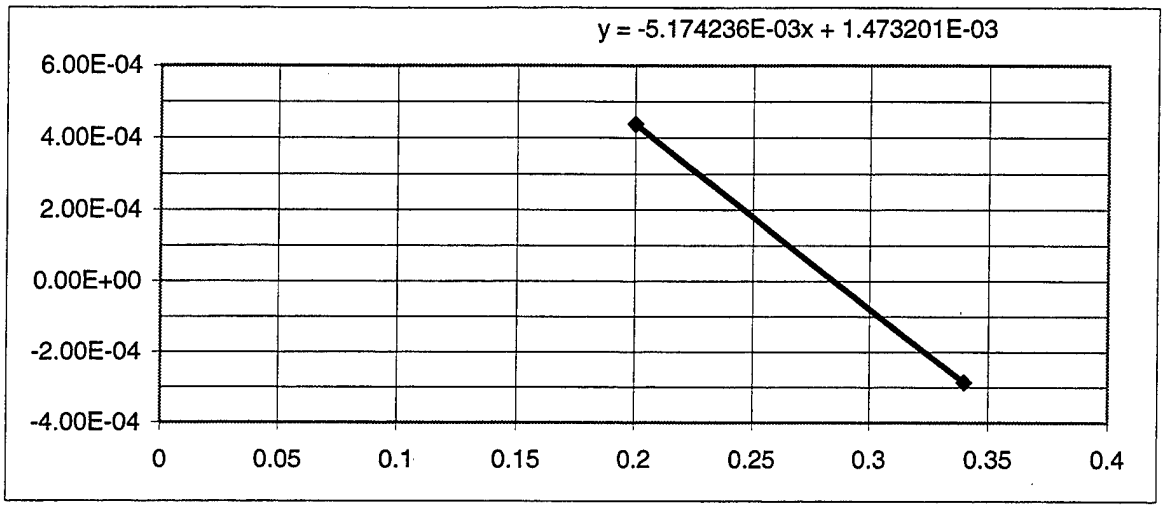

Figure 5-27 Curvefit of Ka vs time rate of change of AOA amplitude (N-S case)

Using this k_α value indeed produces the oscillation shown in Figure 5-28 and the slope $-6.783E{\cdot}10^{-5}$ shown in Figure 5-29.

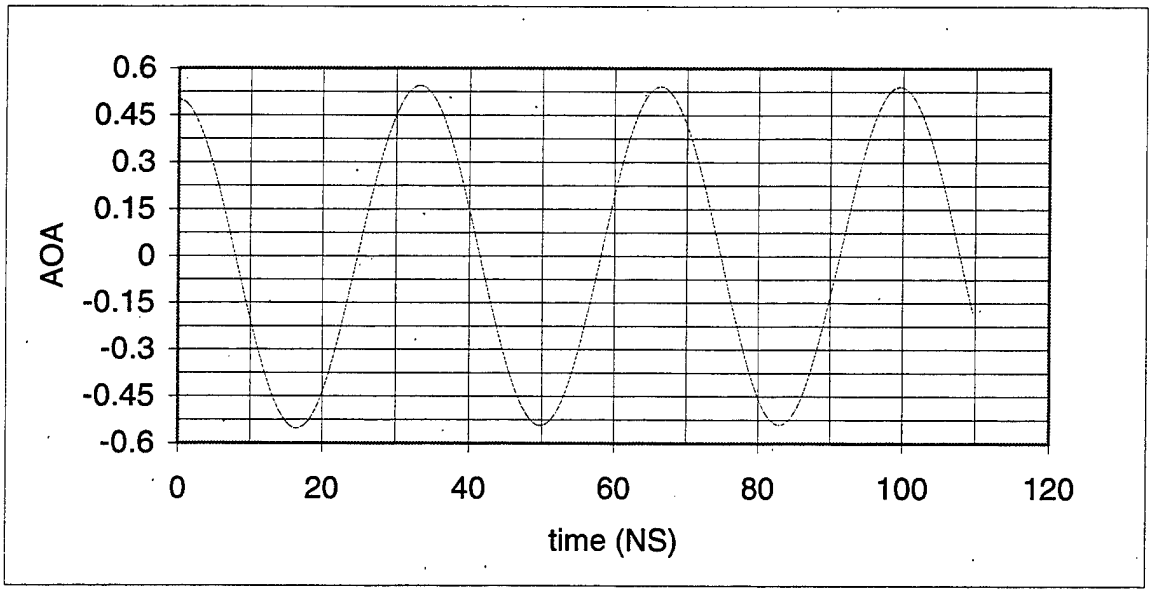

Figure 5-28 Unsteady case solution - Kα=0.252 Critical flutter case (N-S)

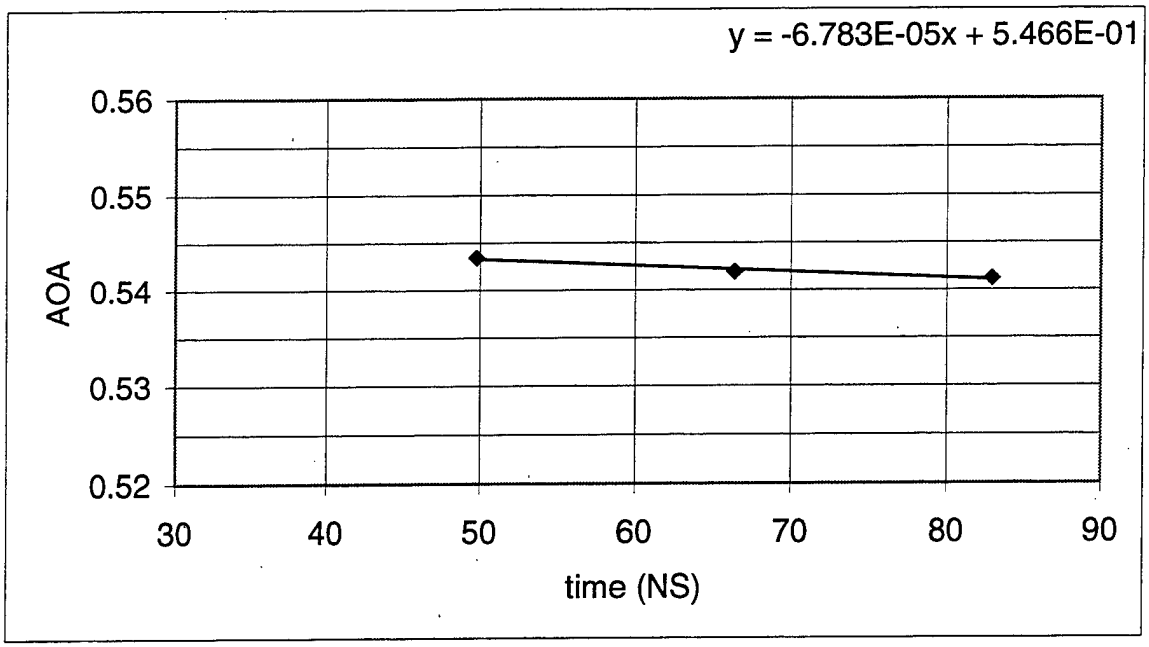

Figure 5-29 Time rate of change of AOA amplitude for Kα=0.324 Critical flutter (N-S case)

From the airfoil motion we find that the average period of oscillation is 33.215 (non-dimensional time) and reduced frequency of oscillation 0.270.

J. EULER-NS RESULTS COMPARISON

Due to time constraints the N-S study was performed only for NACA 0015 airfoil and M=0.7. The critical reduced frequency values for pivot points between $-0.85<Xp<0.15$ are presented in Figure 5-30 and compared with the Euler predictions.

It is seen that the values of critical reduced frequencies found with the Euler calculations are up to 23% higher than the N.S predictions. As expected, viscous flow effects reduce the possibility of flutter. From Eq.(4.5) it is seen that the same airfoil at the same Mach number with 60% less torsional rigidity will have the same flutter stability.

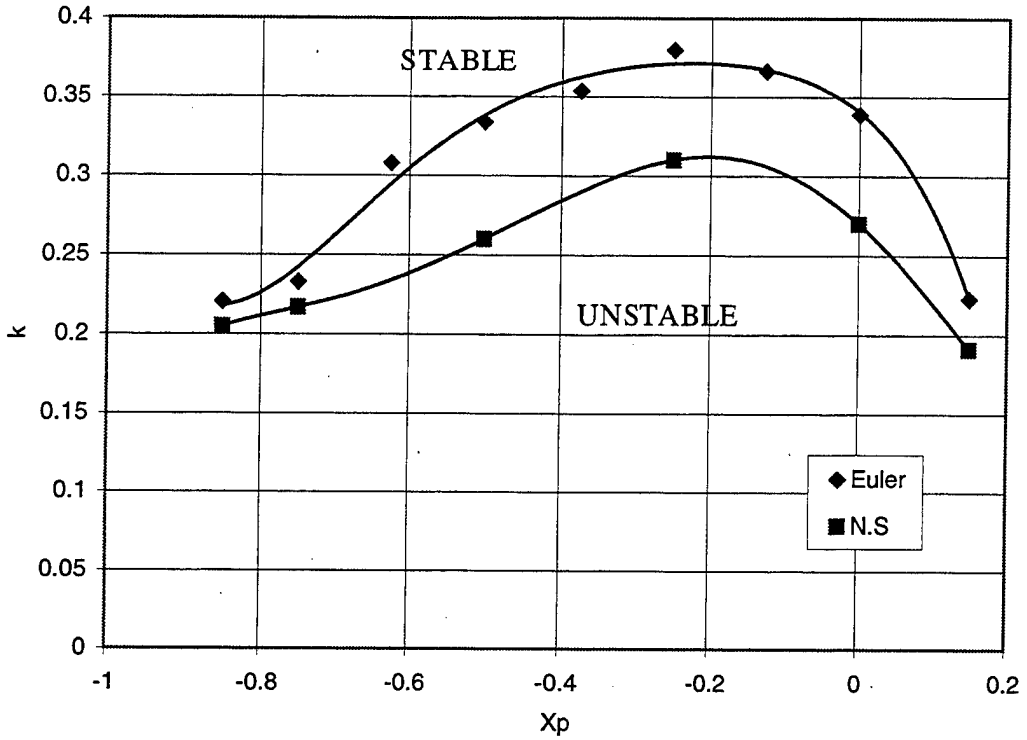

Figure 5-30 Euler – NS reduced frequency results for NACA 0015 and M=0.7

Table 5-8 shows the numerical differences between the above calculations for Euler and Navier-Stokes cases.

Xp	0.15	0.00	-0.25	-0.50	-0.75	-0.85
k(Euler)	0.223	0.339	0.380	0.334	0.233	0.221
k (N-S)	0.191	0.270	0.310	0.260	0.217	0.205
Difference	14.3%	20.3%	18.4%	22.1%	6.8%	7.2%

Table 5-8 Numerical differences of reduced frequency between Euler and N-S calculations for NACA 0015 and M=0.7

The reduced natural pitching frequency k_α values computed with the N-S and Euler codes are presented in Figure 5-31 indicating that the minimum torsional stiffness necessary to prevent flutter is smaller using viscous flow calculations.

In order to explain this finding it is instructive to examine the pressure distributions and Mach number contour plots for both cases in steady AOA of 0.5° (Figure 5-32 to Figure 5-39). The main difference of the graphs has to do with the strength of the shock above the airfoil. For the Euler case it is seen that a relatively strong shock is formed over the airfoil. The graphs that come from the Navier-Stokes calculations show that the shock over the airfoil is very weak. This is due to the boundary layer which smooths the shock.

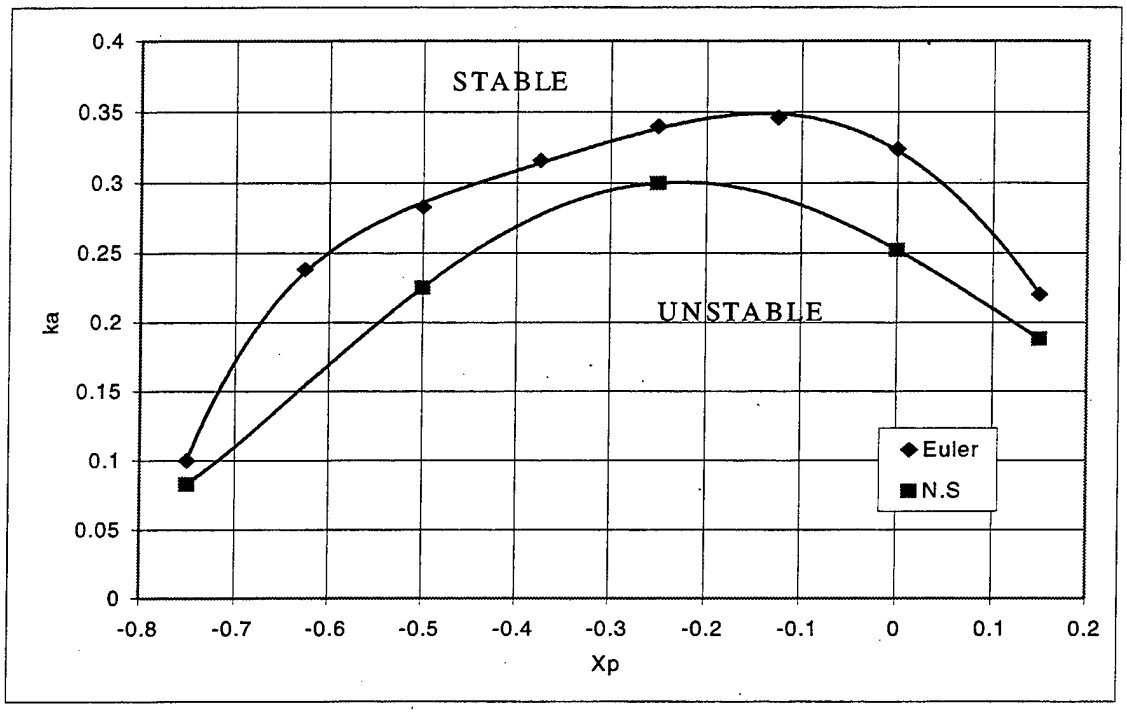

Figure 5-31 Euler – NS reduced natural pitching frequency results for NACA 0015 and M=0.7 i_α=100

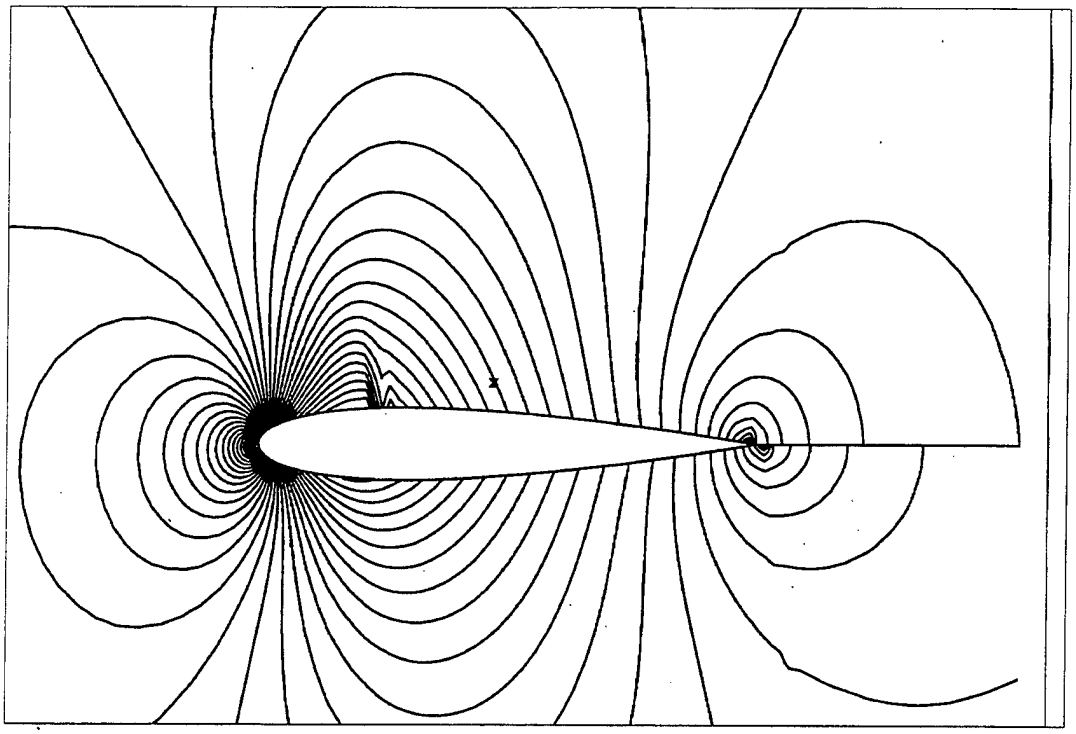

Figure 5-32 Pressure distribution contours for NACA 0015 M=0.7 steady AOA (Euler)

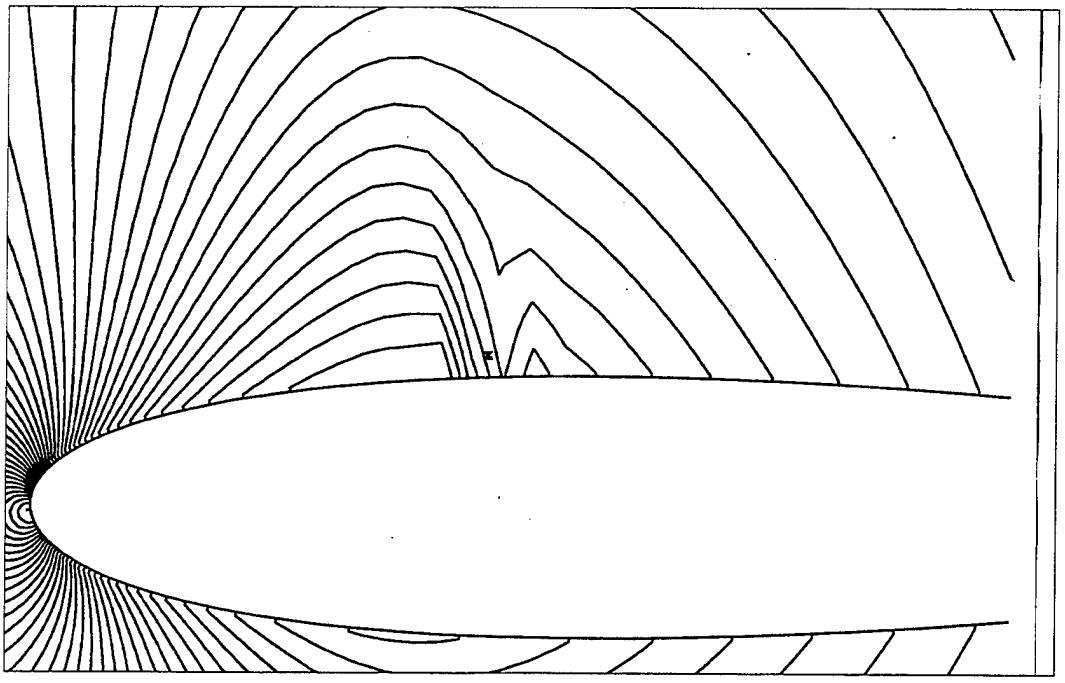

Figure 5-33 Pressure distribution contours for NACA 0015 M=0.7 steady AOA (Euler-detail)

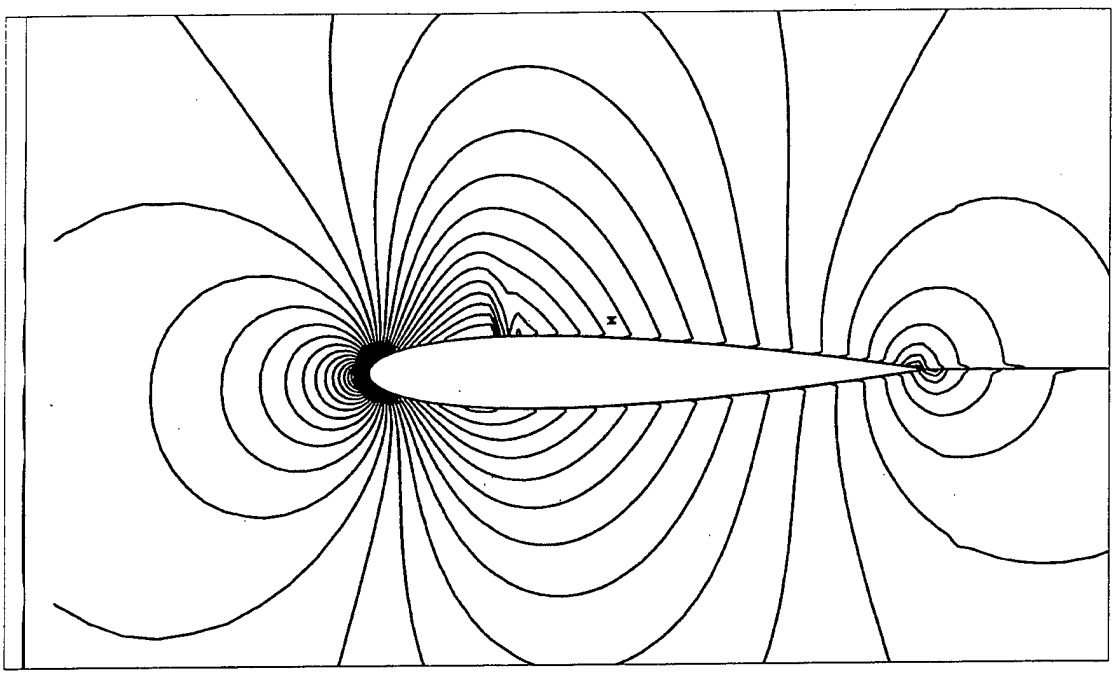

Figure 5-34 Mach contours for NACA 0015 M=0.7 steady AOA (Euler)

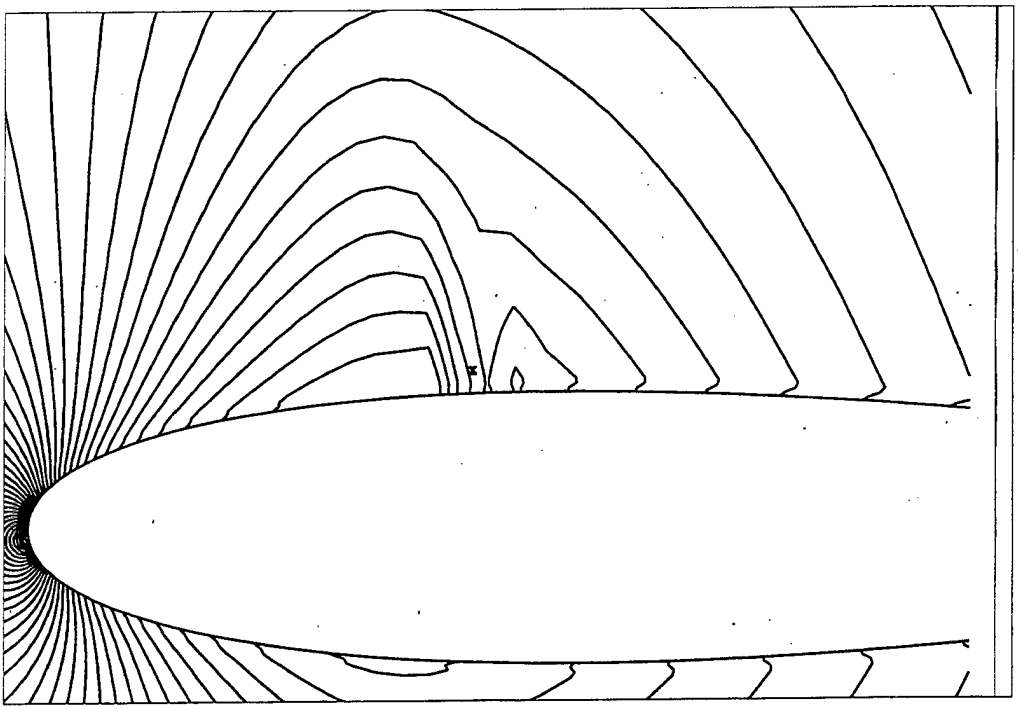

Figure 5-35 Mach contours for NACA 0015 M=0.7 steady AOA (Euler-detail)

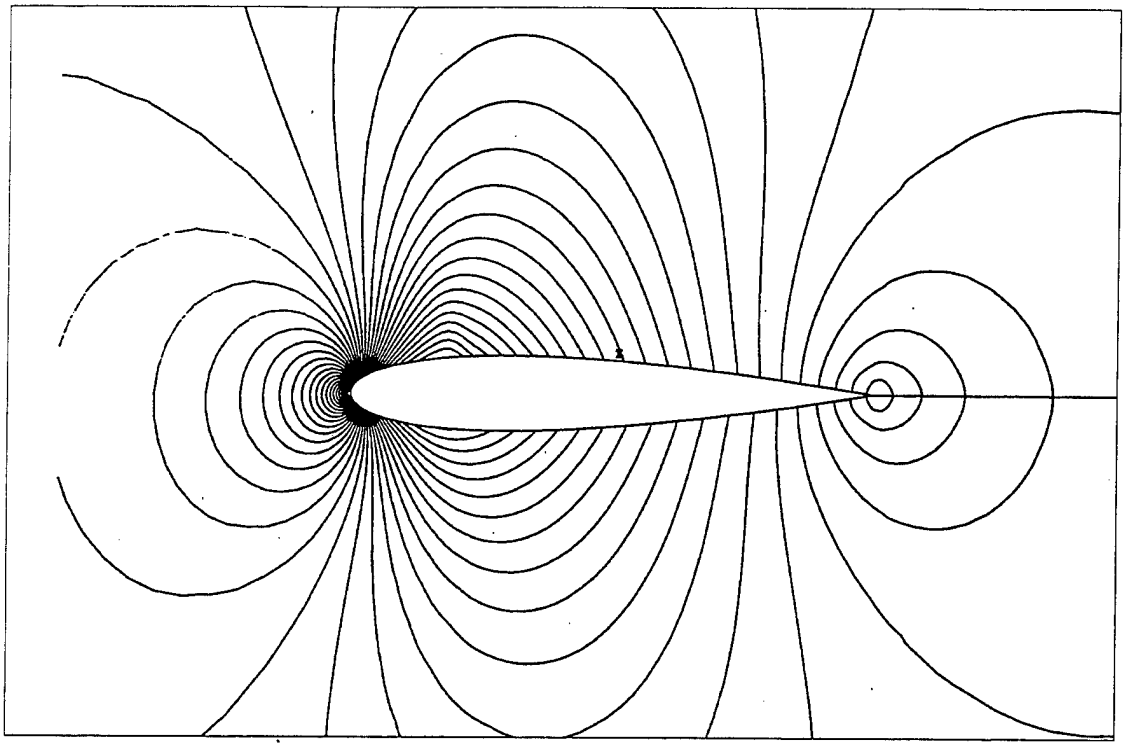

Figure 5-36 Pressure distribution contours for NACA 0015 M=0.7 steady AOA (N-S)

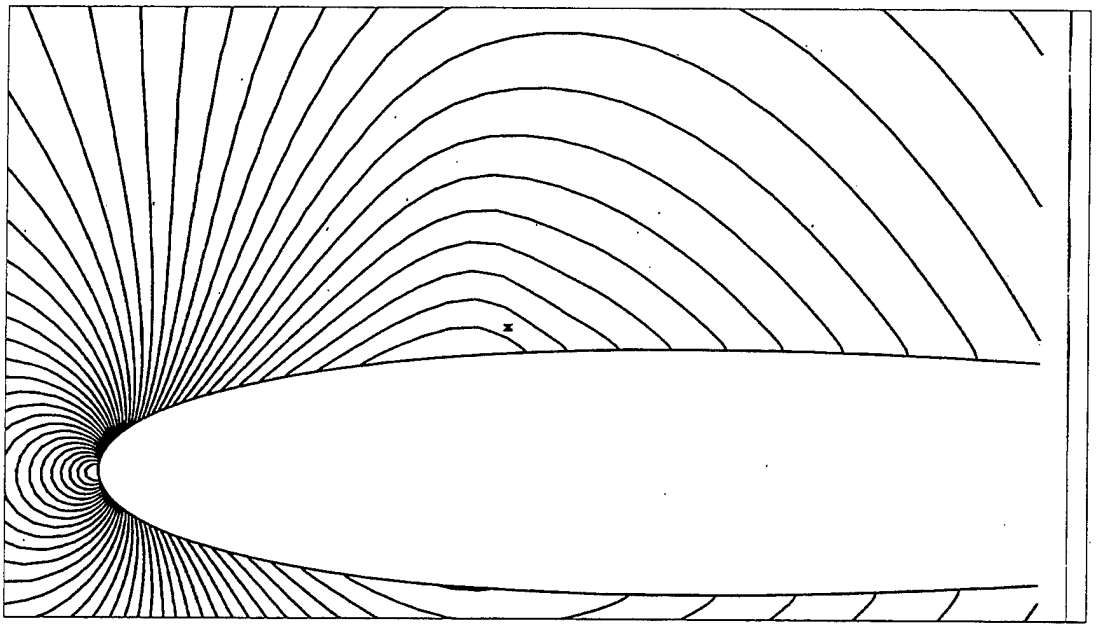

Figure 5-37 Pressure distribution contours for NACA 0015 M=0.7 steady AOA (N-S-detail)

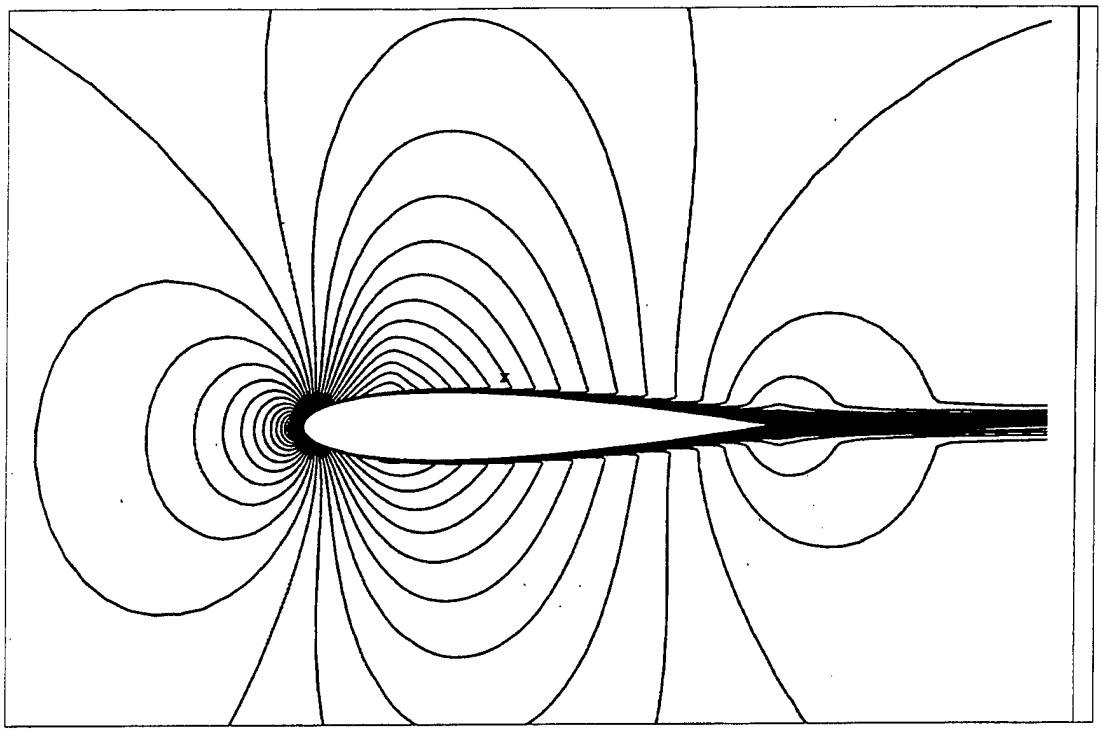

Figure 5-38 Mach contours for NACA 0015 M=0.7 steady AOA (N-S)

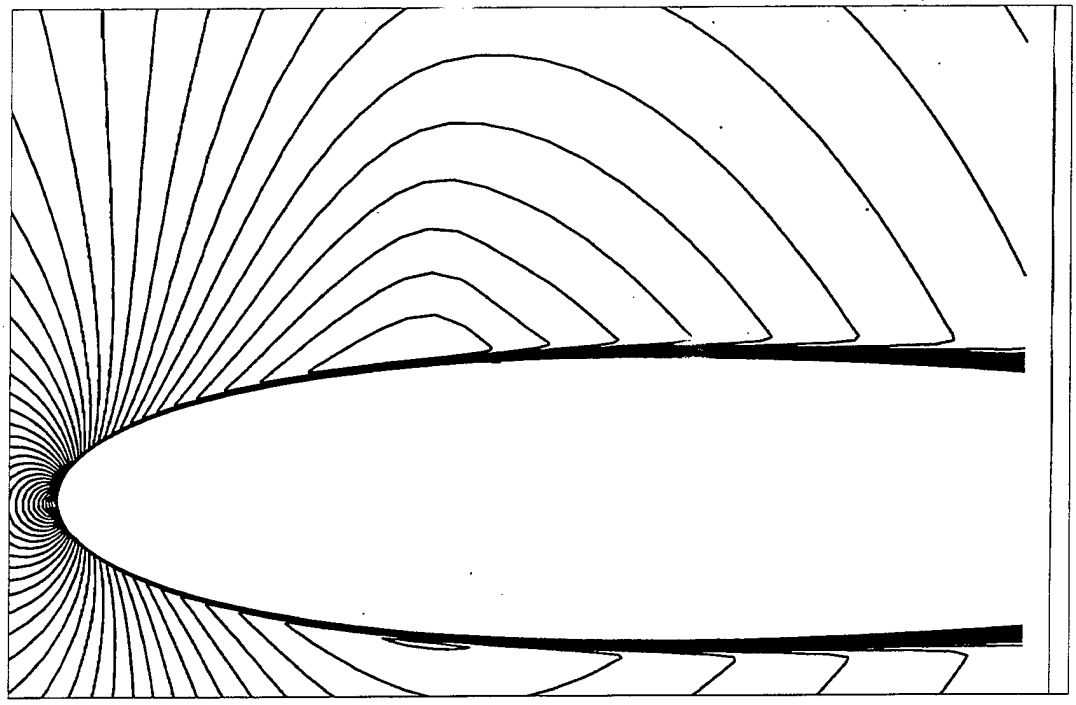

Figure 5-39 Mach contours for NACA 0015 M=0.7 steady AOA (N-S-detail)

K. PANEL – EULER CODE COMPARISON

Another interesting area of study is the comparison of results from the Euler code for non-viscous low subsonic flow with those from the UPOT panel code which calculates inviscid incompressible flow over the airfoil. The calculations were again made for flow the NACA 0015. The results for M=0.3, 0.2, 0.1 and incompressible flow are presented in Figure 5-40.

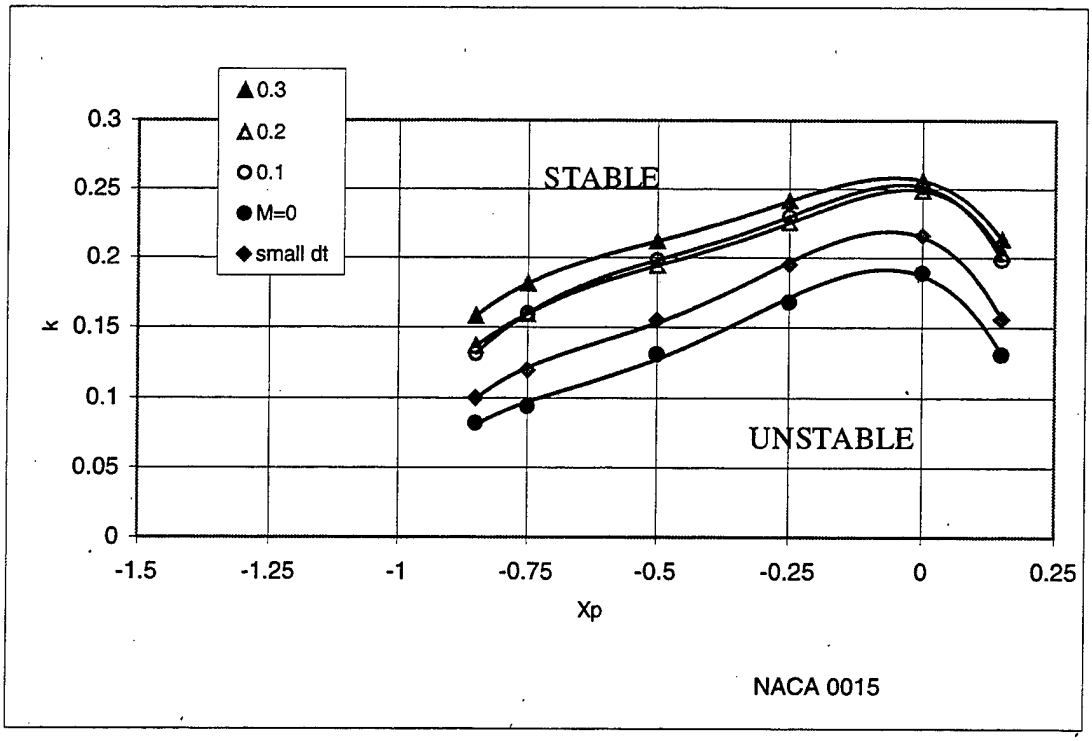

Figure 5-40 Low subsonic Euler code results comparison with UPOT results.

It is seen that the trends predicted by both codes are in good agreement, but there is a significant quantitative difference between the Euler prediction at M=0.1 and the incompressible panel code prediction. This difference could be reduced substantially if the panel code was run with a very small time step, as shown in Figure 5-40 and Figure 5-41.

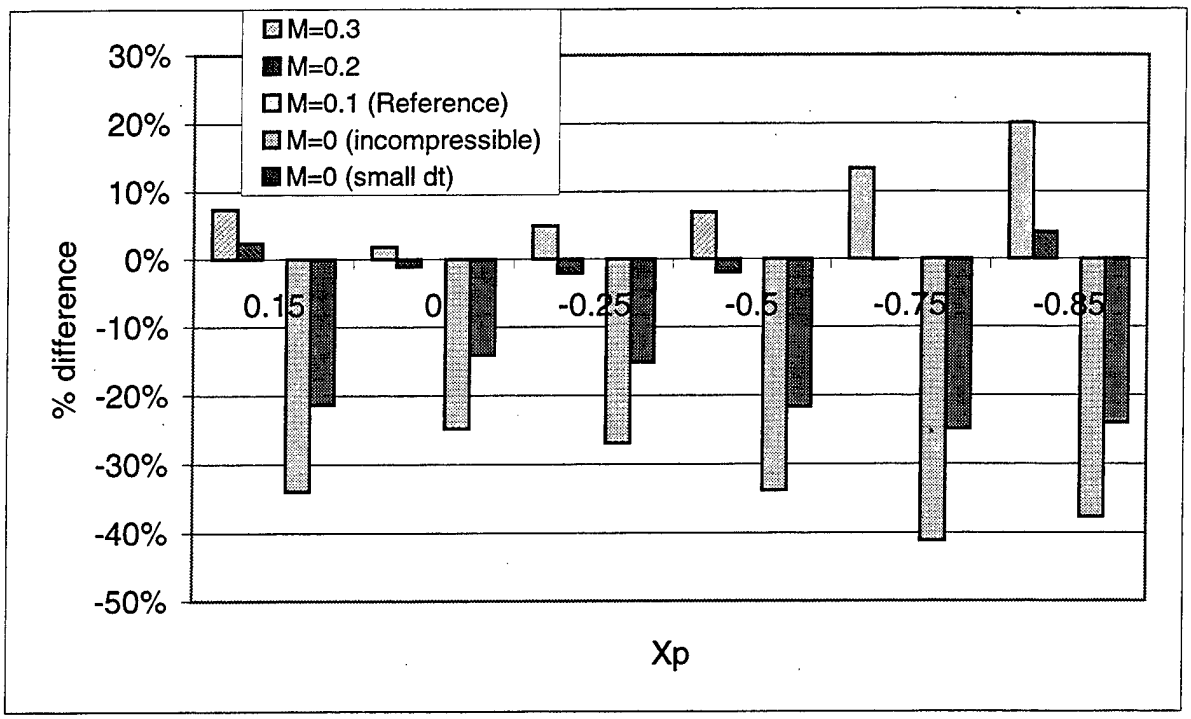

Figure 5-41 % differences between Euler and UPOT results (w.r.t M=0.1 results)

VI. SUMMARY

The time domain flutter analysis of NACA 0006, NACA 0009, NACA 0012 and NACA 0015 airfoils presented in this thesis leads to the following major conclusions:

A. Linearized incompressible and linearized subsonic compressible flow theory yields unconservative estimates of single-degree-of-freedom torsional airfoil flutter.

B. Torsional flutter region increases with increasing airfoil thickness and Mach number.

C. Viscous flow effects have a stabilizing influence.

D. Pitch axis locations upstream of the quarter chord point may induce flutter, especially in the range between the leading edge and a point a half-chord upstream of the leading edge.

E. Flutter boundaries computed with the incompressible panel code UPOT require very small time steps; however, even for the smallest time step used, the UPOT computed flutter boundaries differed from Euler computed boundaries by a significant amount.

F. Euler computations converged relatively quickly for high subsonic Mach numbers, but required increasingly large times for completion as the Mach number was decreased toward 0.1. Every Euler computation could be completed in about 12 to 24 hours.

G. Navier-Stokes computation times typically were 4 to 6 times longer on the Department's SGI work stations.

VII. RECOMMENDATIONS

It will be interesting to study the effect of the following parameters:

A. Reynolds Number

Extend the calculation to Reynolds numbers other than $1 \cdot 10^6$

B. Mach Number

Extend the calculations to cover the transonic Mach number range and investigate the effect of shock motion and shock boundary layer interaction on flutter

C. Moment of Inertia

Investigate the effect of moment of inertia variation on flutter

D. Two-Degree-of-Freedom Flutter

Extend the single-degree-of-freedom analysis to the bending-torsion flutter problem and investigate the effect of airfoil thickness on this type of flutter.

LIST OF REFERENCES

1. Fung, Y.C, "Theory of Aeroelasticity," Dover 1969.
2. Fletcher, C.A., "Computational Techniques for Fluid Dynamics," Springer Verlag, VOL I -II, 1990.
3. Dowell, E.H., et al "A Modern Course in Aeroelasticity," Sijthoff & Noordhoff 1978.
4. Bisplinghoff, R.L., and Ashley H., "Principles of Aeroelasticity," Dover, 1962.
5. Krothapalli A., "Recent Advances in Aerodynamics," Springer Verlag, 1983.
6. Bisplinghoff R.L., Ashley H., Halfman R.L., "Aeroelasticity," Addison-Wesley, 1951.
7. Lambourne,N.C., "Flutter in One Degree of Freedom" Part V Chapter 5, AGARD Manual on Aeroelasticity, General Ed. W. P. Jones, Oct 1961.
8. Schlichting,H., "Boundary Layer Theory, McGraw-Hill Book Company,",1966.
9. Cricelli, A.M., "Unsteady Airfoil Flow Solutions on Moving Zonal Grids," Master's Thesis, Naval Postgraduate School, 1992.
10. Baldwin, B.S., Lomax, H., "Thin Layer Approximation and Algebraic Model for Separated Turbulent Flows," AIAA Paper 78-257, Jan 1978.
11. Rai, M.M. and Chakravarthy, S.R., "An Implicit Form of the Osher Upwind Scheme," AIAA Journal Vol.24, No 5, May 1986, pp-735-743.
12. Cowles L.J., "High Reynolds Number, Low Mach Number Steady Flow Field Calculations over NACA 0012 Airfoil Using Navier-Stokes and Interactive Boundary Layer Theory," Master's Thesis, Naval Postgraduate School,1987.
13. Jones K.D. and Platzer M.F., "Airfoil Geometry and Flow Compressibility Effects on Wing and Blade Flutter," AIAA Paper 98-0517, January 1998.
14. Jones K.D. and Platzer M.F., "Time Domain Analysis of Low-Speed Airfoil Flutter," AIAA Journal, Vol 34, No 5, May 1996.

15. Teng, N.H., "The Development of a Computer Code for the Numerical Solution of Unsteady, Inviscid and Incompressible Flow over an Airfoil," Master's Thesis, Naval Postgraduate School, 1987.

INITIAL DISTRIBUTION LIST

1. Defense Technical Information Center.....2
   8725 John J.Kingman Road, Ste 0944
   Ft.Belvoir, VA 22060-6218

2. Dudley Knox Library 2
   Naval Postgraduate School
   411 Dyer Rd.
   Monterey, CA 93943-5101

3. Chairman.....1
   Department of Aeronautics and Astronautics, Code AA
   Naval Postgraduate School
   699 Dyer Rd, Room 137
   Monterey, CA 93943-5106

4. Dr. Max F.Platzer.....7
   Department of Aeronautics and Astronautics, Code AA/PL
   Naval Postgraduate School
   699 Dyer Rd, Room 137
   Monterey, CA 93943-5106

5. Dr. Kevin. D. Jones.....1
   Department of Aeronautics and Astronautics, Code AA
   Naval Postgraduate School
   699 Dyer Rd, Room 137
   Monterey, CA 93943-5106

6. CAPT. Constantinos Kakkavas 2

Peloponnisou 19

Vrilissia 15235

Athens, GREECE